EFFECT OF Mn SUBSTITUTION ON THE STRUCTURAL AND MAGNETIC PROPERTIES OF $Fe_{2.5}Zn_{0.5-x}Mn_xO_4$

A Dissertation Submitted to the Department Of Physics,
Bangladesh University of Engineering & Technology,
Dhaka, in Partial Fulfillment of Requirement
for the Degree of Master of
Philosophy in Physics

SUBMITTED

By

MARZIA SHARMIN

EXAMINATION ROLL NO.: 1009143024F

SESSION: October- 2009

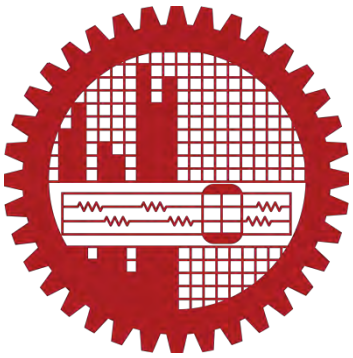

DEPARTMENT OF PHYSICS

BANGLADESH UNIVERSITY OF ENGINEERING & TECHNOLOGY

DHAKA 1000, BANGLADESH

CANDIDATE'S DECLARATION

It is hereby declared that this thesis or any part of it has not been submitted elsewhere for the award of any degree or diploma.

MARZIA SHARMIN

BANGLADESH UNIVERSITY OF ENGINEERING & TECHNOLOGY
DEPARTMENT OF PHYSICS, DHAKA 1000, BANGLADESH

CERTIFICATION OF THESIS

The thesis titled "**EFFECT OF Mn SUBSTITUTION ON THE STRUCTURAL ANDMAGNETIC PROPERTIES OF $Fe_{2.5}Zn_{0.5-x}Mn_xO_4$**" submitted by **MARZIA SHARMIN**, Roll No.: 1009143024F, Session: October 2009, has been accepted as satisfactory in partial fulfillment of the requirement for the degree of **Master of Philosophy** in Physics on 28.03.2015.

BOARD OF EXAMINERS

1. Dr. A. **K. M. Akther Hossain** — **Chairman**
   Professor
   Department of Physics, BUET, Dhaka.
   (Supervisor)

2. Dr. Afia Begum — **Member (Ex-Officio)**
   Professor and Head
   Department of Physics, BUET, Dhaka

3. Dr. Md. Feroz Alam Khan — **Member**
   Professor
   Department of Physics, BUET, Dhaka

4. Dr. Md. Mahbubul Haque — **Member (External)**
   Senior Scientific Officer
   Materials Science Division
   Atomic Energy Centre, Dhaka-1000.

DEDICATED TO

MY

BELOVED PARENTS

ACKNOWLEDGEMENTS

First of all I express all my admiration and devotion to the almighty Allah- Rabbul Alamin, the most beneficial who has enabled me to perform this research work and to submit this thesis.

I express my profound gratitude to my honorable supervisor Prof. Dr. A.K.M. Akther Hossain, Department of Physics, Bangladesh University of Engineering and Technology (BUET), for his constant direction, constructive criticism and inspiration in pursuing the whole investigation of the present research. Words are always insufficient to express his working capacities and unending enthusiasm for scientific rigorousness for innovative investigations. This always becomes the everlasting source of inspiration for his students.

I am very grateful to Prof. Dr. Afia Begum, Head, Department of Physics, BUET, Dhaka, Bangladesh for his valuable suggestions and inspiration. I like to express my gratitude to, Prof.Dr. Md. Abu Hashan Bhuiyan, Prof. Dr. Jiban Podder, Prof. Dr. Md. Feroz Alam Khan, Dr. Md. Rafi Uddin, Dr. Md. Forhad Mina, Dr. Mohammed Abdul Basith, Md. Azizar Rahman and all other teachers of Physics Department, for their cooperation.

I would like to give special thank to Dr. Abdul Gafur, Senior Scientific Officer and Md Rakibul Qadir,Engineer, Pilot Plant & Process Development Center, BCSIR for providing X-ray Diffraction data and Rietveld analysis of XRD data. I am grateful to the authority of Glass & Ceramic department of BUET for granting permission to use their FESEM. I wish to thank specially my senior research worker and PhD students of the department, Md. Belal Hossen, Mohammed. Kamrul Haque Bhuiyan, Sajal Chandra Mazumdar, Mohammad. Julhash Miah and others for their cooperation throughout the study.

Ultimately, I would mention a very special gratefulness for the moral support and sustaining inspiration provided by the members of my family. This dissertation would never have been possible without their love and affection.

The Author

Marzia Sharmin

ABSTRACT

Polycrystalline $Fe_{2.5}Zn_{0.5-x}Mn_xO_4$ with x= 0.00-0.50 have been synthesized by the standard solid state reaction technique. Pellet- and toroid -shaped samples are prepared from the ferrite powders and sintered at various temperatures in air for 5 hours (1100-1250°C). Structural and surface morphology are studied by X-ray diffraction (XRD) and Field Emission Scanning Electron Microscope (FESEM). The magnetic properties of these ferrites are characterized with high frequency (10 kHz-120 MHz) using Impedance Analyzer. The influence of microstructure, various cation distribution and sintering temperature on the complex initial permeability of these samples are discussed. XRD pattern show the formation of spinel structure. Lattice parameters are calculated using the Nelson -Riley function. Lattice parameters are also analyzed by the Rietveld quantitative analysis. It is also found that the lattice constant increases with increasing Mn content, obeying Vegard's law due to larger ionic radius (0.89Å) of Mn^{2+} compared to Zn^{2+} (0.74Å). The micrograph shows that both sintering temperatures and cations substitutions have great influence on various properties. As the sintering temperature increases, the bulk density increases (depending on compositions), and hence the porosity decreases for all compositions. The initial permeability increases for substitution up to x=0.40 and beyond this slightly decrease. It is also observed that the real part of initial permeability ($\mu_i^{/}$) increases with sintering temperatures because high sintering temperature helps to develop uniform grain. The $\mu_i^{/}$ remains fairly constant in the frequency range up to some critical frequency which is called resonance frequency. The highest $\mu_i^{/}$ has been observed sintered at 1250 ºC because of the homogenious microstructure with a uniform grain size distribution. The relative quality factor, *Q*, increases with increasing sintering temperature and Mn content up to x=0.40 then decreases for increasing the Mn content. The highest *Q* value (1013) is observed for $Fe_{2.5}Zn_{0.10}Mn_{0.40}O_4$ sintered at 1250ºC.

CONTENTS

LIST OF TABLES

LIST OF SYMBOLS AND ABBREVIATIONS

Mn	Manganese
Zn	Zinc
B	Magnetic induction
CMR	Colossal magnetoresistance
F (θ)	Nelson-Riley function
f_r	Resonance frequency
g	Landé splitting factor
H_{cr}	Critical field
J	Exchange integral
K	Total anisotropy

K_1	Magnetocrystalline anisotropy constant
L_s	Self-inductance of the sample core
L_o	Inductance of the winding coil without sample
M	Magnetization
M_s	Saturation magnetization
N_A	Avogadro's number
P	Porosity
P_{intra}	Intragranular porosity
P_{inter}	Intergranular porosity
P_e	Eddy-current loss
Q	Relative quality factor
T_c	Curie temperature
T_n	Néel temperature
T_s	Sintering temperature
tanδ	Loss factor
Z	Complex impedance
α	Restoring force coefficient
β	Viscous damping factor
γ	Domain wall energy
ω	Angular velocity
δ_w	Domain wall thickness
μ_i	Initial permeability
$\mu^{/}$	Real part of complex permeability
$\mu^{//}$	Imaginary part of complex permeability
μ_B	Bohr magneton
χ_{spin}	Intrinsic rotational susceptibility
χ_w	Domain wall susceptibility
ρ_{th}	Theoretical Density
ρ_B	Bulk Density

CHAPTER 1

INTRODUCTION

1.1 General Introduction

There is an intense demand for high performance and miniaturization of many electronic devices. For some devices soft magnetic materials of high permeability is desired. With the rapid development of mobile communication and information technology, the electronic devices with small size, low cost and high performance is in demand. Many researchers have worked on different types of ferrites in order to improve their electrical and magnetic properties. There does not exist an ideal ferrite sample that meets the requirements of low eddy current loss and usefulness at frequencies of the gigahertz. Each one has its own advantages and disadvantages. Scientists still continue their efforts to achieve the optimum parameters of ferrites, like high saturation magnetization, high permeability, high resistivity etc. Since the research on ferrites is so vast, it is difficult to collect all of the experimental results and information about all types of ferrites in every aspect. Most modern soft ferrites have spinel type crystal structure. Spinel ferrites of different compositions have been studied and used for a long time to get useful products. It has tetrahedral *A* site and octahedral *B* site in AB_2O_4 crystal structure. It shows various magnetic properties depending on the compositions and cation distribution. Various cations can be placed in *A* site and *B* site to tune its magnetic properties. Depending on *A* site and *B* site cations it can exhibit ferromagnetic, antiferromagnetic, spin (cluster) glass, and paramagnetic behaviour [1, 2]. The general chemical formula of such ferrites is $MeFe_2O_4$, where *Me* represents one or several of the divalent transition metals. These types of ferrites are subjects of intense theoretical and

experimental investigation due to their remarkable behaviour of magnetic and electric properties [3-9].

Magnetic properties of ferrites strongly depend on their chemical compositions and additives or substitutions. Small amount of foreign ions in the ferrite can dramatically change the properties of ferrites. Therefore most of the latest ferrites products contain a small amount of additives. Non magnetic Zn is a very promising and interesting candidate among them. The magnetic properties of Zn substituted ferrites have attracted considerable attention because of the importance of these materials for high frequency applications. Again in order to get higher initial permeability, ferrites were often doped with ZnO, which activated sintering mechanism and increased sintered density.

Kulkarni et al. [10], Maria, et al. [11] and Dawoud, et al. [12] studied magnetic ordering in Cu-Zn ferrite and complex permeability of $Zn_xCu_{1-x}Fe_2O_4$ prepared by a standard solid state reaction technique. It was reported that preparation condition of the samples and substitution of Cu had an influence on the magnetic properties of these ferrites. In our laboratory, structural and magnetic properties of Cu substituted Zn based various polycrystalline $Fe_{2.5}Zn_{0.5-x}Cu_xO_4$ were investigated [13]. It was observed that the initial permeability increased up to x=0.3 and beyond this substitution it decreased. In the present research, high spin Mn will be substituted in Zn based $Fe_{2.5}Zn_{0.5-x}Mn_xO_4$ in order to investigate its structural and magnetic properties.

1.2 Objectives of the Present Work

Ferrites are especially convenient for high frequency uses because of their high resistivity. The high frequency response of the complex permeability is therefore very useful in determining the convenient frequency range in which a particular ferrite material can be used.

The mechanism of eddy current losses and damping of domain wall motion can be understood from the relative magnitudes of the real and imaginary parts of the complex permeability. The effect of composition and microstructure on the frequency response is therefore very useful.

The main objectives of the present research are as follows:

- Preparation of various $Fe_{2.5}Zn_{0.5-x}Mn_xO_4$ ferrites (x=0-0.50 in the step of 0.1) samples by solid state reaction technique.
- Study of crystal structure (X-ray diffraction) and hence determination of density and porosity of various samples.
- Investigation of surface morphology (grain size).
- Measurement of initial permeability as a function of frequency (10kHz-120MHz) for all samples having various microstructures (e. g. grain size).

Possible outcome of the research is as follows:

Due to substitution of various cations, spinel lattice may be either compressed or expanded depending on ionic radius and hence there is a change of cation distribution in A- and B-sites of AB_2O_4 spinel structure. The crystal structure is expected to change for the substitution of Mn in $Fe_{2.5}Zn_{0.5-x}Mn_xO_4$. Due to the structural change there may be a variation of magnetic interaction between A-site and B-site cations and hence a change of magnetic properties is expected in $Fe_{2.5}Zn_{0.5-x}Mn_xO_4$. The results of the present research will be helpful for practical applications of these ferrites.

1.3 Summary of the Thesis

The thesis consists of following components:

Chapter 1 deals with the importance of ferrites and objectives of the present work.

Chapter 2 gives a brief overview of the materials, theoretical background as well as crystal structure of the spinel ferrites.

Chapter 3 gives the details of the sample preparation and descriptions of different experimental setup that have been used in this research work.

Chapter 4 is devoted to the results of various investigations of the study and a brief discussion.

The conclusions drawn from the overall experimental results and discussion are presented in Chapter 5.

References:

[1] Peelamedu, R., Grimes, C., Agrawal, D., and Roy, R., "Ultralow dielectric constant Nickel-Zinc ferrites using microwave sintering." J. Mater. Res., Vol-18(10), pp 2292-2296, 2003.

[2] Hossain, A.K.M. Akhter, Mahmud, S.T., Seki, M., Kawai, T. and Tabata, H., "Structural, Electriial transport and magnetic properties of $Ni_{1-x}Zn_xFe_2O_4$",J. Magn. Magn. Mater., Vol-312, pp 210-219, 2007.

[3] Valenzuela, R., "Magnetic Ceramics", Cambridge University Press, Cambridge (1994).

[4] Schiessl, W., Potzel, W., Karzel, H., Steiner, M., and Kalvius, G. M., "Magnetic properties of the $ZnFe_2O_4$ spinel," Phys. Rev. B, Vol-**53**, No. 14, pp 9143-9152, (1996).

[5] Hossain, A.K.M. Akther, Tabata. H. and Kawai, T.,"Magnetoresistive properties of $Zn_{1-x}Co_xFe_2O_4$ ferrites," J. Magn. Magn. Mater., Vol-320, pp 1157-1162, 2008.

[6] Sousa, M. H., Touriaho, F. A., Depayrot, J., Da Silva, G.J. and Lara, M. C. F., New Electric Double-Layered Magnetic Fluids Based on Copper, Nickel and Zinc Ferrite Nanostructures". J. Phys. Chem., Vol-105, pp 1169-1175, 2001.

[7] Drofenik, M.,Znidarsic, M.A. and Zajc, I.,"High resistivity grain boundaries in doped MnZn ferrites for high frequency power supplies".J. Appl. Phys. Vol-82,pp 333-340,1997.

[8] Inaba, H., Abe, T.,Kitano, Y., and Shimomura, J., "Mechanism of core loss and Grain-boundary structure of Niobium-Doped Manganese-Zinc Ferrite." J. Solid State Chem., Vol-121, pp 117-128, 1996.

[9] Verma, A., Goel, T. C., R. G. Mendiratta and P. Kishan, "Magnetic properties of nickel-zinc ferrites prepared by the citrate precursor method," Journal of Magnetism and Magnetic Materials, **208**, 13 (2000).

[10] Kulkarni, R.G., PatiI, V. U., "Magnetic ordering in Cu-Zn ferrite", J. Mater. Sci., Vol-17 pp 843—848. 1982

[11] Maria, K. H., Choudhury, S. and Hakim, M.A., "Complex Permeability and Transport Properties Of Zn Substituted Cu Ferrites," J. Bangl. Acade. Sci., Vol- 34, No. 1, pp 1-8, 2010.

[12] Dawoud, H. A. and Shaat, S. K. K., "Initial Permeability and Dc Conductivity of Cu – Zn Ferrite", The Isla. Unive. J. (Series Of Natural Studies And Engineering), Vol-14, No.1, pp 165-182, 2006.

[13] Rahman, M. A.,"The effect of Cu substitution on the magnetic properties of $Fe_{2.5}Zn_{0.5-x}Cu_xO_4$."M.Phil.Thesis, BUET, 2013.

CHAPTER 2

THEORITICAL BACKGROUND

2.1 General aspects of magnetism

2.1.1 Origin of magnetism

The origin of magnetism lies in the orbital and spin motions of electrons and how the electrons interact with one another. The best way to introduce the different types of magnetism is to describe how materials respond to magnetic fields. It is just that some materials are much more magnetic than others. The main distinction is that in some materials there is no collective interaction of atomic magnetic moments, whereas in other materials there is a very strong interaction between atomic moments. The magnetic moment of an electron in orbit is given by

$$\mu = \pi r^2 (ev/2\pi r) = evr/2 \quad \ldots \quad \ldots \quad \ldots \quad \ldots \quad \ldots \quad \ldots \quad (2.1)$$

Where r is the radius of orbit, e - charge of an electron and v is the velocity of an electron.

The angular momentum of an electron must be an integral multiple of Planck's const.

$$mvr = nh/2\pi \quad \ldots \quad \ldots \quad \ldots \quad \ldots \quad \ldots \quad \ldots \quad \ldots \quad (2.2)$$

Where m is the mass of an electron and h is the Planck's const.

If the electron revolves in the first orbit then n=1

Therefore orbital magnetic moment of an electron is given by from (2.1) and (2.2)

$$\mu = eh/4\pi m \quad \ldots \quad \ldots \quad \ldots \quad \ldots \quad \ldots \quad \ldots \quad \ldots \quad (2.3)$$

This is known as Bohr magnetron, the smallest possible orbital magnetic moment.

A simple electromagnet can be produced by wrapping copper wire into the form of a coil and

connecting the wire to a battery. A magnetic field is created in the coil but it remains there only while electricity flows through the wire. The field created by the magnet is associated with the motions and interactions of its electrons, the minute charged particles which orbit the nucleus of each atom. Electricity is the movement of electrons, whether in a wire or in an atom, so each atom represents a tiny permanent magnet in its own right. The circulating electron produces its -own orbital magnetic moment, measured in Bohr magnetrons (μ_B), and there is also a spin magnetic moment associated with it due to the electron itself spinning, like the earth, on its own axis (illustrated in Figure 2.1). In most materials there is resultant magnetic moment, due to the electrons being grouped in pairs causing the magnetic moment to be cancelled by its neighbor.

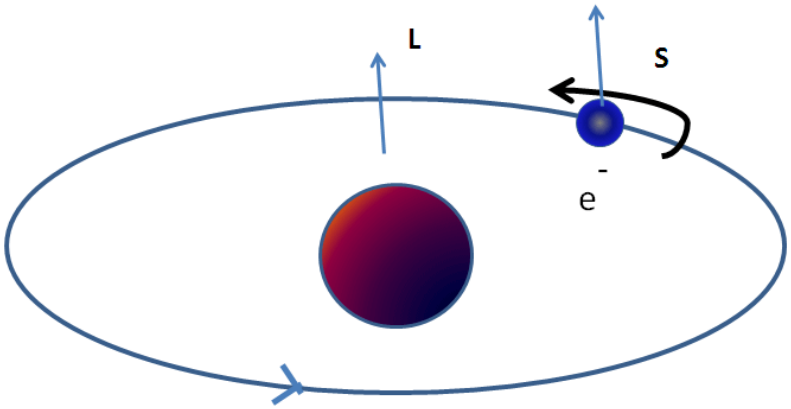

Figure 2.1. A spin magnetic moment associated with it due to the electron itself spinning like the earth on its own axis.

In certain magnetic materials the magnetic moments of a large proportion of the electrons align, producing a unified magnetic field. The field produced in the material (or by an electromagnet) has a direction of flow and any magnet will experience a force trying to align it with an externally applied field, the smallest possible magnetic moment due to spin of the electron is $\mu = eh/4\pi m$. According to quantum theory the spin of electrons has only two possibilities +1/2 or -1/2. Similar to eqn (2.3) we can write in the form

$$\mu = (e/2m)\, S \qquad \ldots \quad \ldots \quad \ldots \quad \ldots \quad \ldots \quad \ldots \quad \ldots \qquad (2.4)$$

Where S is the spin quantum number here given by (1/2).(h/2π)

In short,

$$\mu = g\,(e/2m).S \quad \ldots \quad \ldots \quad \ldots \quad \ldots \quad \ldots \quad \ldots \quad \ldots \quad (2.5)$$

Here g is the term known as g- factor. When g=2, the spin contribution arises and when g=1 the orbital contribution arises. The mass of the nucleus is so large that the magnetic moment contribution can be neglected compared to the electronic magnetic moment. The gryomagnetic ratio is proportional to the g-factor and 'g' arises due to the precession of the electrons similar to the precession of a top in a gravitational force. The value of g tells us whether the origin of magnetic moment is spin or orbital motion of electrons.

2.1.2 Magnetic moment of atoms

The strength of a magnetic dipole, called the magnetic dipole moment, may be thought of as a measure of a dipole's ability to turn itself into alignment with a given external magnetic field. In a uniform magnetic field, the magnitude of the dipole moment is proportional to the maximum amount of torque on the dipole, which occurs when the dipole is at right angles to the magnetic field [1].

The magnetic moment or magnetic dipole moment is a measure of the strength of a magnetic source. In the simplest case of a current loop, the magnetic moment is defined as:

$$\mu_m = I \int da \quad \ldots \quad \ldots \quad \ldots \quad \ldots \quad \ldots \quad \ldots \quad \ldots \quad (2.6)$$

Where a is the vector area of the current loop, and the current, I is constant. By convention, the direction of the vector area is given by the right hand rule (moving one's right hand in the current direction around the loop, when the palm of the hand is 'touching' the loop's surface, and the straight thumb indicate the direction).

In the more complicated case of a spinning charged solid, the magnetic moment can be found by the following equation:

$$\vec{\mu}_m = \frac{1}{2}\int \vec{r} \times \vec{J} d\tau \ldots \quad \ldots \quad \ldots \quad \ldots \quad \ldots \quad \ldots \quad \ldots \quad (2.7)$$

where, $d\tau = r^2 \sin\theta \, dr \, d\theta \, d\varphi$, J is the current density.

Magnetic moment can be explained by a bar magnet which has magnetic poles of equal magnitude but opposite polarity. Each pole is the source of magnetic force which weakens with distance. Since magnetic poles come in pairs, their forces interfere with each other because while one pole pulls, the other repels. This interference is greatest when the poles are close to each other i.e. when the bar magnet is short. The magnetic force produced by a bar magnet, at a given point in space, therefore depends on two factors: on both the strength P of its poles and on the distance d separating them. The force is proportional to the product, $\mu = PR$, where, μ describes the 'magnetic moment' or 'dipole moment' of the magnet along a distance R and its direction as the angle between R and the axis of the bar magnet. Magnetism can be created by electric current in loops and coils so any current circulating in a planar loop produces a magnetic moment whose magnitude is equal to the product of the current and the area of the loop. When any charged particle is rotating, it behaves like a current loop with a magnetic moment.

The equation for magnetic moment in the current-carrying loop, carrying current I and of area vector a for which the magnitude is given by:

$$\vec{\mu}_m = I\vec{a} \qquad \ldots \quad \ldots \quad \ldots \quad \ldots \quad \ldots \quad \ldots \quad \ldots \qquad (2.8)$$

where, $\vec{\mu}_m$ is the magnetic moment, a vector measured in ampere-square meters, or equivalent joules per tesla, I is the current, a scalar measured in amperes, and $\vec{a}$ is the loop area vector, having as x, y and z coordinates the area in square meters of the projection of the loop into the yz-, zx- and xy-planes.

2.1.3 Magnetic moment of electrons

The electron is a negatively charged particle with angular momentum. A rotating electrically charged body in classical electrodynamics causes a magnetic dipole effect creating magnetic poles of equal magnitude but opposite polarity like a bar magnet. For magnetic dipoles, the dipole moment points from the magnetic south to the magnetic north pole. The electron exists in a magnetic field which exerts a torque opposing its alignment creating a potential

energy that depends on its orientation with respect to the field. The magnetic energy of an electron is approximately twice what it should be in classical mechanics. The factor of two multiplying the electron spin angular momentum comes from the fact that it is twice as effective in producing magnetic moment. This factor is called the electronic spin g-factor. The persistent early spectroscopists, such as Alfred Lande, worked out a way to calculate the effect of the various directions of angular momentum. The resulting geometric factor is called the Lande g-factor.

The intrinsic magnetic moment of a particle with charge q, mass m, and spin s, is

$$\vec{\mu}_m = g\frac{q}{2m}\vec{s} \quad \ldots \quad \ldots \quad \ldots \quad \ldots \quad \ldots \quad \ldots \quad (2.9)$$

Where, the dimensionless quantity g is called the g-factor.

The g-factor is an essential value related to the magnetic moment of the subatomic particles and corrects for the precession of the angular momentum. One of the triumphs of the theory of quantum electrodynamics is its accurate prediction of the electron g-factor, which has been experimentally determined to have the value 2.002319. The value of 2 arises from the Dirac equation, a fundamental equation connecting the electron's spin with its electromagnetic properties, and the correction of 0.002319, called the anomalous magnetic dipole moment of the electron, arises from the electron's interaction with virtual photons in quantum electrodynamics. Reduction of the Dirac equation for an electron in a magnetic field to its non-relativistic limit yields the Schrödinger equation with a correction term which takes account of the interaction of the electron's intrinsic magnetic moment with the magnetic field giving the correct energy [2].

The total spin magnetic moment of the electron is

$$\vec{\mu}_s = -g_s\mu_B(\vec{s}/\hbar) \ldots \quad \ldots \quad \ldots \quad \ldots \quad \ldots \quad \ldots \quad \ldots \quad (2.10)$$

Where $g_s = 2$ in Dirac mechanics, but is slightly larger due to Quantum Electrodynamics

effects, μ_B is the Bohr magnetron and s is the electron spin. The z component of the electron magnetic moment is

$$\vec{\mu}_Z = -g_s \mu_B m_s \ldots \quad \ldots \quad \ldots \quad \ldots \quad \ldots \quad \ldots \quad \ldots \quad (2.11)$$

Where, m_s is the spin quantum number.

The total magnetic dipole moment due to orbital angular momentum is given by

$$\vec{\mu}_s = -\frac{e}{2m_e} L = -\mu_B \sqrt{l(l+1)} \ldots \quad \ldots \quad \ldots \quad (2.12)$$

Where, μ_B is the Bohr magnetron.

The z-component of the orbital magnetic dipole moment for an electron with a magnetic quantum number m_l is given by

$$\vec{\mu}_Z = -\mu_B m_l \quad \ldots \quad \ldots \quad \ldots \quad \ldots \quad \ldots \quad (2.13)$$

2.1.4 Magnetic Behavior

The magnetic properties of a matter are fundamentally the result of the electrons of the atom, which have a magnetic moment by means of the electron motion. There are two types of electronic motion, spin and orbital, and each has a magnetic moment associated with it. Since the response of a material to a magnetic field (H) is characteristic of the magnetic induction or the flux density (B) and the effect that a material has upon the magnetic induction in a magnetic field is represented by the magnetization (M). Thus a universal equation can be established, relating these three magnetic quantities, by

$$B = \mu_0 (H+M) \ldots \quad \ldots \ldots \quad \ldots \quad \ldots \quad (2.14)$$

$$B = \mu H \quad \ldots \ldots \quad \ldots \quad \ldots \quad (2.15)$$

Where, μ_0 is a universal constant of permeability in a free space and μ is the permeability of a material. In equation (2.14), one can see that $\mu_0 H$ is the magnetic induction generated by the field alone and $\mu_0 M$ is the additional magnetic induction contributed by a material. The magnetic susceptibility (χ) is defined as the ratio of magnetization to magnetic field

$$\chi = \frac{M}{H} \quad \ldots \quad \ldots \quad \ldots \quad \ldots \quad \ldots \quad \ldots \quad \ldots \quad (2.16)$$

The permeability and susceptibility of a material is correlated with respect to each other by

$$\mu=\mu_0(1+\chi) \quad \ldots \quad \ldots \quad \ldots \quad \ldots \quad \ldots \quad \ldots \quad \ldots \quad (2.17)$$

The magnetic behavior of materials can be classified into the following five major groups:

1. **Diamagnetism**
2. **Paramagnetism**
3. **Ferromagnetism**
4. **Antiferromagnetism**
5. **Ferrimagnetism**

Materials in the first two groups are those that exhibit no collective magnetic interactions and are not magnetically ordered. Materials in the last three groups exhibit long-range magnetic order below a certain critical temperature [1,2]. Ferromagnetic and ferrimagnetic materials are usually what we consider as being magnetic (i.e., behaving like iron). The remaining three are so weakly magnetic that they are usually thought of as "nonmagnetic". The varieties of magnetic orderings are schematically presented in Fig. 2.2.

A brief description of the above mentioned classes of magnetic materials are described below:

1. Diamagnetism

Diamagnetism is a fundamental property of all matter, although it is usually very weak. It is due to the non-cooperative behavior of orbiting electrons when exposed to an applied magnetic field. Diamagnetic substances are composed of atoms which have no net magnetic moments (i.e., all the orbital shells are filled and there are no unpaired electrons). However, when exposed to a field, a negative magnetization is produced and thus the susceptibility is negative. It obeys Lenz's law. The other characteristic behavior of diamagnetic materials is that the susceptibility is temperature independent.The typical values of susceptibility on the order of 10^{-5} to 10^{-6}. Most of the materials are diamagnetic, including Cu, B, S, N_2 and most

organic compounds.

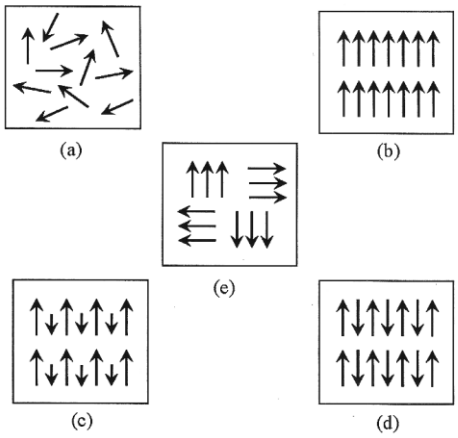

Figure2.2. Varieties of magnetic orderings (a) paramagnetic, (b) ferromagnetic, (c) ferrimagnetic, (d) antiferromagnetic and (e) superparamagnetic.

2. Paramagnetism

Paramagnetic materials possess a permanent dipole moment due to incomplete cancellation of electron spin and/or orbital magnetic moments (unpaired electrons). In the absence of an applied magnetic field the dipole moments are randomly oriented; therefore the material has no net macroscopic magnetization. When a field is applied these moments tend to align by rotation towards the direction of the applied field and the material acquires a net magnetization [4]. The magnetic moment can be oriented along an applied field to give rise to a positive susceptibility and the values of susceptibility are very small with the order of 10^{-5} to 10^{-3}. O_2, NO, Mn and Cr are just a few examples of the paramagnetic materials. The susceptibility of a paramagnetic material is inversely dependent on temperature, which is known as Curie law (Figure 2.3a)

$$\chi = \frac{C}{T} \ldots \quad \ldots \quad \ldots \quad \ldots \quad \ldots \qquad (2.18)$$

Where C is the Curie constant.

3. Ferromagnetism

Ferromagnetic material differs from diamagnetic and paramagnetic materials in many different ways. In a ferromagnetic material, the exchange coupling between neighboring moments leads the moments to align parallel with each other. In ferromagnetic materials, this permanent magnetic moment is the result of the cooperative interaction of large numbers of atomic spins in what are called domains regions where all spins are aligned in the same direction. The exchange force is a quantum mechanical phenomenon due to the relative orientation of the spins of two electrons.

Therefore, the ferromagnetic materials generally can acquire a large magnetization even in absence of a magnetic field, since all magnetic moments are easily aligned together. The susceptibility of a ferromagnetic material does not follow the Curie law, but displayed a modified behavior defined by Curie-Weiss law (Figure 2.3b).

$$\chi = \frac{C}{T - \theta} \quad \ldots \quad \ldots \quad \ldots \quad \ldots \quad \ldots \quad \ldots \quad \ldots \quad (2.19)$$

C is a constant and θ is called Weiss constant. For ferromagnetic materials, the Weiss - constant is almost identical to the Curie temperature (Tc). At temperature below Tc, the magnetic moments are ordered whereas above Tc, material losses magnetic ordering and show paramagnetic character. The elements Fe, Ni, and Co and many of their alloys are typical ferromagnetic materials.

Two distinct characteristics of ferromagnetic materials are:

- Spontaneous magnetization and
- The existence of magnetic ordering temperature (Curie temperature)

The spontaneous magnetization is the net magnetization that exists inside a uniformly magnetized microscopic volume in the absence of a field. The magnitude of this magnetization, 0K, is dependent on the spin magnetic moments of electrons. The saturation magnetization is the maximum induced magnetic moment that can be obtained in a magnetic

field (Hsat); beyond this field no further increase in magnetization occurs. Saturation magnetization is an intrinsic property, independent of particle size but dependent on temperature.

Even though electronic exchange forces in ferromagnets are very large, thermal energy eventually overcomes the exchange and produces a randomizing effect. This occurs at a particular temperature called the Curie temperature (Tc). Blow the Curie temperature, the ferromagnet is ordered and above it, disordered. The saturation magnetization goes to zero at the Curie temperature. The Curie temperature is also an intrinsic property.

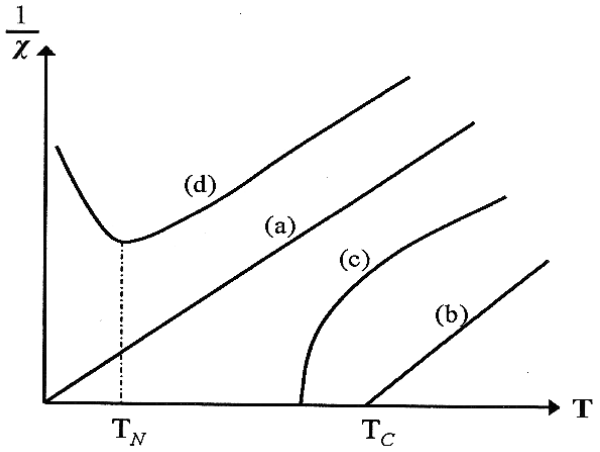

Figure2.3. The inverse susceptibility varies with temperature T for (a) paramagnetic, (b) ferromagnetic, (c) ferrimagnetic, (d) antiferromagnetic materials. T_N and T_c are Néel temperature and Curie temperature, respectively.

4. Antiferromagnetism

Antiferromagnetic material aligns the magnetic moments in a way that all moments are anti-parallel to each other, the net moment is zero. The anti-ferromagnetic susceptibility is followed the Curie-Weiss law with a negative θ as in equation (2.14). The inverse susceptibility as a function of temperature is shown in Fig. 2.3(d). Common examples of materials with antiferromagnetic ordering include MnO, FeO, CoO and NiO.

5. Ferrimagnetism

Ferrimagnetic material has the same anti-parallel alignment of magnetic moments as an

antiferromagnetic material does. However, the magnitude of magnetic moment in one direction differs from that of the opposite direction. As a result, a net magnetic moment remains in the absence of external magnetic field. The behavior of susceptibility of a ferrimagnetic material also obeys Curie-Weiss law and has a negative θ as well in Fig. 2.3(c). In ionic compounds, such as oxides, more complex forms of magnetic ordering can occur as a result of the crystal structure. The magnetic structure is composed of two magnetic sub lattices (called A and B) separated by oxygen. The exchange interactions are mediated by the oxygen anions. When this happens, the interactions are called indirect or super exchange interactions. The strongest super exchange interactions result in an antiparallel alignment of spins between the A and B sub lattice. In ferrimagnets, the magnetic moments of the A and B sub lattices are not equal and result in a net magnetic moment. Ferrimagnetisrn is therefore similar to ferromagnetism. It exhibits all the hallmarks of ferromagnetic behavior like spontaneous magnetization, Curie temperature, hysteresis, and remanence. However, ferro- and ferrimagnets have very different magnetic ordering.

2.1.5 Hysteresis Loop

In addition to the Curie temperature and saturation magnetization, ferromagnets and ferrimagnets can retain a memory of an applied field once it is removed. This behavior is called hystresis and a plot of the variation of magnetization with magnetic field is called a hysteresis loop.

Another hysteresis property is the coercivity of remanence (H_r) as in Fig. 2.4. This is the reverse field which, when applied and then removed, reduces the saturation remanence to zero is always larger than the coercive force. The initial susceptibility (χ_0) is the magnetization in low fields, on the order of the earth's field (50-100 μT). The various hysteresis parameters are not solely intrinsic properties but are dependent on grain size, domain state, stresses, and temperature. Because hysteresis parameters are dependent on

grain size, they are useful for magnetic grain sizing of natural samples.

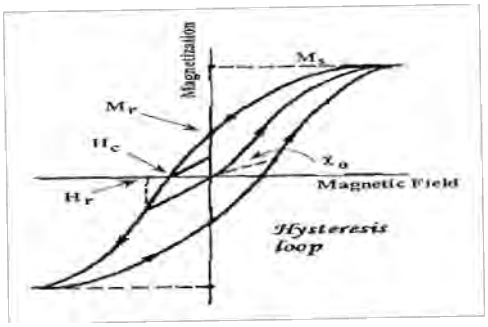

Figure2.4. Hysteresis loop

2.1.6 Magnetic Domains

In 1907 Weiss proposed that a magnetic material consists of physically distinct regions called domains and each of which was magnetically saturated in different directions (the magnetic moments are oriented in a fixed direction) as shown schematically in Fig. 2.5. Even each domain is fully magnetized but the material as a whole may have zero magnetization. The external applied field aligns the domains, so there is net moment. At low fields this alignment occurs through the growth of some domains at the cost of less favorably oriented ones and the intensity of the magnetization increases rapidly. Growth of domains stops as the saturation region is approached and rotation of unfavorably aligned domain occurs. Domain rotation requires more energy than domain growth. In a ferromagnetic domain, there is parallel alignment of the atomic moments. In a ferrite domain, the net moments of the anti ferromagnetic interactions are spontaneously oriented parallel to each other. Domains typically contain from 10^{12} to 10^{15} atoms and are separated by domain boundaries or walls called Bloch walls. The formation of domains allows a ferro or ferri-material to minimize its total magnetic energy.

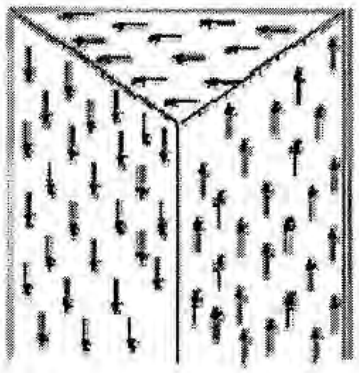

Figure2.5. Illustration of domains in ferromagnetic materials

The magnetic energy is composed of several types of energy [5, 6]:

i) Magnetostatic or demagnetization energy: The magnetized material behaves like a magnet, with a surrounding magnetic field. This field acts to magnetize the material in the direction opposite from its own magnetization, causing a magneto static energy which depends on the shape of the material. This magneto static energy can be reduced by reducing the net external field through the formation of domains inside the material.

ii) Magneto crystalline anisotropy energy: In some materials the domain magnetization tends to alien in a particular crystal direction (the so-called easy axis). The material is easiest to magnetize to saturation or demagnetize from saturation if the field is applied along an easy axis. The energy difference between aligning the domain in the easy and another direction (hard direction) is called magneto crystalline anisotropy energy. Anisotropy energy is the energy needed to rotate the moment from the easy direction to a hard direction. For materials with cubic crystalline structure (such as ferrites), the energy is expressed in terms of anisotropy constants and the direction to which the magnetization rotates.

$E_k=K_1\sin^2\theta+K_2\sin^4\theta$ …. (Hexagonal structure)

$E_k=K_1(\alpha_1^2\,\alpha_2^2+\alpha_2^2\,\alpha_3^{2+}\,\alpha_3^2\,\alpha_1^2)+K_2(\alpha_1^2\alpha_2^2\alpha_3^2+\ldots\ldots$ (Cubic Structure)

where, K is the anisotropy constant, θ is the angle between the easy axis and the direction of magnetization, and α's are the direction cosines, which are the ratios of the individual components of

the magnetization projected on each axis divided by the magnitude of the magnetization. A crystal is higher in anisotropy energy when the magnetization points in the hard direction rather than along the easy direction. The formation of domains permits the magnetization to point along the easy axis, resulting in a decrease in the net anisotropy energy.

c) Magnetostrictive energy: In a magnetic field, the material may change its dimensions on the order of several parts per million. This change in dimension results in what is called magnetostrictive energy, which is lowered by a reduction in the size of the domains, requiring the formation of more domains.

d) Domain wall energy: This is energy resulting from the increase or decrease in the width of the walls due to the growth/shrinkage of domains.

The magnetization in a domain changes by two mechanisms: rotation of the magnetic dipoles toward the direction of the applied field and change in the domain volume. In the first case, a certain amount of anisotropy energy is needed to rotate the magnetization in a crystal from the easy to another axis. In the second mechanism, the volume of the domain changes, changing its contribution to the bulk magnetization, while the magnetization direction is unchanged. The change in the magnetization intensity of a domain depends on how close its direction is to the direction of the applied field. If the magnetization direction is close, the intensity in the domain increases, whereas if it is far, the intensity decreases.

The domain volume changes due to motion of the domain wall. This movement is originated by a torque that rotates the moments of the domain in line with the field, moving the center of the wall toward the domain opposed to the field. Consequently, the volume of the domains whose direction is favorable is increased whereas the domains with unfavorable direction decrease in volume [5]. In order to explain the fact that ferromagnetic materials with spontaneous magnetization could exist in the demagnetized state Weiss proposed the concept of magnetic domains. The magnetization within the domain is saturated and will always lie in the easy direction of magnetization when there is no externally applied field. The direction of the domain alignment across a large volume of material is more or less random and hence the

magnetization of a specimen can be zero.

Magnetic domains exist in order to reduce the energy of the system. A uniformly magnetized specimen as shown in Fig. 2.6 (a) has a large magneto static energy associated with it. This is the result of the presence of magnetic free poles at the surface of the specimen generating a demagnetizing field, H_d. From the convention adopted for the definition of the magnetic moment for a magnetic dipole the magnetization within the specimen points from the South Pole to the North Pole, while the direction of the magnetic field points from north to south. Therefore, the demagnetizing field is in opposition to the magnetization of the specimen. The magnitude of H_d is dependent on the geometry and magnetization of the specimen. In general if the sample has a high length to diameter ratio (and is magnetized in the long axis) then the demagnetizing field and the magneto static energy will be low.

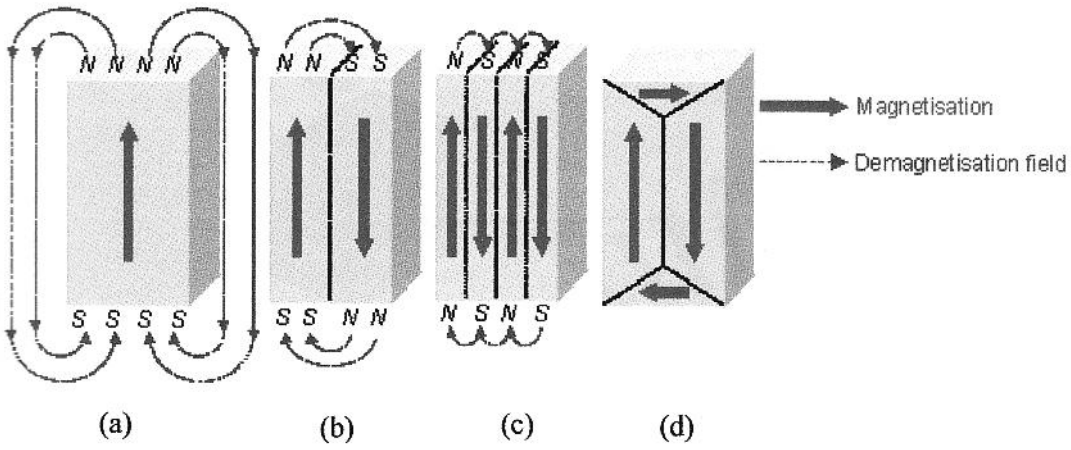

Figure2.6. Schematic illustration of the break up of 'magnetization into domains (a) single domain, (b) two domains, (c) four domains and (d) closure domains.

The break up of the magnetization into two domains as illustrated in figure 2.6(b) reduces the magneto static energy by half. In fact if the magnet breaks down into N domains then the magneto static energy is reduced by a factor of 1/N, hence figure 2.6(c) has a quarter of the magneto static energy of Fig. 2.6(a). Figure 2.6(d) shows a closure domain structure where the, magneto static energy is zero, this is only possible for materials that do not have a strong

uniaxial anisotropy, and the neighboring domains do not have to be at 180˚ to each other.

2.1.7 Structure of domain wall

The introduction of a domain raises the overall energy of the system, therefore the division into domains only continues while the reduction in magneto static energy is greater than the energy required to form the domain wall. The energy associated with a domain wall is proportional to its area. The schematic representation of the domain wall, shown in Fig. 2.7, illustrates that the dipole moments of the atoms within the wall are not pointing in the easy direction of magnetization and hence are in a higher energy state. In addition, the atomic dipoles within the wall are not at 180˚ to each other and so the exchange energy is also raised within the wall. Therefore, the domain wall energy is an intrinsic property of a material depending on the degree of magneto crystalline anisotropy and the strength of the exchange interaction between neighboring atoms. The thickness of the wall will also vary in relation to these parameters, as strong magneto crystalline anisotropy will favor a narrow wall, whereas a strong exchange interaction will favor a wider wall.

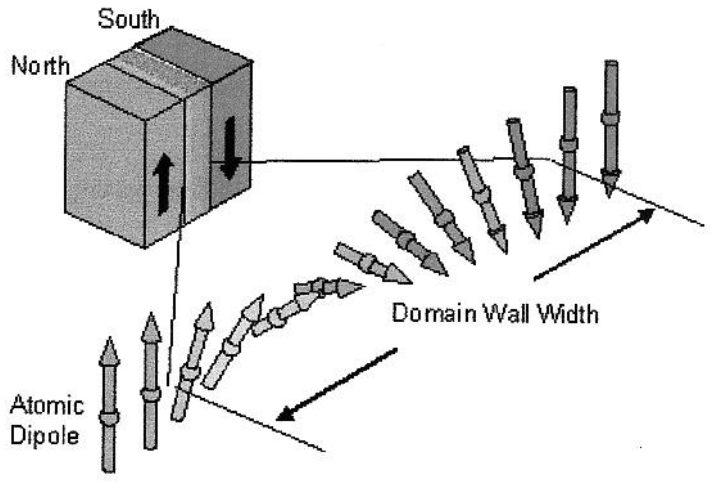

Figure2.7. Schematic representation of a 180° domain wall

A minimum energy can therefore be achieved with a specific number of domains within a specimen. This number of domains will depend on the size and shape of the sample (which will affect the magneto static energy) and the intrinsic magnetic properties of the material (which will affect the magneto static energy and the domain wall energy). Ferromagnetic materials get their magnetic properties not only because their atoms carry a magnetic moment but also because the material is made up of small regions known as magnetic domains. In each domain, all of the atomic dipoles are coupled together in a preferential direction. During solidification, a trillion or more atom moments are aligned parallel so that the magnetic force within the domain is strong in one direction. Ferromagnetic materials are said to be characterized by "spontaneous magnetization" since they obtain saturation magnetization in each of the domains without an external magnetic field being applied. Even though the domains are magnetically saturated, the bulk material may not show any signs of magnetism because the domains develop themselves and are randomly oriented relative to each other.

Ferromagnetic materials become magnetized when the magnetic domains within the material are aligned. This can be done by placing the material in a strong external magnetic field or by passing electrical current through the material. Some or all of the domains can become aligned. The more domains that are aligned, the stronger the magnetic field in the material. When all of the domains are aligned, the material is said to be magnetically saturated. When a material is magnetically saturated, no additional amount of external magnetization force will cause an increase in its internal level of magnetization. In an unmagnetized sample of material, the domains point in random directions, or form closed loops, so that there is no overall magnetization of the sample. Ina magnetized sample, the domains are aligned so that their magnetic effects combine to produce a strong overall magnetism.

2.1.8 Microstructure

A polycrystalline is much more than many tiny crystals bonded together. The interfaces between the crystals, or the grain boundaries which separate and bond the grains, are complex and interactive interfaces. The whole set of a given material's properties (mechanical, chemical and especially electrical and magnetic) depend strongly on the nature of the microstructure.

In the simplest case, the grain boundary is the region, which accommodates the difference in crystallographic orientation between the neighboring grains. For certain simple arrangements, the grain boundary is made of an array of dislocations whose number and spacing depends on the angular deviation between the grains. The ionic nature of ferrites leads to dislocation patterns considerably more complex than in metals, since electrostatic energy accounts for a significant fraction of the total boundary energy [2].

For low-loss ferrite, Ghate [3] states that the grain boundaries influence properties by

1) creating a high resistivity intergranular layer,
2) acting as a sink for impurities which may act as a sintering aid and grain growth modifiers,
3) providing a path for oxygen diffusion, which may modify the oxidation state of cations near the boundaries.

In addition to grain boundaries, ceramic imperfections can impede domain wall motion and thus reduce the magnetic property. Among these are pores, cracks, inclusions, second phases, as well as residual strains. Imperfections also act as energy wells that pin the domain walls and require higher activation energy to detach. Stresses are micro structural imperfections that can result from impurities or processing problems such as too rapid a cool. They affect the domain dynamics and are responsible for a much greater share of the degradation of properties than would expect [3].

Grain growth kinetics depends strongly on the impurity content. A minor dopant can drastically change the nature and concentration of defects in the matrix, affecting grain boundary motion, pore mobility and pore removal [2]. The effect of a given dopant depends on its valence and solubility with respect to host material. If it is not soluble at the sintering temperature, the dopant becomes a second phase which usually segregates to the grain boundary.

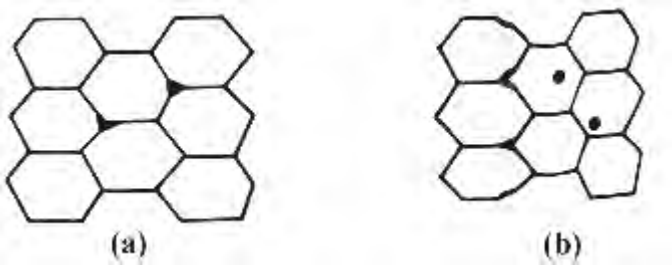

Figure2.8. Porosity character: (a) intergranular, (b) intragranular.

The porosity of ceramic samples results from two sources, intragranular porosity and intergranular porosity, Fig. 2.8. An undesirable effect in ceramic samples is the formation of exaggerated or discontinuous grain growth which is characterized by the excessive growth of some grains at the expense of small, neighboring ones, Fig. 2.9. When this occurs, the large grain has a high defect concentration. Discontinuous growth is believed to result from one or several of the following: powder mixtures with impurities; a very large distribution of initial particle size; sintering at excessively high temperatures; in ferrites containing Zn and /or Mn, a low O_2 partial pressure in the sintering atmosphere. When a very large grain is surrounded by smaller ones, it is called ‘duplex’ microstructure.

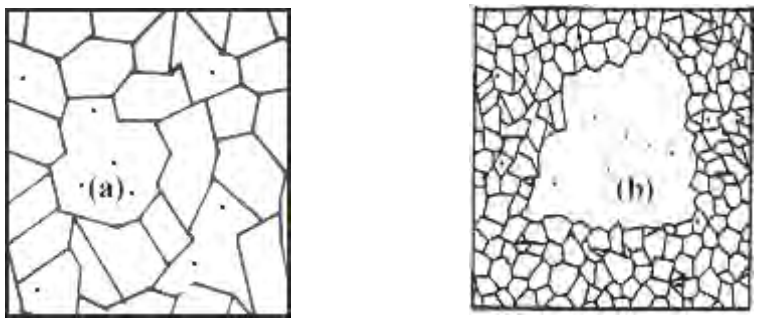

Figure2.9. Grain growth (a) discontinuous, (b) duplex (schematic).

2.1.9 Theories of initial permeability

For high frequency applications, the desirable property of a ferrite is the high initial permeability with low loss. The present goal of the most of the recent ferrite researches is to fulfill this requirement. The initial permeability μ_i is defined as the derivative of induction B with respect to the initial field H in the demagnetization state.

$$\mu_i = \frac{dB}{dH},\ dH \to 0,\ B \to 0 \ldots\ldots \quad \ldots \quad \ldots \quad \ldots \quad (2.20)$$

At microwave frequency, and also in low anisotropic amorphous materials, dB and dH may be in different directions, the permeability thus a tensor character. In the case of amorphous materials containing a large number of randomly oriented magnetic atoms the permeability will be scalar. As we have

$$B = \mu_0(H + M) \ldots \quad \ldots \quad \ldots \quad \ldots \quad \ldots \quad (2.21)$$

and susceptibility,

$$\chi = \frac{dM}{dH} = \frac{d}{dH}\left(\frac{B}{\mu_0} - H\right) = \frac{1}{\mu_0}(\mu - 1) \quad \ldots \quad \ldots \quad \ldots \quad (2.22)$$

The magnetic energy density

$$E = \frac{1}{\mu_0}\int HdB \quad \ldots \quad \ldots \quad \ldots \quad \ldots \quad \ldots \quad (2.23)$$

For time harmonic fields $H = H_0 \sin\omega t$, the dissipation can be described by a phase difference δ between H and B. In the case of permeability, defined as the proportional constant between

the magnetic field induction B and applied intensity H;

$$B = \mu H \ldots \quad \ldots \quad \ldots \quad \ldots \quad \ldots \qquad (2.24)$$

If a magnetic material is subjected to an ac magnetic field as we get,

$$B = B_0 e^{i\omega t} \quad \ldots \quad \ldots \quad \ldots \quad \ldots \quad \ldots \qquad (2.25)$$

Then it is observed that the magnetic flux density B experiences a delay. This is caused due to the presence of various losses and is thus expressed as,

$$B = B_0 e^{i(\omega t - \delta)} \quad \ldots \quad \ldots \quad \ldots \quad \ldots \quad \ldots \qquad (2.26)$$

where δ is the phase angle and marks the delay of B with respect to H, the permeability is then given by

$$\mu = \frac{B}{H} = \frac{B_0 e^{i(\omega t - \delta)}}{H_0 e^{i\omega t}} = \frac{B_0 e^{-i\delta}}{H_0} = \frac{B_0}{H_0}\cos\delta - i\frac{B_0}{H_0}\sin\delta = \mu^{/} - i\mu^{//} \qquad (2.27)$$

Where $\mu^{/} = \frac{B_0}{H_0}\cos\delta$ … … … … … (2.28)

And $\mu^{//} = \frac{B_0}{H_0}\sin\delta$ … … … … … (2.29)

The real part μ' of complex permeability μ as expressed in equation (2.28) represents the component of induction B, which is in phase with H, so it corresponds to the normal permeability. If there are no losses, we should have μ= μ'. The imaginary part μ'' corresponds to that part of B, which is delayed by phase δ from H. The presence of such a component requires a supply of energy to maintain the alternation magnetization, regardless of the origin of delay. It is useful to introduce the loss factor or loss tangent (tanδ). The ratio of μ'' to μ', as is evident from equation gives.

$$\frac{\mu^{//}}{\mu^{/}} = \frac{\frac{B_0}{H_0}\sin\delta}{\frac{B_0}{H_0}\cos\delta} = \tan\delta \ldots \quad \ldots \quad \ldots \quad \ldots \quad \ldots \qquad (2.30)$$

This tanδ is called the loss factor. The Q-factor or quality factor is defined as the reciprocal of

this loss factor i.e.

$$\text{Quality factor} = \frac{1}{\tan\delta} \qquad \ldots \quad \ldots \quad \ldots \quad \ldots \quad \ldots \quad (2.31)$$

And the relative quality factor, $Q = \dfrac{\mu'}{\tan\delta}$

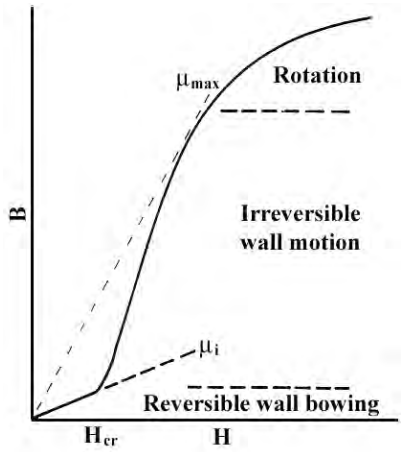

Figure2.10. Schematic magnetization curve showing the important parameter: initial permeability, μ_i (the slope of the curve at low fields) and the main magnetization mechanism in each magnetization range.

The behavior of μ' and μ" versus frequency is called the complex permeability spectrum. The initial permeability of a ferromagnetic substance is the combined effect of the wall permeability and rotational permeability mechanism.

2.1.10 Mechanisms of Permeability

The mechanisms can be explained as follows: A demagnetized magnetic material is divided into number of Weiss domains separated by Bloch walls. In each domain all the magnetic moments are oriented in parallel and the magnetization has its saturation value M_S. In the walls the magnetization direction changes gradually from the direction of magnetization in

one domain to that in the next. The equilibrium positions of the walls result from the interactions with the magnetization in neighboring domains and from the influence of pores; crystal boundaries and chemical in homogeneities which tend to favor certain wall positions.

2.1.11 Wall Permeability

The mechanism of wall permeability arises from the displacement of the domain walls in small fields. Lets us consider a piece of material in the demagnetized state, divided into Weiss domains with equal thickness L by means of 180˚ Bloch walls (as in the Fig. 2.11). The walls are parallel to the YZ plane. The magnetization M_s in the domains is oriented alternately in the +Z or -Z direction. When a field H with a component in the +Z direction is applied, the magnetization in this direction will be favored. A displacement dx of the walls in the direction shown by the dotted lines will decrease the energy density by an amount [47, 48]:

$$\frac{2M_s H_z dx}{L}$$

This can be described as a pressure M_sH_z exerted on each wall. The pressure will be counteracted by restoring forces which for small deviations may assume to be kdx per unit wall surface. The new equilibrium position is then given by

$$d = \frac{M_s H_z dx}{L}$$

From the change in the magnetization

$$\Delta M = \frac{2M_s d}{L},$$

the wall susceptibility χ_w may be calculated. Let H makes the angle θ with Z direction. The magnetization in the θ direction becomes

$(\Delta M)_\theta = \frac{2M_s d}{L}\cos\theta$, And with $H_z = H\cos\theta$ and $d = \frac{2M_s H_z}{K}$

we obtain

$$\chi_w = \frac{(\Delta M)_\theta}{H} = \frac{4M_s^2 \cos^2 \theta}{KL} \quad \ldots \quad \ldots \quad \ldots \quad \ldots \quad \ldots \quad (2.32)$$

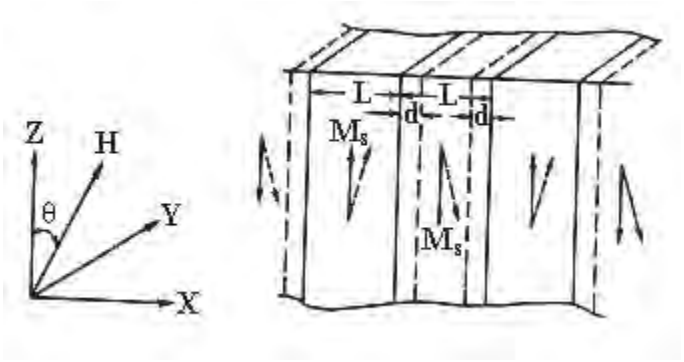

Figure 2.11. Magnetization by wall motion and spin rotation.

2.1.12 Rotational Permeability

The rotational permeability mechanism arises from rotation of the magnetization in each domain. The direction of M can be found by minimizing the magnetic energy E as a function of the orientation. Major contribution to E comes from the crystal anisotropy energy. Other contributions may be due to the stress and shape anisotropy. The stress may influence the magnetic energy via the magnetostriction. The shape anisotropy is caused by the boundaries of the sample as well as by pores, nonmagnetic inclusions and in homogeneities. For small angular deviations, α_x and α_y may be written as

$$\alpha_x = \frac{M_x}{M_s} \quad \text{and} \quad \alpha_y = \frac{M_y}{M_s}$$

For equilibrium z-direction, E may be expressed as [47, 48]

$$E = E_0 + \frac{1}{2}\alpha_x^2 E_{xx} + \frac{1}{2}\alpha_y^2 E_{yy}$$

Where it is assumed that x and y are the principal axes of the energy minimum. Instead of E_{xx} and E_{yy}, the anisotropy field H_x^A and H_y^A are often introduced. Their magnitude is given by

$$H_x^A = \frac{E_{xx}}{2M_s} \text{ and } H_y^A = \frac{E_{yy}}{2M_s},$$

H_x^A and H_y^A represent the stiffness with which the magnetization is bound to the equilibrium direction for deviations in the x and y direction, respectively. The rotational susceptibilities $\chi_{r,x}$ and $\chi_{r,y}$ for fields applied along x and y directions, respectively are

$$\chi_{r,x} = \frac{M_s}{H_x^A} \text{ and } \chi_{r,y} = \frac{M_s}{H_y^A}.$$

For cubic materials it is often found that H_x^A and H_y^A are equal. For $H_x^A = H_y^A = H^A$ and a field H which makes an angle θ with the Z direction (as shown in Fig. 2.16) the rotational susceptibility, $\chi_{r,c}$ in one crystallite becomes

$$\chi_{r,c} = \frac{M_s}{H^A}\sin^2\theta \quad \ldots \quad \ldots \quad \ldots \quad \ldots \quad \ldots \quad (2.33)$$

A polycrystalline material consisting of a large number of randomly oriented grains of different shapes, with each grain divided into domains in a certain way. The rotational susceptibility χ_r of the material has to be obtained as a weighted average of $\chi_{r,c}$ of each crystallite, where the mutual influence of neighboring crystallites has to be taken into account. If the crystal anisotropy dominates other anisotropies, then H^A will be constant throughout the material, so only the factor $\sin^2\theta$ (equation 2.33) has to be averaged. Snoek [9] assuming a linear averaging of $\chi_{r,c}$ and found

$$\chi_r = \frac{2M_s}{3H^A}$$

The total internal susceptibility

$$\chi = \chi_w + \chi_r = \frac{4M_s^2 \cos^2 \theta}{KL} + \frac{2M_s}{3H^A} \qquad (2.34)$$

If the shape and stress anisotropies cannot be neglected, H^A will be larger. Any estimate of χ_r will then be rather uncertain as long as the domain structure, and the pore distribution in the material are not known. A similar estimate of χ_w would require knowledge of the stiffness parameter K and the domain width L. These parameters are influenced by such factors as imperfection, porosity and crystallite shape and distribution which are essentially unknown.

2.2 Soft Magnetic Materials

The wide variety of magnetic materials can be divided into two groups, the magnetically soft and the magnetically hard. Soft magnetic materials are those materials that are easily magnetized and demagnetized. Soft magnetic materials have low magneto crystalline anisotropy resulting in reduced coercivity and high permeability. They typically have intrinsic coercivity less than 1000 Arn^{-1}. They are used primarily to enhance and/or channel the flux produced by an electric current. The main parameter, often used as a figure of merit for soft magnetic materials, is the high relative permeability μ_r (where $\mu_r = B/\mu_0 H$), which is a measure of how readily the material responds to the applied magnetic field. The other main parameters of interest are the coercivity, the saturation magnetization and the electrical conductivity.

The types of applications for soft magnetic materials fall into two main categories: AC and DC. In DC applications the material is magnetized in order to perform an operation and then demagnetized at the conclusion of the operation, e.g. an electromagnet on a crane at a scrap yard still be switched on to attract the scrap steel and then switched off to drop the steel. In AC applications the material will be continuously cycled from being magnetized in one direction to the other, throughout the period of operation, e.g. a power supply transformer. A high permeability will be desirable for each type of application but the significance of the

other properties varies.

For DC applications the main consideration for material's election is most likely to be the permeability. This would be the case, for example, in shielding applications where the flux must be channeled through the material. Where the material is used to generate a magnetic field or to create a force then the saturation magnetization may also be significant. For AC applications the important consideration is how much energy is lost in the system as the material is cycled around its hysteresis loop. The energy loss can originate from three different sources: (1) hysteresis loss, which is related to the area contained within the hysteresis loop; (2) eddy current loss, which is related to the generation of electric currents in the magnetic material and the associated resistive losses and (3) anomalous loss, which is related to the movement of domain walls within the material. Hysteresis losses can be reduced by the reduction of the intrinsic coercivity, with a consequent reduction in the area contained within the hysteresis loop. Eddy current losses can be reduced by decreasing the electrical conductivity of the material and by laminating the material, which has an influence on overall conductivity and is important because of skin effects at higher frequency. Finally, the anomalous losses can be reduced by having a completely homogeneous material, within which there will be no hindrance to the motion of domain walls.

2.2.1 Soft ferrites

At high frequency metallic soft magnetic materials simply cannot be used due to the eddy current losses. Therefore, soft ferrites, which are ceramic insulators, become the most desirable material. These materials are ferrimagnetic with a cubic crystal structure and the general composition $MO.Fe_2O_3$, where M is a transition metal such as nickel, manganese, magnesium or zinc [2]. The magnetically soft ferrites first came into commercial production in 1948.

MnZn ferrite, sold commercially as ferroxcube, can be used at frequencies up to 10 MHz, for example in telephone signal transmitters and receivers and in switch mode power supplies (also referred to as DC-DC converters). For this type of application the driving force to increase frequency is to allow

miniaturization.

Additionally, part of the family of soft ferrites, are the microwave ferrites, e.g. yttrium iron carnet. These ferrites are used in the frequency range from 100 MHz to 500 GHz, for waveguides for electromagnetic radiation and in microwave devices such as phase shifters.

2.2.2 Cubic ferrites with spinel structure

The cubic ferrite has the general formula $MO.Fe_2O_3$ where M is one of the divalent cations of the transition elements such as Mn, Ni, Mg, Zn, Cd, Cu, Co etc. A combination of these ions is also possible and it can be named as solid solution of two ferrites or mixed spinel ferrites. Generally, M represents a combination of ions which has an average valence of two. The trivalent iron ion in $MO.Fe_2O_3$ can partially be replaced by another trivalent ion such as Al^{3+} or Cr^{3+} giving rise to mixed crystals. The structure of ferrite is derived from the $MgAl_2O_4$ determined by Bragg [7]. These ferrites crystallize in the FCC spinel structure. The spinel lattice is composed of a close-packed oxygen arrangement in which 32 oxygen ions form the unit cell (the smallest repeating unit in the crystal network). These anions are packed in a face centered cubic (FCC) arrangement leaving two kinds of spaces between anions: tetrahedral coordinated sites (A), surrounded by four nearest oxygen atoms, and octahedral coordinated sites (B), surrounded by six nearest neighbor oxygen atoms. These are illustrated in Fig. 2.12. In total, there are 64 tetrahedral sites and 32 octahedral sites in the unit cell, of which only 8 tetrahedral sites and 16 octahedral sites are occupied, resulting in a structure that is electrically neutral [2, 5].

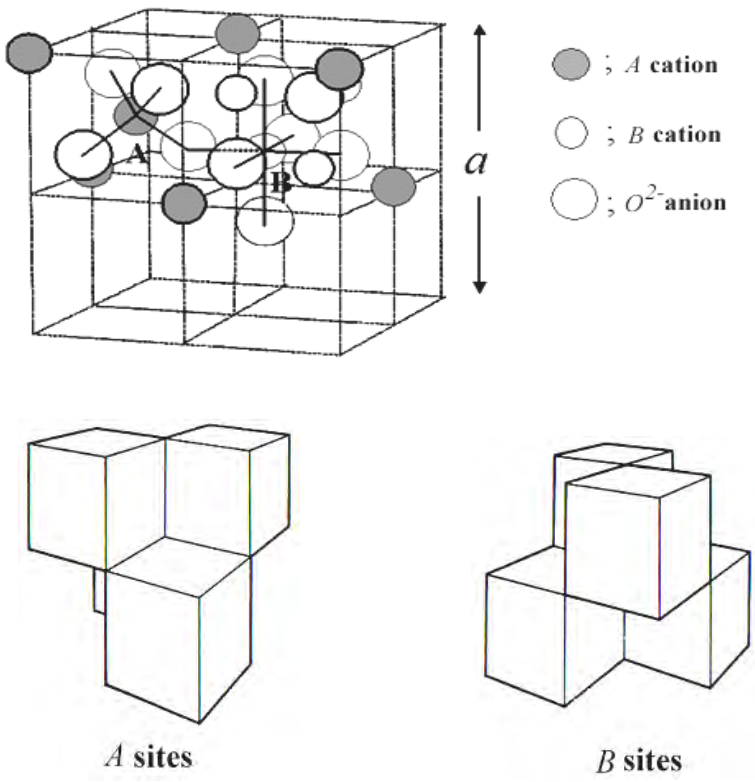

Figure 2.12. Schematic of two subcells of a unit cell of the spinel structure, showing octahedral and tetrahedral sites.

The localization of ions either in the A or B sites depends fundamentally on the ion and lattice sizes. Also it has been observed to depend on the temperature and the orbital preference for specific coordination. In general, divalent ions are larger than trivalent ions. This is because trivalent ion nuclei produce greater electrostatic attraction, hence their electron orbits contract.

The octahedral sites are larger that the tetrahedral sites, thus, the divalent ions are localized in the octahedral sites whereas trivalent ions are in the tetrahedral sites [5].

According to the site occupancy of the metal ions, the spinel ferrites are classified as:

(a) Normal spinel: where the tetrahedral A-sites are occupied by divalent metal ions and trivalent ions occupy B sites. A majority of these ferrites present paramagnetic behavior,

(b) Inverse spinel: where all the divalent ions are present in the octahedral site while trivalent

ions are located on both A and B sites. The spin moments of the trivalent ions in an inverse spine] are canceled (direction of moment on A sites is opposed to B sites) whereas the spin moments of the divalent ions are aligned, resulting in a net magnetic moment [6] and

(c) Mixed spinel: where divalent ions are present both in tetrahedral and octahedral sites.

The cubic ferrite is easily magnetized and demagnetized; it has high permeability and saturation magnetization, low electrical conductivity, and the anisotropy energy is dominated by the anisotropy constant K_1. If K_1, is greater than zero, the easy direction is the cube edge direction (100) whereas if K_1, is less than zero, the body direction is preferred (111). For most ferrites the value of K, is negative, with the exception of cobalt ferrite [5].

2.2.3 Cation distribution in ferrites

The cation distribution in the spinel ferrite $Me^{2+}Fe^{3+}O_4$ can be as follows [5]:

- Normal spinel ferrite : The Me^{2+} cations are in tetrahedral positions, while the two Fe^{3+} cations are in octahedral sites which is represented as $(Me^{2+})_A[Fe^{3+}]_BO_4$
- Inverse spinel ferrite : In this case the Me^{2+} cation and one of the Fe^{3+} cations are in octahedral positions while the second Me^{3+} cation occupies tetrahedral sites. The arrangement is as $(Fe^{3+})_A[Me^{2+}Fe^{3+}]_BO_4$.
- Mixed spinel ferrite : The arrangement of the form $(Me^{2+}_{1-\delta}Fe^{3+}_{1-\delta})[Me^{2+}_{1-x}Fe^{3+}_{1+x}]O_4$ is often referred as mixed spinel, where δ is called the inversion parameter. δ = 0 for completely normal and δ = 1 for completely inverse spinels $0 < \delta < 1$ for mixed spinels.

The factors affecting the cation distribution over A and B sites are as follows [5]

- The size of the cations
- The electronic configurations of the cations
- The electronic energy
- The saturation magnetization of the lattice

Smaller cations (trivalent) prefer to occupy the A-sites. The cations have special preference

for A and B sites and the preference depends on the following factors:

- Ionic radius
- Size of interstices
- Sintering temperature
- Orbital preference for the specific coordination

Zn^{2+}, Cd^{2+}, Ga^{2+}, In^{3+}, Ge^{2+} etc. have strong preference for A-sites while Ni^{2+}, Cr^{3+}, Ti^{4+}, Sn^{4+} etc. have the preference for B-sites. Mg^{2+}, Fe^{3+}, $A1^{3+}$, Mn^{2+}, Cu^{2+}, Co^{2+} are distributed among A and B-sites. Moreover, the electrostatic energy also affects the cation distribution in the spinel lattice.

2.2.4 Magnetic exchange interaction

The exchange energy between the two atoms having spins S_i and S_j can be expressed universally in terms of Heigenburg Hamiltonian [8]

$$H = -\sum J_{ij} S_i S_j \quad \ldots \quad \ldots \quad \ldots \quad \ldots \quad \ldots \quad (2.35)$$

Where, J_{ij} the exchange integral represents the strength of the exchange coupling between the spin angular momentum i and j. It is well known that the favored situation is the one with the lowest energy and there are two ways in which the wave functions can combine for lowering the energy by H. These are:

If J_{ij} is positive, the parallel spin configuration will minimize the system total energy and all spins aligned to each other in the ground state. This is the case leading to ferromagnetic ordering.

If J_{ij} is negative, J_{ij} favors the antiparallel alignment of spins and consequently gives rise to antiferromagnetic ordering.

2.2.5 Super exchange interaction

The magnetic interaction in magnetic oxide (ferrites) cannot be explained on the basis of direct exchange interaction because of the following facts:

- The magnetic ions are located too far apart from each other shielded by the nonmagnetic anion (oxygen). This is because these are not band type semiconductor [10]. The non-magnetic anion is situated in the line joining magnetic cations.
- Super exchange interactions appear, i.e., indirect exchange via anion p-orbital's that may be strong enough to order the magnetic moments.

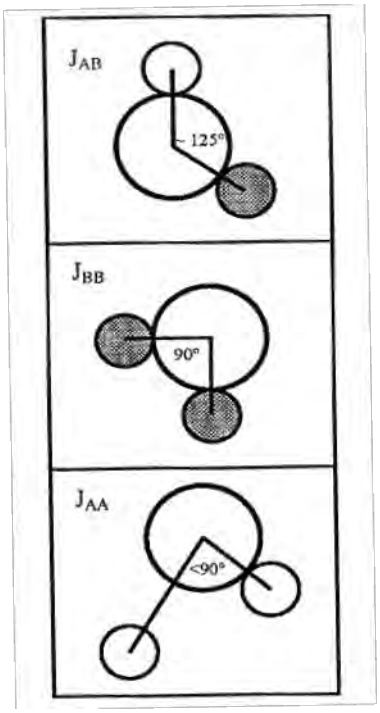

Figure2.13. Three major types of super exchange interactions in spinel ferrites are as follows: J_{AB}, J_{BB} and J_{AA}. The small empty circle is A site, the small solid circle is B site, and the large empty circle is oxygen anion.

Ferrimagnetic oxides are one kind of magnetic systems in which there exist at least two equivalent sub lattices for the magnetic ions. The antiparallel alignment between these sub lattices (ferrimagnetic ordering) may occur provided the inter-sub lattice exchange interactions are anti ferromagnetic (AF) and some requirements concerning the signs and

strengths of the intra-sub lattice interactions are fulfilled. Since usually in ferrimagnetic oxides the magnetic cations are surrounded by bigger oxygen anions (almost excluding the direct overlap between cation orbitals) magnetic interactions occur via indirect super exchange mediated by the p oxygen orbitals. It is well-known that the sign of these super exchange interactions depends both on the electronic structure of the cations and their geometrical arrangement [11]. In most of ferrimagnetic oxides, the crystallographic and electronic structure give rise to antiferromagnetic inter and intra-sub lattice competing interactions. The magnitude of negative exchange energies between two magnetic ions M and M' depends upon the distances from these ions to the oxygen ion O^{2-}, via which the superexchange takes place, and on the angle M-O^2-M' (φ). According to the super exchange theory, the angle φ=l80° gives rise to the greatest exchange energy, and this energy decreases very rapidly as the distance between the ions increases. If A and B are the tetrahedral and octahedral ions respectively in a spinel structure, the A-B interaction is the greatest and A-A exchange interaction is the weakest [8].

2.2.6 Two sub lattices in spinel ferrites

The term 'magnetic sub lattice' is widely used in the study of magnetic structures of the whole spectrum of magnetic materials [12]. In the case of ferromagnetic materials, the 'magnetic sub lattice' is exactly the same as the crystal structure and no problem arises. In the case of antiferromagnetics, the importance of the direction of the magnetic moments is evident and makes clear the existence of two magnetic sub lattices, as for example, in MnO. The difference between the two magnetic sub lattices is the direction of their magnetic moment. However, ferrimagnetic materials are considerably more complex and the application of the molecular field theory to spinels has pointed to the problem of a clear definition of the concept of magnetic sub lattices. In spinel ferrites the metal ions are separated by the oxygen ions and the exchange energy between spins of neighboring metal

ions is found to be negative, that is, antiferromagnetic. This is explained in terms of super exchange interaction of the metal ions via the intermediate oxygen ions [13]. There are a few points to line out about the interaction between two ions in tetrahedral (A) sites:

- The distance between two A ions (~3.5 Å) is very large compared with their ionic radius (0.67 Å for Fe^{3+}),
- The angle A-0^{2-} -A (φ=79°38') is unfavorable for super exchange interaction [8],
- The distance from one A ion to O^{2-} is not the same as the distance from the other A ion to O^{2-} as there is only one A nearest neighbor to an oxygen ion (in figure 2.10, M and M' are A ions, r = 3.3 Å and q = 1.7 Å) [8]. As a result, two nearest A ions are connected via two oxygen ions.

These considerations led us to the conclusion that super exchange interaction between A ions is very unlikely. This conclusion together with the observation that direct exchange is also unlikely in this case [8] support the assumption that $J_{AA} = 0$ in the spinet ferrites. According to Néel's theory, the total magnetization of a ferrite divided into two sub lattices A and B is:

$$M_T(T)=M_B(T)-M_A(T) \quad \ldots \quad (2.36)$$

Where, T is the temperature, $M_B(T)$ and $M_A(T)$ are A and B sub lattice magnetizations. Both $M_B(T)$ and $M_A(T)$ are given in terms of the Brillouin function $B_{si}(x_i)$;

$$M_B(T)= M_B(T= 0)\, B_{sB}(x_s) \quad \ldots \quad (2.37)$$

$$M_A(T)= M_A(T= 0) \quad \ldots \quad (2.38)$$

with

$$\chi_B = \frac{\mu_B g_A S_A}{k_B T} M_B N_{AB} \quad \ldots \quad (2.39)$$

$$\chi_B = \frac{\mu_B g_B S_B}{k_B T} (M_B N_{BB} + M_A N_{AB}) \quad \ldots \quad (2.40)$$

The molecular field coefficients N_{ij}, are related to the exchange constants J_{ij} by the following

expression:

$$J_{ij} = \frac{n_j g_i g_j \mu_B^2}{2 z_{ij}} N_{ij} \quad \ldots \quad \ldots \quad \ldots \quad \ldots \quad \ldots \quad (2.41)$$

with r_{ij} the number of magnetic ions per mole in the jth sub lattice, g the Lande factor, μ_B is the Bohr magneton and z_{ij} the number of nearest neighbors on the j^{th} sub lattice that interact with the i^{th} ion.

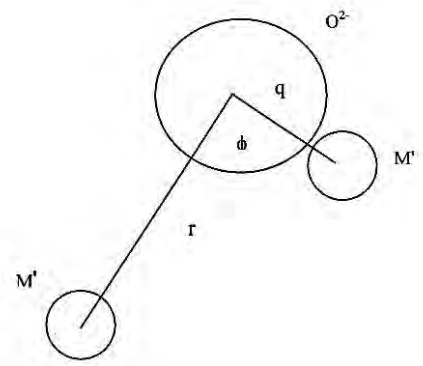

Figure2.14. Schematic representation of ions M and M' and the 0^{2-} ion through which the super exchange is made. R and q are the centre to centre distances from m M and M' respectively to O^{2-} and φ is the angle between them.

According to Néel's theory and using $J_{AA} = 0$, equating the inverse susceptibility $1/\chi = 0$ at $T = T_c$ we obtain for the coefficients of the molecular field theory N_{AB} and N_{BB} of the following expression:

$$N_{BB} = \frac{T_C}{C_B} - \frac{C_A N_{AB}^2}{T_C} \quad \ldots \quad \ldots \quad \ldots \quad \ldots \quad \ldots \quad (2.42)$$

Where, C_A and C_B are the Curie constants for each sub lattice. Equations (2.36) and (2.42) constitute a set of equations with two unknown, N_{AB} and N_{BB}, provided that M_A and M_B are a known function of T.

2.3 Magnetic Structure of Substituted Ferrites

2.3.1 Néel's collinear model of ferrites

Soft ferrites belong to the cubic spinel structure. According to Néel's theory, the magnetic ions are assumed to be distributed among the tetrahedral A and octahedral B-sites of the spinel structure. The magnetic structure of such crystals essentially depends upon the type of magnetic ions residing on the A and B sites and the relative strengths of the inter- (J_{AB}) and intra-sub lattice exchange interactions (J_{AA}, J_{BB}). Negative exchange interactions exist between A–A, A–B and B–B ions. When A–B antiferromagnetic interaction is the dominant one, A and B sub lattices will be magnetized in opposite direction below a transition temperature. When the A–A (or B–B) interaction is dominant, Néel found that the above transition will not take place and he concluded that the substance remains paramagnetic down to the lower temperature. But this conclusion was not correct, as in the presence of strong interactions, some kind of ordering may be expected to occur at low temperature as claimed by Yafet and Kittel [14].

2.3.2 Non-collinear model

In general, all the interactions are negative (antiferromagnetic) with $|J_{AB}| \gg |J_{BB}| \gg |J_{AA}|$. In such situation, collinear or Néel type of ordering is obtained. Yafet and Kittel theoretically considered the stability of the ground state of magnetic ordering, taking all the three exchange interactions into account and concluded that beyond a certain value of J_{BB}/J_{AB}, the stable structure was a non-collinear triangular configuration of moment wherein the B-site moments are oppositely canted relative to the A-site moments. Later on Leyons et. al. [15] extending these theoretical considerations showed that for normal spinel the lowest energy correspond to conical spinel structure for the value of $3J_{BB}S_B/2J_{AB}S_A$ greater than unity. Initially one can understand why the collinear Néel structure gets perturbed when J_{BB}/J_{AB} increases. Since all these three exchange interactions are negative (favoring anti

ferromagnetic alignment of moments) the inter- and intra-sub lattice exchange interaction compete with each other in aligning the moment direction in the sub lattice. This is one of the origins of topological frustration in the spinel lattice. By selective magnetic directions of say A -sub lattice one can effectively decrease the influence of J_{AB} vis-a-vis J_{BB} and thus perturb the Néel ordering. The first neutron diffraction study of such system i.e., $Zn_xNi_{l-x}Fe_2O_4$ was done at Trombay [16] and it was shown to have the Y-K type of magnetic ordering followed by Néel ordering before passing on to the paramagnetic phase [17].

It was found that ferrites which have been substituted sufficiently with non-magnetic atoms showed significant departure from Néel collinear model. These theoretical models have been used to explain these departures:

- A paramagnetic centre model in which a number of magnetic nearest neighbors determines whether a magnetic ion remains paramagnetic or contributes to the magnetization
- A uniform spin canting relative to the average magnetization and
- A localized canting where the canting angle of a magnetic ion spin depends on the local magnetic environment.

The discrepancy in the Néel's theory was resolved by Yafet and Kittel [14] and they formulated the non-collinear model of ferrimagnetism. They concluded that the ground state at 0K might have one of the following configurations:

- Have an antiparallel arrangement of the spins on two sites
- Consists of triangular arrangements of the spins on the sub lattices
- An antiferromagnetic in each of the sites separately.

2.3.3 Re-entrant spin glass behavior

When a piece of material is cooled down its constituent atoms or molecules become more and more ordered. Some systems, however, seem to become disordered again when the temperature continues

to decrease. Such a behavior is commonly referred to as reentrant transition, because the system reenters a disordered phase when lowering the temperature. When such a system is cooled from a high temperature, it first exhibits a transition from paramagnetic (PM) to a ferromagnetic (FM) phase. Upon further lowering the temperature, the spins are progressively frozen below a freezing temperature T_f. The low temperature spin frozen state is called a reentrant spin glass (SG) or mixed state, in which ferromagnetic order is argued to coexist with spin-glass order [18,19]. If the cooling proceeds, a transition to a RSG phase occurs. For comparison, in a diluted spin glass, spins freeze directly from a paramagnetic state. This contradictory behavior was first seen in binary liquid mixtures [20]. After that it has been observed and investigated in a variety of different physical systems, e.g., magnets [21], superconductors [22], and liquid crystals [23]. When there is a majority of the ferromagnetic interactions and a minority of the anti ferromagnetic interactions to create substantial spin frustration effect, the situation may drastically change. Such random spin systems are called a reentrant ferrornagnet. The system exhibits two phase transitions at T_{RSG} and T, ($T > T_{RSG}$)2 the reentrant spin glass (RSG) phase below T_{RSG} and the ferromagnetic (FM) phase between T_{RSG} and T_c In a reentrant spin glass, the fact that the FM state occurs at higher temperatures than the SG state suggests larger entropy for the FM state than for the SG state [24].

The usual mechanism for reentrance is the existence of interactions that are capable of lowering the entropy in some huddler way while at the same time reducing the energy of the system. Reentrant behavior in random ferromagnets has been observed in many systems. Neutron scattering on $Eu_xSr_{1-x}S$ [25] has indicated that the long range order disappears at temperatures below the reentrant irreversibility's. This suggests a transition to a low temperature reentrant phase. This phase should be characterized by lack of long range ferromagnetic order and a diverging spin glass correlation length.

2.3.4 Spin glass behavior

The introduction of randomness and disorder may dramatically change the physical properties of a

magnetic material. Spin glasses (SG's) are disordered magnetic systems with competing ferromagnetic and antiferromagnetic interactions. The combination of randomness with these competing interactions causes "spin frustration". Below a SG freezing temperature T_g, a highly irreversible met stable frozen state occurs without any usual long-range spatial spin order [24, 26, 27]. Spin glass was first observed by Canella and Mydosh [24] in 1972 by observing a peak in the ac susceptibility, and predicted the existence of a phase transition to a low temperature spin glass phase.

A spin glass is a magnetic material in which the exchange interaction, J_{ij}, between atomic Spins S_j, is a random variable. A positive sign favors an antiparallel alignment of a spin pair, while a negative sign favors an antiparallel alignment. A consequence of such random exchange Interactions between the moments is a ft˙ustrated system, i.e., for a representative spin there is no obvious direction relative to its neighbors to align

$$H = -\sum J_{ij} S_i S_j \quad \ldots \quad \ldots \quad \ldots \quad \ldots \quad \ldots \quad (2.43)$$

If $J_{jj} = J > 0$, parallel orientation of the spins is favored and at low temperatures all spins will be aligned ferromagnetically. Such a system has two phases. At temperature high compared to J, the entropy dominates the energy and the spins fluctuate almost independently. In this paramagnetic phase, the expectation value of a spin is $<S_i>$ (< > denotes the time average over long times). At temperature low compared to J, the energy dominates the entropy and the spins of the system are predominantly aligned in the same direction, i.e. $<S_i> \neq 0$. This phase is called ferromagnetic. A transition between the two phases occurs at a finite critical temperature, T_c. An order parameter is associated to the transition, with the property that it is zero above and non-zero below the phase transition. For $J_{ij} = J < 0$, the low temperature phase is antiferromagnetic with the spins aligned anti-parallel. If $J_{ij} = 0$, the Hamiltonian describes a system being paramagnetic at all temperatures.

If positive and negative interactions are mixed the situation becomes more complicated. Then there is a possibility that not all of the exchange interactions can be satisfied simultaneously. This property is called frustration [28]. An example of frustration is given in Fig. 2.15. Here

the frustration arises due to bond disorder, but it may also arise from randomness in spin positions (site disorder). If only a small fraction of the interactions are of opposite sign the ground state will still be ferromagnetic or antiferromagnetic, with only a small fraction of the spins misaligned. If the density of positive and negative interactions is comparable, the system will be strongly frustrated. Such systems are called spin glasses (SG).

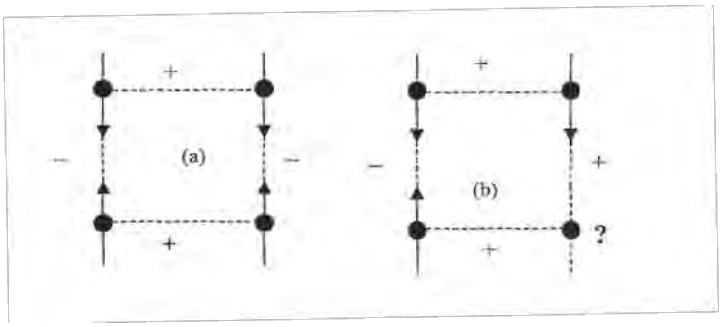

Figure2.15. Examples of (a) an unfrustrated and (b) a frustrated spin configuration.

Edwards and Anderson [29] proposed the following Hamiltonian to describe a spin-glass

$$H = -\sum_{ij} J_{ij} S_i S_j + H \sum_i S_i \quad \ldots \quad \ldots \quad \ldots \quad \ldots \quad \ldots \quad (2.44)$$

Where, H is an applied magnetic field. The interactions are random and symmetrically disordered around zero, i.e. [Jij] =0 and [Jij2] =j2. The order parameter is not the same as in the other models since the magnetization is zero without an external field. Edwards and Anderson [29] proposed the order parameter q = [$<S_i>$].

Ferrites represent the most important and interesting class of magnetic oxides where magnetic disorder and exchange frustration, introduced by size mismatch of cations and competition between super exchange interactions amongst A and B site moments, gives rise to various king of magnetic order [30].

In recent years, aging dynamics, of SG systems has been extensively studied theoretically

[31, 32] and experimentally [33-37] The low temperature SG phase below a SG freezing temperature T_g exhibits intriguing non-equilibrium dynamics which is characterized by the chaotic nature and ageing behavior. The zero-field SG never reaches equilibrium. The non-equilibrium character can be experimentally observed from an age-dependence of the magnetic response. When the SG system is quenched from a high temperature above the SG transition temperature T_g to a low temperature T below T_g (this process is called the zero-field cooled (ZFC) aging protocol), the initial state is not thermodynamically stable and relaxes to more stable state. The aging behaviors depend strongly on their thermal history within the SG phase. The rejuvenation (chaos) and memory effects are also significant features of the aging dynamics. These effects are typically measured from the low frequency AC magnetic susceptibility. The SG phase is also susceptible to any perturbation in the form of temperature or field changes, which consequently, if large enough, effectively reinitializes the ageing process (temperature chaos). Both aging behavior and chaotic nature of the low temperature SG phase have been viewed first as additional difficulty in the understanding of SG's. However, it proved to be a key feature of the SG behavior, offering the unique opportunity to explore the nature of the SG phase.

2.4 Transport Properties

2.4.1 Conduction Mechanism in ferrites

Ferrites are ferromagnetic semiconductors that could be used in electronic devices. The increasing demand for low loss ferrites resulted in detailed investigations on conductivity and on the influence of various substitutions on the electrical conductivity, thermoelectric power, etc. The conduction mechanism in ferrites is quite different from that in semiconductors. In ferrites, the temperature dependence of mobility affects the conductivity and the carrier concentration is almost unaffected by temperature variation. In

semiconductors, the band type conduction occurs, where in ferrites, the cations are surrounded by closed pack oxygen anions and as a first approximation can well be treated as isolated from each other. There will be a little direct overlap of the anion charge clouds or orbital. In other words, the electrons associated with particular ion will largely remain isolated and hence a localized electron model is more appropriate than a collective electron (band) model. This accounts for the insulating nature of ferrites. These factors led to the hopping electron model [38]. An appreciable conductivity in these ferrites is found to be due to the presence of iron ion ions with different valence states at crystallographically different equivalent lattice sites [39]. Conduction is due to exchange of 3d electron, localized at the metal ions, from Fe^{3+} to Fe^{2+}. Various models have been suggested to account for the electrical properties. These are as follows

- Hopping model of electrons
- Small polaron model

2.4.2 Hopping model of electrons

In ferrites, there is a possibility in exchanging valence of a considerable fraction of metal ions and especially that of iron. The temperature dependence of conductivity arises only due to mobility and not due to the number of charge carriers in the sample. It is noted that for hopping conduction mechanism;

- The mobility has a minimum value much lower than the limiting value (0.1 cm/VS) taken as minimum for band conduction [40].
- The independence of Seebeck coefficient on temperature is due to the fact that in hopping model the number of charge carriers is fixed.
- Thermally activated process with activation energy E_a called hopping activation energy.

- Occurrence of n-p transitions with charge carriers in the Fe^{2+} or oxygen concentration in the system.

2.4.3 Small polaron model

A small polaron is a defect occurred when an electronic carrier becomes trapped at a given site as a consequence of the displacement of adjacent atoms or ions. The entire defect then migrates by an activated hopping mechanism. Small polaron formation can take place in materials whose conduction electrons belong to incomplete inner (d or f) shells which due to small electron overlap; tend to form extremely narrow bands [41-46]. The migration of small polaron requires the hopping of both the electron and the polarized atomic configuration from one site to an adjacent site [49]. The small polaron model also explains the low mobility, temperature independence of the Seebeck coefficient and thermally activated hopping.

2.5 Literature Review

Double oxides of iron and other metals are important members of ferrimagnetic system commonly known as ferrites. The outstanding properties of ferrites are their complex magnetic structure, which can be varied to tailor their magnetic properties for various high frequency applications. In this chapter we describe a brief overview of the ferrites. The basic issue of ferrimagnetisms, crystal structure of the spinel ferrites and effect of Mn substitution of Mn-Zn spinel ferrites are discussed.

References:

[1] Cullity, B. D., Introduction to Magnetic Materials, Addison-Wisley Publishing Company, Inc., California, 1972.

[2] Valenzuela, R., Magnetic Ceramics, Cambridge University Press, Cambridge, 1994.

[3] Goldman, A., Handbook of Modern Ferromagnetic Materials, Kulwer Acad. Pub, Boston, U.S.A 1999.

[4] Callister, W., "Materials Science and Engineering an introduction", Sixth ed. New York: JoHn Wiley

and Sons, Inc, 2003.

[5] Goldman, A., "Modern Ferrite Technology", New York, 1990.

[6] Spaldin, N., "Magnetic materials: Fundamentals and device applications", Cambridge: Cambridge University press, 2003.

[7] Bragg, W. H., "The structure of magnetite and the spinets", Nature, Vol-95, pp 561, 1915.

[8] Smit and Wijn, W. J. P., Ferrites, Philips Technical Library Wiley, New York, 1959.

[9] Snoek, J. L., "Dispersion and absorptions in magnetic ferrites at frequencies above Mc/s", Physica, Vol- 14, pp 207, 1948

[10] Viswanathan, B., Murthy, VRK, "Ferrite Materials Science and Technology", Spring Verlag, noarosa Publishing House, New Delhi, pp 143, 1990.

[11] Krupicka, S., and Novak, P., "Oxide spinets. In E. P. Wohlfarth, editor", Ferromagnetic Materials, Vol-3, chapter 4, pp 189-304, 1982.

[12] Fuentes, V., Aburto, S., and Valenzuela, R., "Magnetic sublattices in nickel ferrite", J.Mag. Mag. Mater., Vol- 69, No. 3, pp 233-236, 1987.

[13] P. W. Anderson, in Magnetism, Vol-1, Eds, G. T. Rado and H. Suhl, Academic Press, New York, 1963.

[14] Yafet, Y., and Kittel, C., "Antiferromagnetic arrangements in ferrites", Phys. Rev., Vol- 87, pp 290, 1952.

[15] Leyons, D. H., Keplan, T. A., Dwight, K. and Menyuk, N., "Classical theory of the ground spin-state in cubic spinels", Phys. Rev., Vol- 126, pp 540, 1962.

[16] Murthy, N. S. S., Natera, M. G., Youstif, S. I., Begum, R. J. and Srivatava, C. M., "YafetKittel angles in Zinc-Nickel ferrites", Phys. Rev., Vol- 181, No. 2, pp 969, 1969.

[17] Nogues, M., Dorman, J.L., Teillet, T. and Villers, G., "Randomly canted structures in the ferrite $Zn_xMg_{1-x}Fe_2O_4$", J. Mag.Mag. Mater., Vol-415, pp 104-107, 1992.

[18] Gabay, M. and Toulouse, G., "Coexistence of spin-glass and ferromagnetic orderings", Phys.Rev. Lett., Vol- 47, pp 201, 1981.

[19] Moore, M. A., and Brag, A. J., "Critical behaviour at the spin glass transition in a magnetic field", J.Phys. C, Vol- 15, No. 10, pp L301, 1982.

[20] McEwan, B. C., "Studies in mutual solubility. Part 11. The mutual solubility of glycerol and alcohols, aldehydes, phenols, and their derivatives", J.Chem. Soc., Vol- 123, pp 2284, 1923.

[21] Binder, K. and Young, A. P., "Spin glasses: Experimental facts, theoretical concepts, and open questions", Rev.Mod. Phys., Vol- 58, pp 801, 1986.

[22] Fischer, O., and Maple, M. B., "Superconductivity in Ternary Compounds I+H", (SpringerVerlag), 1982.

[23] Cladis, P. E., "New liquid-crystal phase diagram", Phys. Rev. Lett., Vol- 35, pp 48, 1975.

[24] Mydosh, J.A., "Spin Glasses-An Experimental Introduction", Taylor and Francis, London, 1993.

[25] Shapiro, S. M., Aeppli, G., Maletta, H., Motoya, K., "Neutron scattering studies of magnetic correlations in reentrant spin glasses", Ph vsica B+C, Vol- 137, pp 96, 1986.

[26] Mezard, M., Parisi, G., and Virasoro, M.A., Spin Glass Theory and Beyond World Scientific, Singapore, 1987

[27] Fisher, K.H., and Hertz, J.A., Spin Glasses, Cambridge University Press, 1991

[28] Mattsson, J., "Dynamics of random magnets", PhD thesis, Uppsala University, Sweden, 1994.

[29] Edwards, S., and Anderson, P., "Theory of spin glasses", J.Phys. F., Vol- 5, pp 965, 1975.

[30] Belayachi, A., Dormann, J.L., Nogues, M., "Critical analysis of magnetically semi-disordered systems: critical exponents at various transitions", J.Phys. Condens.Matt., Vol- 10, pp 1599, 1995.

[31] Bernardi, L.W., Yoshino, H., Hukushima, K., Takayama, H., Tobo, A., and Ito, A., "Aging of the zero-field-cooled magnetization in Ising spin glasses: experiment and numerical simulation", Phys. Rev. Lett., Vol- 86, pp 720, 2001.

[32] Yoshino, H., Lemaitre, A., and Bouchaud, J.P., "Multiple domain growth and memory in the droplet model for spin-glasses.", The European Physical Journal B (EPJ B), Vol- 20, pp 367, 2001

[33] Djurberg, C., Jonason, K., and Nordblad, P., "Magnetic relaxation phenomena in a CuMn spin glass", The European Physical Journal B (EPJ B), Vol-10, pp 15, 1999.

[34] Jonsson, T., Jonason, K., Jonsson, P., and Nordblad, P., "Nonequilibrium dynamics in a three-dimensional spin glass", Phys. Rev. B, Vol- 59, pp 8770, 1999

[35] Jonason, K., Nordblad, P., Vincent, E., Hanimann, J., and Bouchaud, J.P., "Memory interference effects in spin glasses", The European Physical Journal B (EPJ B), Vol- 13, pp 99, 2000.

[36] Dupuis, V., Vincent, E., Bouchaud, J.P., Hammann, J., Ito, A., and Katori, H. A., "Aging, rejuvenation, and memory effects in Ising and Heisenberg spin glasses", Phys. Rev. B., Vol- 64, pp 174-204, 2001.

[37] Nordblad, P., "Spin glasses: model systems for non-equilibrium dynamics", J.Phys: Condens. Matt, Vol- 16, pp 5715, 2004.

[38] Samokhvalov, A. A. and Rustamov, A. G., Soviet Physics - Solid State, Vol- 6, pp 749, 1964.

[39] Bossmann, A. J. and Crevecoeur, C., "Mechanism of the electrical conduction in Li-doped NiO", Physics Review, Vol- 144, pp 763, 1966.

[40] Jonker, G.H., Santen, J.H.V., "Magnetic compounds with perovskite structure III. ferromagnetic compounds of cobalt", Physica, Vol- 19, pp 120, 1953.

[41] Bhise, B. V., Ghatage, A. K., Kulkarni, B. M., Lotka, S. D., and Patil, S. A., "Conduction in Mn substituted Ni-Zn ferrites", Bulletin of Material Science, Vol- 19, No. 3, pp 527, 1996.

[42] Patil, M. G., Mahajan, V. C., Bhise, B. V., Chendke, S. M., and Patil, S. A., "Conduction phenomenon in Mn-substituted NiCd ferrites", Physica Status Solidi (b), Vol-144, pp 415, 1994.

[43] Tsay, M.J., Tung, M.J., Chen, C.J. and Liu, T.Y. "The Manufacture of High Permeability Mn-Zn Ferrites by Atmospherical Protect" J; PHYS. IVFRANCE 7 (1997)

[44] Ewais, E. M. M., Hessien, M. M., and El-Geassy, A.H. A. "In-Situ Synthesis of Magnetic Mn-Zn Ferrite Ceramic Object by Solid State Reaction" J. Aust. Ceram. Soc. 44 [1] 57-62 (2008)

[45] Syue, M.R., Wei, F.J., Chou, C.S., and Chao-Ming Fu, "Magnetic and electrical properties of Mn-Zn ferrites synthesized by combustion method without subsequent heat treatments" , J. Appl. Phys. 109, 07A324 (2011)

[46] Amarendra K. S., Abhishek K. S., Goelb,T.C., Mendiratta , R.G. "High performance Ni-substituted Mn–Zn ferrites processed by soft chemical technique" J. Magn.Magn.Mater.281, 276–280(2004)

[47] Stojanovic,G., Srdic,V. and Maletin,M. "Electrical properties of yttrium-doped Zn and Ni–Zn ferrites" p hys. stat. sol. (a) 205, No. 10, 2464–2468 (2008);

[48] Ishaque , M. , Islam , M.U., AzharKhan , M., Rahman , I.Z., Genson , A., Hampshire, S. "Structural, electrical and dielectric properties of yttrium substituted nickel ferrites" Physica B 405, 1532–1540(2010)

[49] Ahmeda, M.A., Okashab, N., Salah, L. "Influence of yttrium ions on the magnetic properties of Ni–Zn ferrites", J. Magn. Magn. Mater. 264 241–250(2003)

CHAPTER 3

SAMPLE PREPARATION AND EXPERIMENTAL TECHNIQUES

3.1 Introduction

A goal common to all the ferrites is the common formation of the spinel structure. Today, the large majority of ferrite powders are made by the conventional Ceramic process or Solid State Reaction method. Most non-conventional process involves producing the powder by a wet method. Among these methods, some are [1]:

1) Co-precipitation
2) Organic precursors
3) Sol-gel synthesis
4) Spray-drying
5) Freeze-drying
6) Combustion synthesis
7) Glass crystallization

In this chapter, we describe the solid state reaction method that is used in this research work.

3.2 Conventional solid state reaction method

In the solid state reaction method, the required composition is usually prepared form the appropriate amount of raw mineral oxides or carbonates by crushing, grinding and milling. The most common type of mill is the ball mill, which consists of a lined pot with hard spheres or rod inside. Milling can be carried out in a wet medium to increase the degree of mixing. This method depends on the solid state inter-diffusion between the raw materials. Solids do not usually react at room temperature over normal time scales. Thus it is necessary

to heat them at higher temperatures for the diffusion length $(2Dt)^{1/2}$ to exceed the particle size, where D is the diffusion constant for the fast-diffusing species, and t is the firing time. The ground powders are then calcined in air or oxygen at a temperature above 1000°C. For some time, this process is continued until the mixture is converted into the correct crystalline phase. The calcined powders are again crushed into fine powders. The pellets or toroid shaped samples are prepared from these calcined powders using die-punch assembly or hydrostatic or isostatic pressure. Sintering is carried out in the solid state, at temperature ranging 1050-1400°C, for times of typically 1-40 h and in various atmospheres (e.g. Air, O_2 and N_2) [2-5]. Fig. 3.1 shows, diagrammatically, the stages followed in ferrite preparation.

The general solid state reaction leading to a ferrite $MeFe_2O_4$ may be represented as

$$MeO + Fe_2O_3 \longrightarrow MeFe_2O_4$$

Where Me is the divalent ions. There are basically four steps in the preparation of ferrite:

1) Preparation of materials to form an intimate mixture with the metal ions in the ratio which they will have in the final product,
2) Heating of this mixture to form the ferrite (often called calcining),
3) Grinding the calcined powders and pressing the fine powders into the required shape,
4) Sintering to produce a highly densified product.

3.3 Details of calcining, pressing and sintering

Calcining is defined as the process of obtaining a homogeneous and phase pure composition of mixed powders by heating them for a certain time at a high temperature and then allowing it to cool slowly. During the presintering stage, the reaction of Fe_2O_3 with metal oxide (say, MeO or Me'_2O_3) takes place in the solid state to form spinel according to the reactions [7]:

$$MeO + Fe_2O_3 \longrightarrow MeFe_2O_4 \text{ (Spinel)}$$

$$2Me'_2O_3 + 4Fe_2O_3 \longrightarrow 4Me'Fe_2O_4 \text{ (Spinel)} + O_2$$

$$Fe_2O_3 + FeO \longrightarrow Fe_3O_4$$

After that Zn and Mn ions are introduced by

$$(1\text{-}x)Fe_3O_4 + xZnO \longrightarrow Zn_xFe_{3-x}O_4$$

$$(1\text{-}x)Fe_3O_4 + xMnCO_3 \longrightarrow Mn_xFe_{3-x}O_4$$

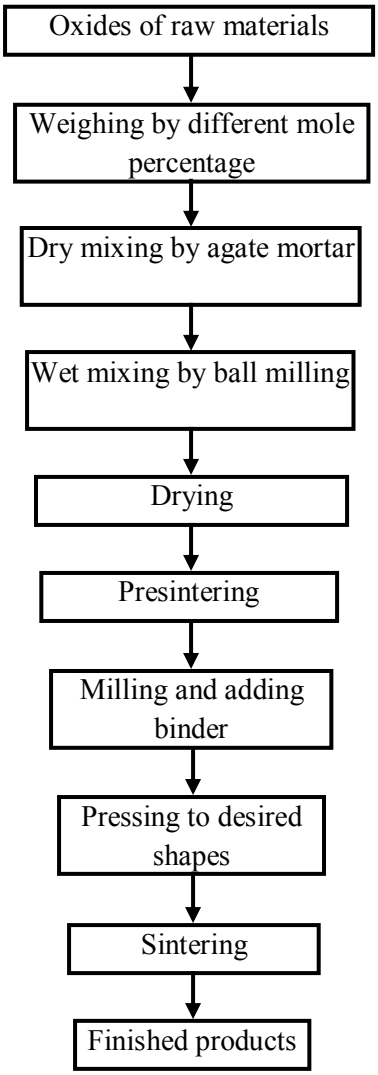

Figure3.1. Flow chart of the stages in preparation of spinel ferrite.

The calcining process can be repeated several times to obtain a high degree of homogeneity. The presintering powders are crushed into fine powders. The ideal characteristics of fine powders are [6]:

1) small particle size (sub micron)
2) narrow distribution in particle size
3) dispersed particles
4) equaled shape of particles
5) high purity
6) homogeneous composition.

A small particle size of the reactant powders provides a high contact surface area for initiation of the solid state reaction; diffusion paths are shorted, leading to more efficient completion of the reaction. Porosity is easily eliminated if the initial pores are very small. A narrow size distribution of spherical particles as well as a dispersed state is important for compaction of the powder during green-body formation. Grain growth during sintering can be better controlled if the initial size is small and uniform.

A binder is usually added prior to compaction, at a concentration lower than 5wt % [6]. Binders are polymers or waxes; the most commonly used binder in ferrite is polyvinyl alcohol. The binder facilitates the particles flow during compacting and increases the bonding between the particles, presumably by forming bonds of the type particle-binder-particle. During sintering, binders decompose and are eliminated from the ferrite. Pressures are used for compacting very widely but are commonly several tons per square inch (i. e., up to 10^8 N m^{-2}).

Sintering is defined as the process of obtaining a dense, tough body by heating a compacted powder for a certain time at a temperature high enough to significantly promote diffusion, but

clearly lower than the melting point of the main component. The driving force for sintering is the reduction in surface free energy of the powder. Part of this energy is transferred into interfacial energy (grain boundaries) in the resulting polycrystalline body [6, 8]. The sintering time, temperature and the furnace atmosphere play very important role on the magnetic property of ferrite materials. The purposes of sintering process are:

1) to bind the particles together so as to impart sufficient strength to the product,
2) to densify the material by eliminating the pores and
3) to homogenize the materials by completing the reactions left unfinished in the presintering step.

Sintering of crystalline solids is dealt by Coble and Burke [9] who found the following empirical relationship regarding rate of grain growth:

$$\bar{d} = kt^n$$

Where $\bar{d}$ is the mean grain diameter, n is about 1/3, t is sintering time and k is a temperature dependent parameter. Sintering is divided into three stages, Fig. 3.2 [6, 10].

Stage1. Contact area between particles increases,

Stage2. Porosity changes from open to closed porosity,

Stage3. Pore volume decreases; grains grow.

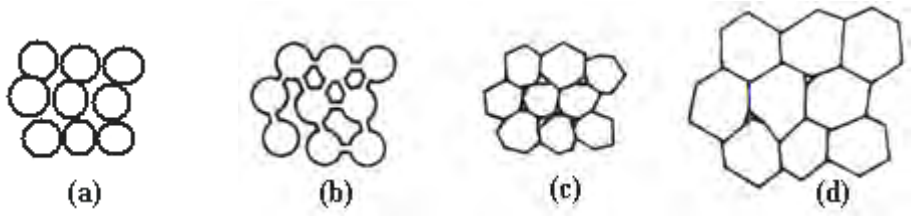

Figure3.2. Schematic representation of sintering stages: (a) green body, (b) initial stage, (c) intermediate stage, and (d) final stage.

In the initial stage, neighboring particles form a neck by surface diffusion and presumably also at high temperatures by an evaporation-condensation mechanism. Grain growth begins during the intermediate stage of sintering. Since grain boundaries are the sinks for vacancies, grain growth tends to decrease the pore elimination rate due to the increase in distance between pores and grain boundaries, and by decreasing the total grain boundary surface area. In the final stage, the grain growth is considerably enhanced and the remaining pores may become isolated.

3.4 Preparation of the present samples

3.4.1 Sample preparation:

Polycrystalline $Fe_{2.5}Zn_{0.5-x}Mn_xO_4$ (x=0 to 0.5 in steps of 0.1) prepared by a solid state reaction technique. Appropriate amount of commercially available high purity powders of $MnCO_3$ (99.9%), ZnO (99.9%) and Fe_3O_4 (99.9%) will be weighed and mixed thoroughly by ball milling. Milling will be carried out in a wet medium (distilled water) to increase the degree of mixing. The mixture calcined at 900ºC for 5 hours. The calcined powder again crashed into fine powders. From the fine powders, toroid- and disk-shaped samples prepared and sintered at various temperatures. During sintering the samples heated/cooled in various heating and cooling rates. It is expected that various heating/cooling rate will produce samples of various surface morphology, electric and magnetic properties.

3.4.2 Structural characterization:

Surface morphology of the samples investigated using an optical microscope. From the observed micrographs of these samples, the grain size determined. X-ray diffraction study carried out to verify the homogeneity and structure of the samples. Density, porosity and lattice parameters also determined.

3.4.3 Complex permeability and magnetization:

Initial permeability and magnetic loss factor measured up to 120 MHz with an Agilent Impedance Analyzer. Detailed analysis carried out for the dependence of permeability as a function of grain size and sintering temperatures.

Figure3.3. Sample (a) disk shaped, (b) Toroid shaped.

3.5 Experimental techniques

3.5.1 X-ray Diffraction

Bragg reflection is a coherent elastic scattering in which the energy of the X-ray is not changed on reflection. If a beam of monochromatic radiation of wavelength λ is incident on a periodic crystal plane at an angle θ and is diffracted at the same angle as shown in Figure 3.4, the Bragg diffraction condition for X-rays is given by

$$2d\,Sin\theta = n\lambda \quad \ldots \quad \ldots \quad \ldots \quad \ldots \quad \ldots \quad \ldots \quad (3.1)$$

Where *d* is the distance between crystal planes and *n* is the positive integer which represents the order of reflection. Equation (3.1) is known as Bragg law. This Bragg law suggests that the diffraction is only possible when $\lambda \leq 2d$ [12].For this reason we cannot use the visible light to determine the crystal structure of a material. The X-ray diffraction (XRD) provides substantial information on the crystal structure.

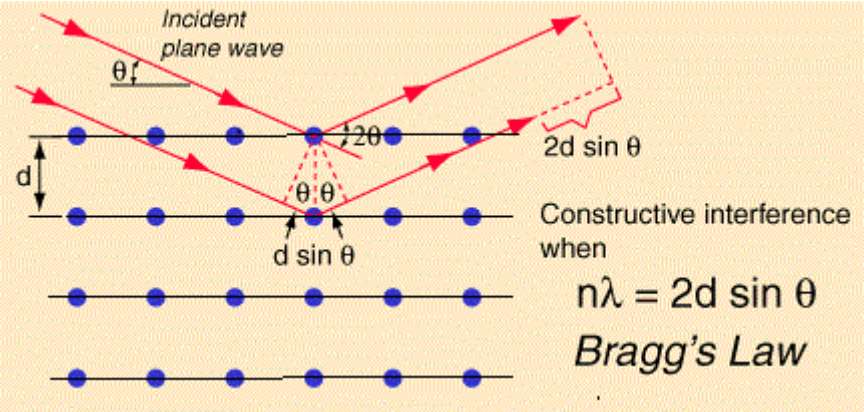

Figure 3.4. Bragg's law of X-ray diffraction.

The XRD was carried out with an X-ray diffractometer for the samples. For this purpose monochromatic *Cu-K_α* radiation was used.

3.5.2 Bruker D8 X-ray diffractometer

XRD provides substantial information on the crystal structure. The wavelength of an X-ray is of the same order of magnitude as that of the lattice constant of crystals and this makes it so useful in structural analysis of crystal structure. To study the crystalline phases, various structural parameters such as, lattice parameter, crystallite size, strain, density etc of the powder samples. Bruker D8 X-ray diffractometer shown in Figure 3.5 was used at the PP and PDC division of Bangladesh council of Scientific and Industrial Research (BCSIR).

The specimens were exposed to Cu-K_α radiation of wavelength, λ = 1.5406Å with a primary beam of 40 kV and 40 mA with a sampling pitch of 0.02° and the data collection rate was 2°/min. A 2θ scan was taken from 35° to 105° to get possible fundamental peaks.

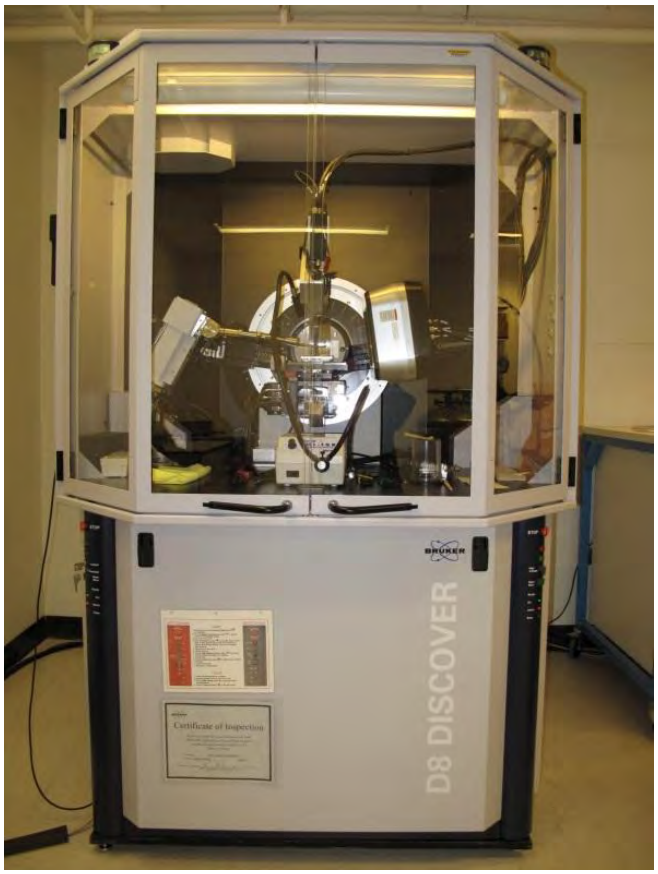

Figure 3.5 Bruker D8 X-ray Diffractometer.

3.5.3 Determination of crystal structure

XRD pattern of a sample provides important information about the crystal structure of the material. From the XRD pattern we can easily find the information of the atomic arrangement by measuring lattice parameter.

XRD can be conducted both by reflection and transmission as shown in Figure 3.6. In our experiment we use classic reflection geometry. The arrangement of the source and the detector was locked coupled.

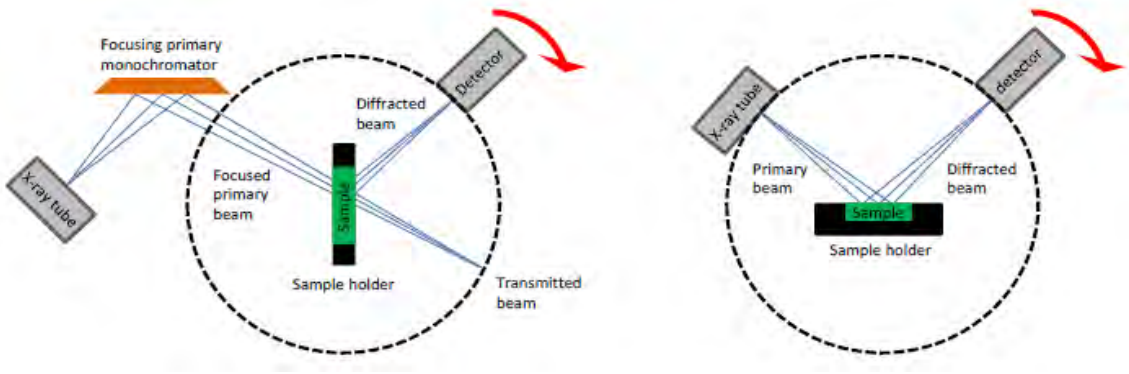

Figure 3.6 X-ray diffraction, (a) classic transmission geometry and (b) Classic reflection geometry.

3.5.4 Determination of lattice parameters

The lattice parameter for each peak of each sample was calculated by using the formula

$$\frac{1}{d_{hkl}} = \left[\left(\frac{h^2 + k^2 + l^2}{a^2}\right)\right]^{\frac{1}{2}} \quad \ldots. \quad \ldots. \quad \ldots. \quad \ldots. \quad \ldots. \quad (3.2)$$

Where *h*, *k* and *l* are the indices of the crystal planes.

We used Nelson-Riley function to calculate the lattice parameter to get a better result. The Nelson-Riley function can be given by,

$$F(\theta) = 1/2\left[\cos^2\theta/\sin\theta + \cos^2\theta/\theta\right] \ldots. \quad \ldots. \quad \ldots. \quad \ldots. \quad (3.3)$$

Plotting $F(\theta)$ Vs. 'a' gives some scattered points. Linear fitting of these points gives a Y-intercept which eventually gives the lattice parameters.

The theoretical density ρ_{th} was calculated using following expression:

$$\rho_{th} = \frac{8M}{N_A a_o^3} g/cm^3 \ldots. \quad \ldots. \quad \ldots. \quad \ldots. \quad \ldots. \quad \ldots. \quad \ldots.$$

(3.4)

Where N_A is Avogadro's number (6.02×10^{23} mol^{-1}), M is the molecular weight.

The porosity was calculated from the relation $\{100(\rho_{th} - \rho_B)/\rho_{th}\}\%$ …. …. (3.5)

Where ρ_B is the bulk density measured by the formula $\rho_B = M/V$ …. …. (3.6)

3.5.5 Rietveld analysis

Profile refinement analysis of the XRD patterns were carried out by TOPAS-3 software, associated with Bruker D8 X-ray diffractometer. The amplitude of light scattered by a crystal is determined by the arrangement of atoms in the diffracting planes and is given by,

$I_{hkl} \propto |F_{hkl}|^2$…. …. …. …. …. …. …. (3.7)

Where, $F_{hkl} = \sum_{j=1}^{m} N_j f_j \exp\left[2\pi i\left(hx_j + ky_j + lz_j\right)\right]$…. …. …. …. …. (3.8)

Where, F_{khl} is called the structure factor, which qualifies the amplitude of light scattered by a crystal. The patterns of atoms in the unit cell scatters strongly in some directions and weakly in others owing to interference of the wavelets scattered by the atoms. F_{hkl} sums the result of scattering from all of the atoms in the unit cell to form a diffraction peak from the (hkl) planes of atoms. f is a scattering factor which can be written as,

$$|f|^2 = \left(f_0 \exp\left[\frac{-B\sin^2\theta}{\lambda^2} \right] + \Delta f' \right)^2 + (\Delta f'')^2 \ldots \quad \ldots \quad \ldots \quad \ldots \quad \ldots$$

(3.9)

Where, $B=8\pi^2U^2$ is called the Debye-Waller temperature factor.

The percentage of phases is based on a simple relationship,

$$W_p = \frac{S_p(Z,M,V)_p}{\sum_i^n S_i(Z,M,V)_i} \quad \ldots \quad \ldots \quad \ldots \quad \ldots \quad \ldots \quad \ldots$$

(3.10)

Where W_p is the relative weight fraction of phase p in a mixture of n phases, and S, Z, M and V are, respectively, the Rietveld scale factor, the number of formula units per unit cell, the mass of the formula unit (in atomic mass units) and the unit cell volume.

There are six different R values which signifies the criterion of fitting such as,

"R-pattern", $R_p = \frac{\Sigma|Y_{o,m} - Y_{c,m}|}{\Sigma Y_{o,m}}$ …. …. …. ….. ….

(3.11)

"R-pattern",(background corrected), $R_p' = \frac{\Sigma|Y_{o,m} - Y_{c,m}|}{\Sigma|Y_{o,m} - Bkg_m|}$ …. …. ….

(3.12)

“R-weighted pattern”, $R_{wp} = \sqrt{\frac{\Sigma W_m (Y_{o,m} - Y_{c,m})^2}{\Sigma W_m Y_{o,m}^2}}$ …. …. …. ….

(3.13)

"R-weighted pattern",(background corrected), $R'_{wp} = \sqrt{\frac{\sum W_m(Y_{o,m}-Y_{c,m})^2}{\sum W_m(Y_{o,m}-Bkg_m)^2}}$ …. ….

(3.14)

"R-expected",$R_{exp} = \sqrt{\frac{\sum M-P}{\sum W_m Y_{o,m}^2}}$ …. …. …. …. ….

(3.15)

"R-expected",(background corrected), $R'_{exp} = \sqrt{\frac{\sum M-P}{\sum W_m (Y_{o,m}-Bkg_m)^2}}$ …. ….

(3.16)

Now, "Goodness of fit", GOF = $\chi^2 = \frac{R_{wp}}{R_{exp}} = \sqrt{\frac{\sum W_m (Y_{o,m}-Y_{c,m})^2}{\sum M-P}}$ …. …. …

(3.17)

"R-Bragg",$R_B = \frac{|I_{Obs,k}-I_{c,k}|}{\sum I_{Obs,k}}$. …. …. …. …. …. ….

(3.18)

3.6 Micro structural investigation

The micro structural study of the ferrite samples was performed in order to have an insight of the grain structures. The samples of different compositions and sintered at different temperatures were chosen for this purpose. The samples were visualized under a high-resolution optical microscope and then photographed.

3.6.1 Scanning Electron Microscopy

The scanning electron microscope (SEM) creates various images by focusing a high energy beam of electrons onto the surface of a sample and detecting signals from the interaction of

the incident electrons with the sample's surface. The type of signals gathered in a SEM varies and can include secondary electrons, characteristic X-rays, and back scattered electrons.

Figure 3.7 JOEL 7500 FE-SEM

The SEM is capable of producing high-resolution images of a sample surface in its primary use mode, secondary electron imaging. Due to the manner in which this image is created, SEM images have great depth of field yielding a characteristic three-dimensional appearance useful for understanding the surface structure of a sample.

3.6.2 Working principle of SEM

Accelerated electrons in an SEM carry significant amounts of kinetic energy and this energy is dissipated as a variety of signals produced by electron-sample interactions when the incident electrons are decelerated in the solid sample. These signals are of six types. They are,

i. Secondary electrons,

ii. Backscattered electrons,

iii. Diffracted backscattered electrons,

iv. Photons (characteristic X-rays and continuum X-rays),

v. Cathodoluminescence and

vi. Chopped beam bombardment generating ultrasonic waves

Secondary and backscattered electrons are used for imaging samples. The secondary electrons are used for showing morphology and topography on samples and backscattered electrons are most valuable for illustration contrast in composition in multiphase samples.

Moreover, the X-ray generation is produced by inelastic collisions of the incident electrons with electrons in discrete orbital or shells of atoms in the sample. As the excited electrons return to lower energy states, they yield X-rays that are of a fixed wavelength. Thus characteristic X-rays are produced in SEM technique.

3.6.3 Instrumentation of SEM

A typical SEM system is generally composed of two subsystems,

i. The electron optical column which produces a finely focused beam of electrons that is scanned in a television type raster over the specimen surface,

ii. A signal detection, processing and display system

Figure.3.8 shows the Schematic diagram of an SEM. In SEM instruments, an electron beam is thermo-ionically emitted from an electron gun fitted with a tungsten filament cathode. Generally, tungsten is used in thermionic electron guns because it has the highest melting point and lowest vapor pressure of all metals, thereby allowing it to be heated for electron emission.

The electron beam, which typically has an energy ranging from a few hundred eV to 40K eV, is focused by one or two condenser lenses to a spot about 0.4nm to 5nm in diameter. The

beam passes through pairs of scanning coils or pairs of deflector plates in the electron column, typically in the final lens, which deflect the beam in the x and y axes so that it scans in arrester fashion over a rectangular area of the sample surface.

When the primary electron beam interacts with the sample, the electrons lose energy by repeated random scattering and absorption within a teardrop-shaped volume of the specimen known as the interaction volume, which extends from less than 100nm to around 5µm into the surface. The size of the interaction volume depends on the electron's landing energy, the atomic number of the specimen and the specimen's density. The energy exchange between the electron beam and the sample results in the reflection of high-energy electrons by elastic scattering, emission of secondary electrons by inelastic scattering and the emission of electromagnetic radiation, each of which can be detected by specialized detectors. The beam current absorbed by the specimen can also be detected and used to create images of the distribution of specimen current. Electronic amplifiers of various types are used to amplify the signals which are displayed as variations in brightness on a cathode ray tube.

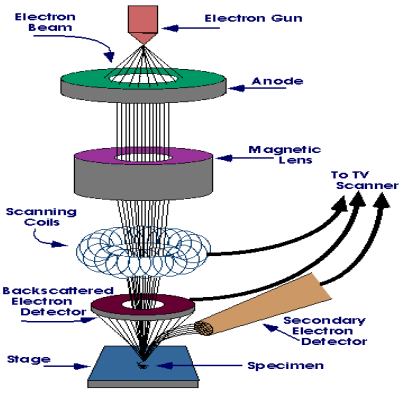

Figure 3.8 Schematic diagram of an SEM

The raster scanning of the CRT display is synchronized with that of beam on the specimen in the microscope and the resulting image is therefore a distribution map of the intensity of the

signal being emitted from the scanned area of the specimen. Then the image is captured and displayed on a computer monitor and finally stored in computer memory.

The micro structural study of the samples was performed in order to get an insight of the grain structures. The samples were visualized under a SEM, JOEL 7500 FE-SEM and then photographed. Average grain diameter of the samples was determined by lineal intercept technique . To do this, several random horizontal and vertical lines were drawn on the micrographs. Therefore, we counted the number of grains intersected and measured the length of the grains along the line traversed. Finally the average grain size was calculated [2].

In the SEM, the magnification is totally determined by the electronic circuitry that scans the beam over the specimen's surface. Magnification can be as high as 300,000×, which is usually more than sufficient. In principle, the resolution of a SEM is determined by the beam diameter on the surface of the specimen. However, the practical resolution depends on the properties of the specimen, the specimen preparation technique, and also on many instrumental parameters, such as the beam intensity, accelerating voltage, scanning speed, distance of the lens from the specimen's surface, and the angle of the specimen with respect to the detector. Under optimum conditions, a resolution of 1 nm can be achieved.

3.7 Complex permeability measurement

For high frequency application, the desirable property of a ferrite is high permeability with low loss. One of the most important goals of ferrite research is to fulfill this requirement. To determine the permeability of the ferrite sample, we compressed the powders to a toroid shape and sintered them for various sintering temperature. The techniques of permeability measurement at frequency characteristics of the present samples are described below:

3.7.1. Techniques for the permeability measurement

Measurements of permeability normally involve the measurements of the change in self-inductance of a coil in presence of the magnetic core. The behavior of a self-inductance can now be described as follows. We assume an ideal lossless air coil of inductance L_0. On insertion of a magnetic core with permeability μ, the inductance will be μL_0. The complex impedance Z of this coil [11] can be expressed as follows:

$$Z = R + jX = j\omega L_0(\mu' - j\mu'') \quad \ldots \quad (3.19)$$

Where, the resistive part is $R = \omega L_0 \mu''$ .... (3.20)

and the reactive part is $X = \omega L_0 \mu'$ .... (3.21)

The permeability can be derived from the complex impedance of a coil, Z, given by equation (4.25). The core is taken as toroidal to avoid demagnetizing effects. The quantity L_o is derived geometrically as shown in the following section:

3.7.2 Frequency dependent permeability

The frequency characteristics of the alloyed samples i.e. the initial permeability spectra were investigated using a *Wayne Kerr Precision Impedance Analyzer (model no. 6500B)* in the solid state physics laboratory, Bangladesh University of Engineering and Technology (BUET).which is shown in Figure 3.9

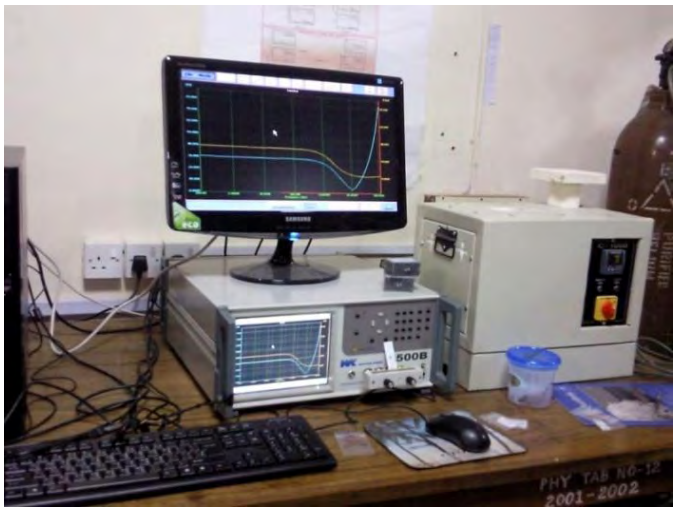

Figure 3.9. Wayne Kerr Impedance analyzer (6500B series) in experimental solid state physics laboratory, BUET.

Figure 3.10 Toroid shaped sample for permeability measurement.

The complex permeability measurements on toroid shaped specimens (one shown in fig. 3.10) were carried out at room temperature (303K) in the frequency range of 100Hz - 120 MHz The real part $(\mu_i^{/})$ of the complex permeability was calculated using the following relations. $\mu_i^{/} = L_s / L_0$, where L_s is the self-inductance of the sample core and $L_0 = \mu_o N^2 S / \pi \bar{d}$ is derived geometrically. Here L_o is the inductance of the winding coil without the sample core, N is the number of turns of the coil (N = 5), S is the area of cross section of the toroidal sample as given below:

$$S = d \times h, \quad \ldots \quad \ldots \quad \ldots. \quad \ldots. \quad \ldots. \quad \ldots. \quad \ldots. \quad (3.22)$$

Where, $d = \frac{d_2 - d_1}{2}$, …. …. …. …. …. …. (3.23)

$d_1 = \text{Inner diameter},$

$d_2 = \text{Outer diameter},$

$h = \text{Height}$

and $\bar{d}$ is the mean diameter of the toroidal sample as given below:

$$\bar{d} = \frac{d_1 + d_2}{2}$$

References:

[1] Goldman , A., Handbook of Modern Ferromagnetic Materials, Kulwer Acad. Pub, Boston, U.S.A (1999).

[2] Hossain, A. K. M. Akther, "Investigation of colossal magneto resistance in bulk and thick film magnetite's," Ph. D. Thesis, Imperial College, London (1998).

[3] Cullity, B. D., Introduction to Magnetic Materials, Addison-Wisley Publishing Company, Inc., California (1972).

[4] Brook, R. J., Sintering: An Overview, Concise Encyclopedia of Advanced Ceramic Materials, Pergamon Press, Oxford, pp. 438 (1991).

[5] Reijnen, P., Science of Ceramics, Academic Press, London (1967)

[6] Valenzuela, R., Magnetic Ceramics, Cambridge University Press, Cambridge (1994).

[7] Slick, P. I., Ferrites for Non-microwave Applications, Vol. 2, North Holland Pub. Co. (1980).

[8] Kingery, W. D., Bowen, H. K. and Uhlman, D. R., Introduction to Ceramics, 2nd edition, Wiley Interscience, Newyork, pp. 476 (1976).

[9] Coble ,R. L. and Burke, J. E., 4th Int. Symp. On the Reactivity of Solids, Amsterdam, pp. 38-51 (1960).

[10] McColm, I. J. and Clark, N. J., Forming, Shaping and Working of high Performance Ceramics, Blackie,Glasgow, pp. 1-338 (1988).

[11] Kittel, C., Introduction to Solid State Physics, 7th edition, Jhon Wiley and Sons, Inc., Singapore (1996).

[12] Goldman, A., "Handbook of Modern Ferromagnetic Materials", Kulwer Acad. Pub., Boston, U.S.A (1999).

CHAPTER 4

RESULTS AND DISCUSSION

The polycrystalline $Fe_{2.5}Zn_{0.5-x}Mn_xO_4$ (x=0.00, 0.10, 0.20, 0.30, 0.40 and 0.50) are studied. All ferrite samples are sintered at 1100, 1150, 1200 and 1250˚C for five hours in air. Structural and surface morphology are studied by X-ray diffraction. The microstructures are studied by field emission scanning electron microscopy (FESEM). The magnetic properties of the ferrites are characterized with high frequency (10 KHz-120 MHz) complex initial permeability. The effects of Mn substitution and sintering temperatures on the complex initial permeability of these ferrites are discussed.

4.1 XRD analysis of the polycrystalline $Fe_{2.5}Zn_{0.5-x}Mn_xO_4$

Fig. 4.1 illustrates the X-ray diffraction (XRD) patterns of various $Fe_{2.5}Zn_{0.5-x}Mn_xO_4$ sintered at 1200˚C in air.

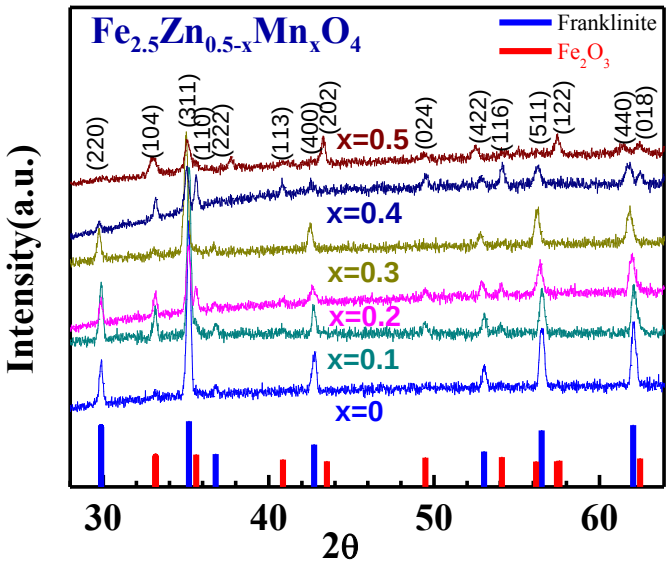

Fig.4.1 The X-ray diffraction patterns of $Fe_{2.5}Zn_{0.5-x}Mn_xO_4$ sintered at 1200˚C in air.

The XRD analysis confirms the $Fe_{2.5}Zn_{0.5-x}Mn_xO_4$ samples have single phase cubic spinel structure. There are some impurity peaks found due to the presence of Fe_2O_3. All the peaks in the patterns matched well with characteristic reflections of spinel structure reported earlier [3]. The XRD peaks are indexed to the crystal plane of spinel ferrite (220), (311), (400), (422), (511) and (440), respectively.

4.2 Rietveld analysis

Figure 4.2 shows the fitted curve given as a output by TOPAS 3 software after Rietveld analysis of the XRD patterns of the $Fe_{2.5}Zn_{0.5-x}Mn_xO_4$ for x=0.0 to 0.5. The upper blue line represents the XRD patterns of the samples, red line represents the standard patterns of the crystallographic models used as a starting model for refinement and the lower grey line represents the difference between our measured XRD patterns and the standard model. We used franklinite ($Fe_{1.96}Zn_{0.68}Mn_{0.36}O_4$) and hematite ($Fe_2O_3$) as starting models for refinement. Following parameters were applied for each refinement: background parameter, scale factor, cell parameter, zero errors, Lorentzian crystallite size, Gaussian lattice strain, preferred orientation spherical harmonics of the order of 4. Various structural parameters such as quantitative phase analysis, lattice parameter, density, crystallite size have been determined by Rietveld's XRD profile refinement analysis. Quality of the fitting was determined by the $\chi 2$ (GOF) value. Rietveld analysis shows that the various $Fe_{2.5}Zn_{0.5-x}Mn_xO_4$ have been formed with a nearly FCC crystal structure which is similar to the structure of $Fe_{1.96}Zn_{0.68}Mn_{0.36}O_4$ .Small percentage has been formed Rhombohedral crystal structure which is nearly similar to the structure of Fe_2O_3.

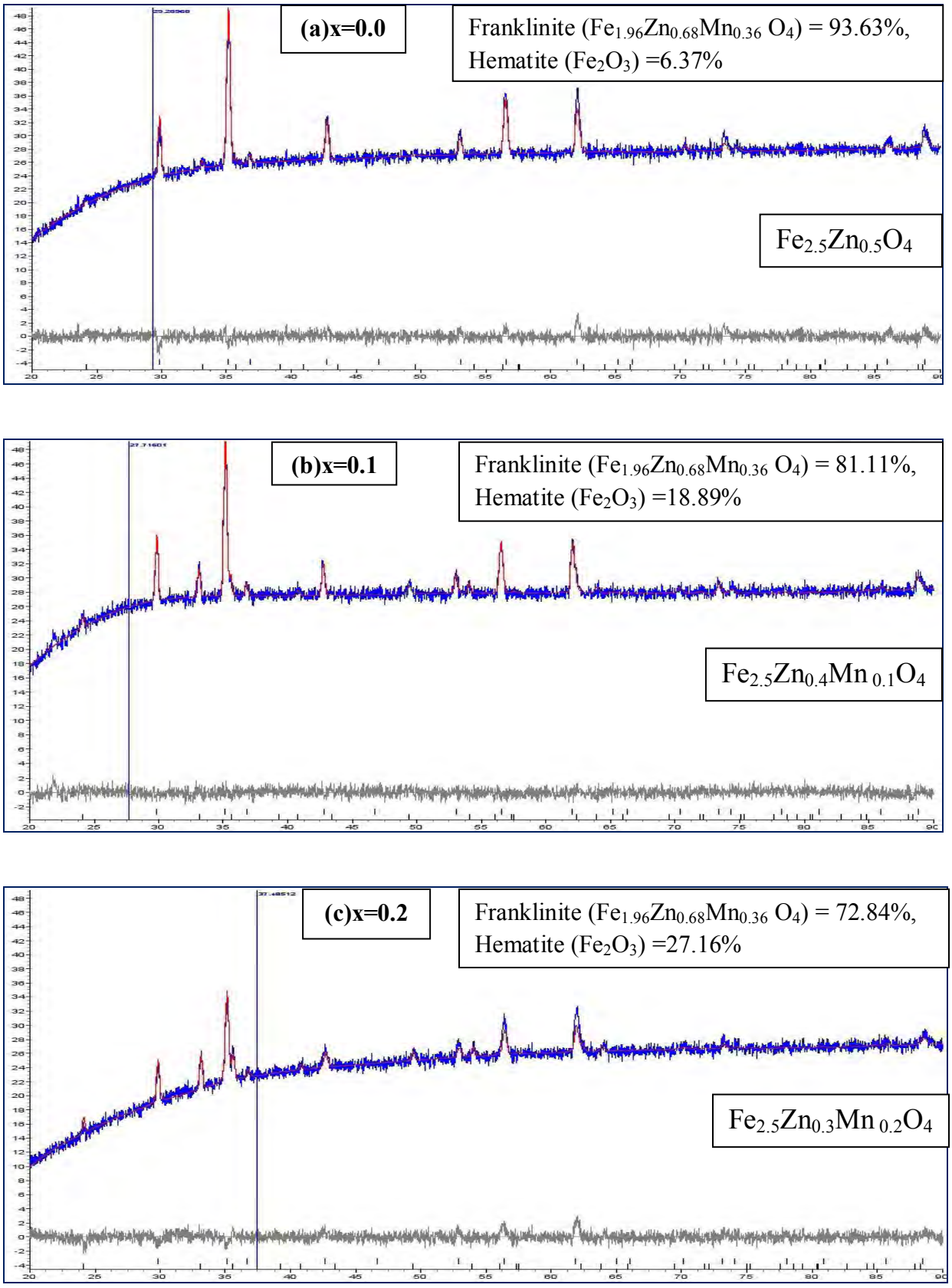

Figure 4.2 Fitted curves for the XRD patterns of $Fe_{2.5}Zn_{0.5-x}Mn_xO_4$, (a) x=0.00, (b) x=0.10, (c) x=0.20 sintered at 1200˚C in air by TOPAS 3 software.

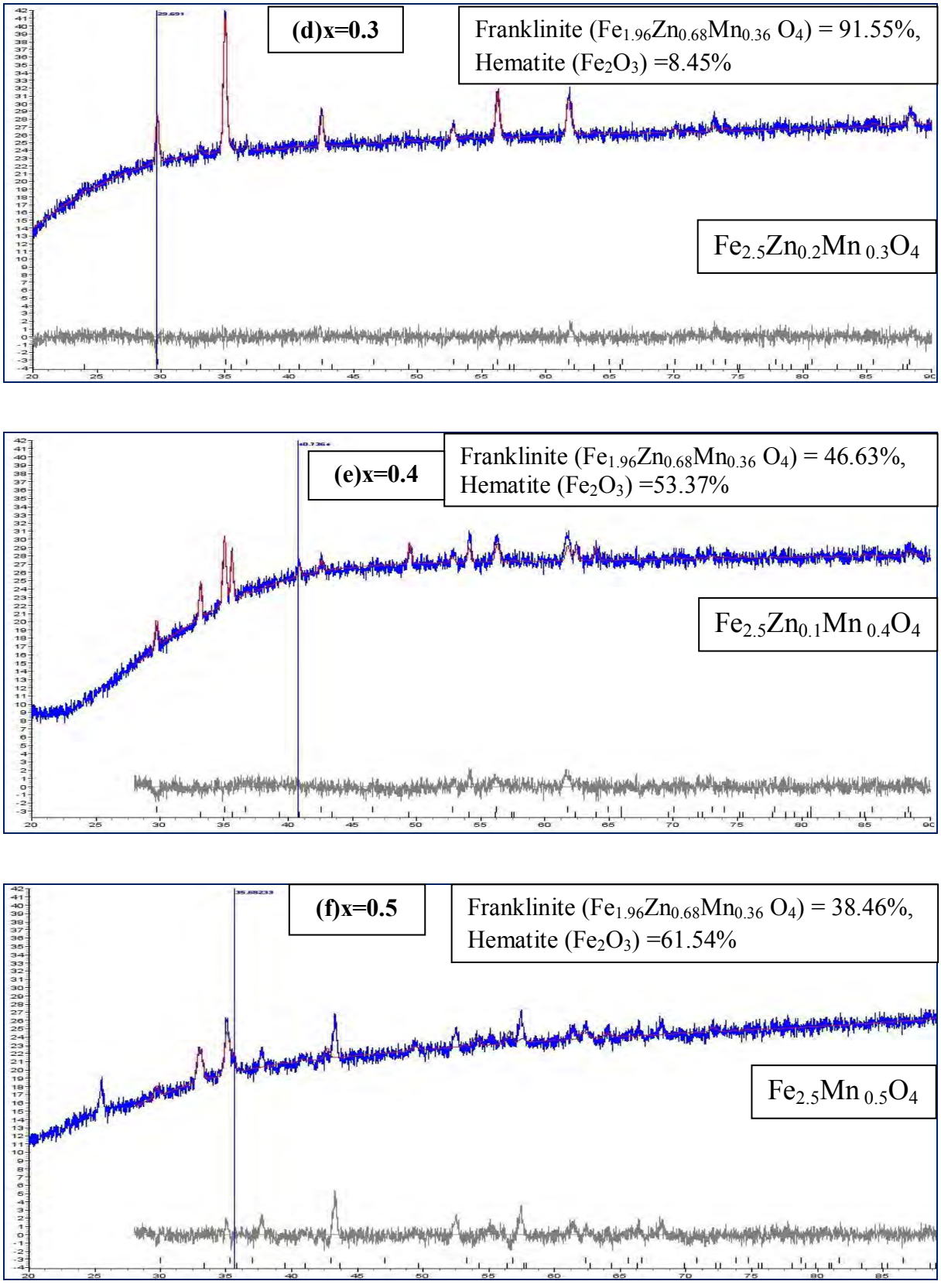

Figure 4.2 Fitted curves for the XRD patterns of $Fe_{2.5}Zn_{0.5-x}Mn_xO_4$ (d) x= 0.30, (e) x= 0.40 and (f) x=0.50 sintered at 1200˚C in air by TOPAS 3 software.

4.2.1 Quantitative phase analysis

Figure 4.3 shows the quantitative phase analysis with Mn content. It shows that the various $Fe_{2.5}Zn_{0.5-x}Mn_xO_4$ have been matched well (100%) with the phase of Franklinite and Hematite.

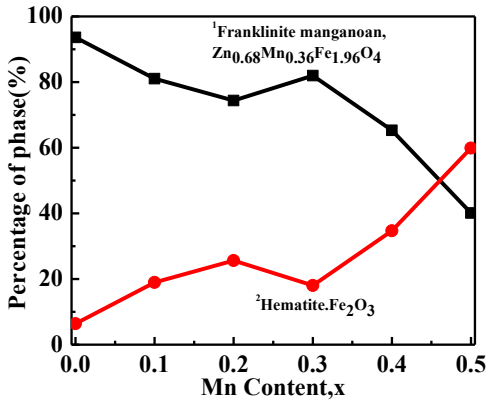

Figure 4.3 Franklinite and Hematite phase with Mn content of various $Fe_{2.5}Zn_{0.5-x}Mn_xO_4$ sintered at 1200˚C.

4.3 Lattice Constants of the polycrystalline $Fe_{2.5}Zn_{0.5-x}Mn_xO_4$

The values of lattice parameters, a_0, obtained from each crystal plane are plotted against Nelson-Riley function F (θ) = ½ [($\cos^2\theta/\sin\theta$) + ($\cos^2\theta/\theta$)] [4] where θ is the Bragg's angle and a straight line is obtained. The values of lattice parameters were estimated from the extrapolation of these lines to F(θ)=0. From a_0Vs F(θ) curve, accurate lattice constant, 'a_0' is calculated for each sample. Fig. 4.4 shows a_0 Vs F(θ) plot for $Fe_{2.5}Zn_{0.4}Mn_{0.1}O_4$.

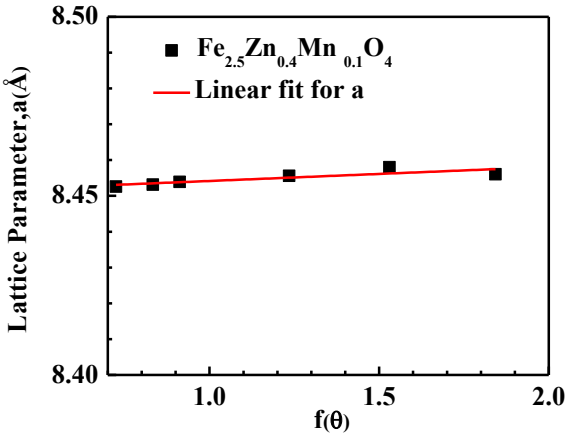

Fig.4.4. Variation of lattice parameter a_0 for $Fe_{2.5}Zn_{0.4}Mn_{0.1}O_4$ with F(θ)

The mean ionic radius of the variant ions for composition $Fe_{2.5}Z_{0.5-x}Mn_xO_4$ can be written as

$$r_{(variant)} = (0.5-x)r_{Zn}+xr_{Mn} \quad (1)$$

where r_{Zn} is the ionic radius of Zn^{2+} ion and r_{Mn} is the ionic radius of Mn^{2+}. The variation of $r_{(variant)}$ with Mn content is shown in Fig. 4.5, where it increases with increasing Mn content. It is clear from Fig. 4.5 that the lattice constant follows an increasing trend with respect to Mn contents. This increase of lattice constant with increase of Mn contents can be explained on the basis of the ionic radii. The ionic radii of the cations used in $Fe_{2.5}Zn_{0.5-x}Mn_xO_4$ are 0.89 Å (Mn^{2+}) and 0.74 Å (Zn^{2+}) [5]. Here Mn^{2+} is substituting by the Zn^{2+} ion. So a small increase in lattice constant is expected due to increasing Mn content. Also it is observed that the radius of the variant cations is increased with increase of Mn content.

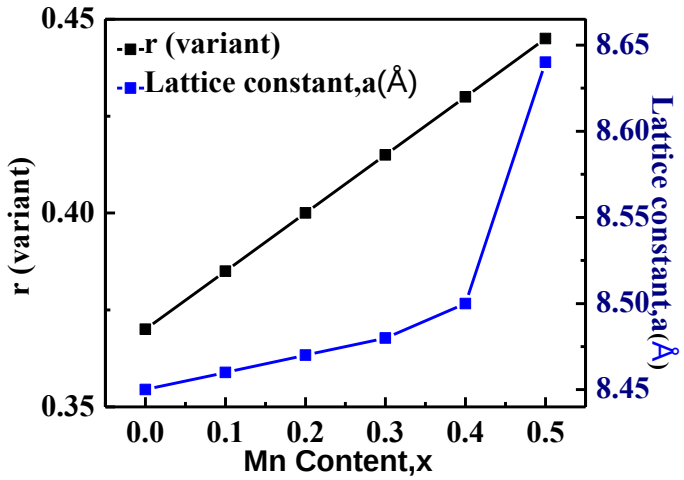

Fig.4.5 Variation of a_0 and $r_{(variant)}$ for various $Fe_{2.5}Zn_{0.5-x}Mn_xO_4$ sintered at 1200˚C in air.

The lattice constant, density, porosity, natural resonance frequency, maximum quality factor and initial permeability of the various $Fe_{2.5}Zn_{0.5-x}$ Mn_xO_4 sintered at different temperatures are given in Table 4.1.

Table 4.1.The lattice constant, density, porosity, natural resonance frequency, maximum Quality factor and initial permeability of the various $Fe_{2.5}Zn_{0.5-x}Mn_xO_4$ (x=0.0-0.5 in the step of 0.1) sintered at various temperatures with fixed dwell time 5h.

Mn Content x	**a_o (Å)**	**T_s (°C)**	**ρ_{th} (g/cm^3)**	**ρ_{exp} (g/cm^3)**	**P (%)**	**f_r (MHz)**	**Q_{max}**	**μ_i' (at 10 MHz)**
0.0	8.4541	1100	5.2	3.84	26	-	-	9
		1150		4.11	21	-	-	8
		1200		4.41	15	-	-	7
		1250		4.46	14	10	259	17
0.1	8.4623	1100	5.16	3.59	30	-	-	8
		1150		3.84	26	-	-	9
		1200		4.24	18	-	-	8
		1250		4.3	17	8	431	21
0.2	8.4722	1100	5.12	3.5	32	-	-	8
		1150		3.76	27	-	-	8
		1200		4.15	19	-	200	13
		1250		4.21	18	7	847	32
0.3	8.4815	1100	5.08	3.44	32	-	-	10
		1150		3.69	27	-	-	8
		1200		4.11	19	7	378	17
		1250		4.15	18	4	987	38
0.4	8.5016	1100	5.02	3.37	33	-	-	9
		1150		3.58	29	-	245	12
		1200		4.04	20	6.2	573	25
		1250		4.08	19	6	1013	33
0.5	8.6426	1100	4.96	3.32	33	-	-	10
		1150		3.51	29	-	830	11
		1200		3.99	20	9.5	488	18
		1250		4.03	19	9	400	18

Theoretical density, ρ_{th}, bulk density, ρ_B, and porosity, P, of the various $Fe_{2.5}Zn_{0.5-x}Mn_xO_4$ are tabulated in the Table 4.1. The ρ_{th} decreases with increasing a_o in the Mn substituted various $Fe_{2.5}Zn_{0.5-x}Mn_xO_4$. Both ρ_{th} and ρ_B decrease in a similar fashion with the increase of Mn content (x) .

4.4 Microstructural analysis of the polycrystalline $Fe_{2.5}Z_{0.5-x}Mn_xO_4$

The FESEM micrographs of various $Fe_{2.5}Zn_{0.5-x}Mn_xO_4$ sintered at 1100, 1150, 1200 and 1250˚C are shown in Fig. 4.6. From these micrographs it is revealed that Mn^{2+} substitutions have significant influence on microstructures of Mn-Zn ferrites. The average grain size increases gradually with increase of Mn^{2+} may be due to the fact that $MnCO_3$ decomposed with the release of CO_2 at 200^0C to produce manganese (II) Oxide and melting point of MnO (1650˚C) is less than that of ZnO (1975˚C). Also as a unit of Mn substitution a new solid solution is found. Chemical preparations of this new solid solution change with increase Mn content. It has been seen that the average grain size is highest for $Fe_{2.5}Mn_{0.5}O_4$. It also noticed that the grain size of all samples increases with the sintering temperatures; T_s porosity follows the opposite trend. It is also observed that those increasing trend of grain diameter and decreasing trend of porosity have impact on density, permeability, real quality factor and loss factor. Grain boundary of various $Fe_{2.5}Zn_{0.5-x}Mn_xO_4$ turns unclear at higher T_s, i.e. at 1200 and 1250˚C, where porosity seems to be suppressed. Density, permeability, real quality factor are higher at those T_s rather than other T_s. Porosity and loss factor are lower at those T_s rather than other T_s. Some cluster form of grain is found at T_s 1100˚C which is much clear for $Fe_{2.5}Zn_{0.1}Mn_{0.4}O_4$, but at higher T_s cluster form turns isolated. $Fe_{2.5}Zn_{0.1}Mn_{0.4}O_4$ shows higher permeability, real quality factor and lower loss factor than other samples.

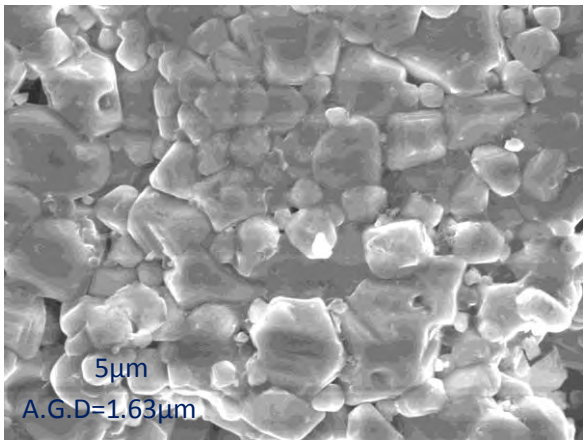

x=0.0

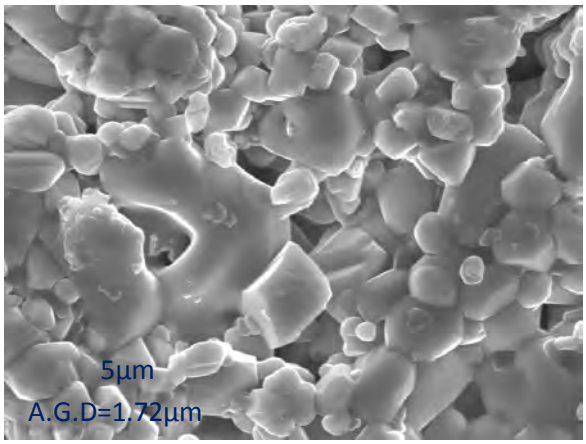

x=0.1

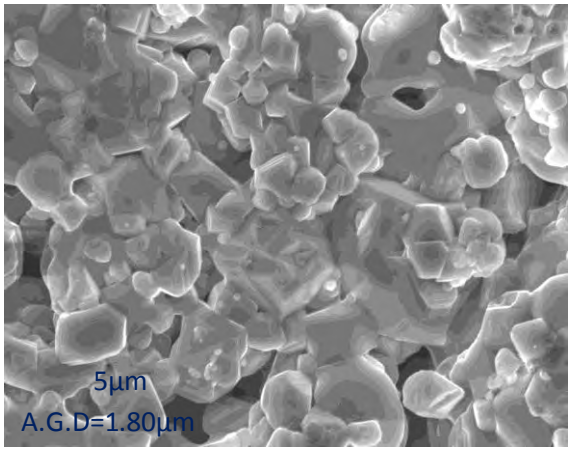

x=0.2

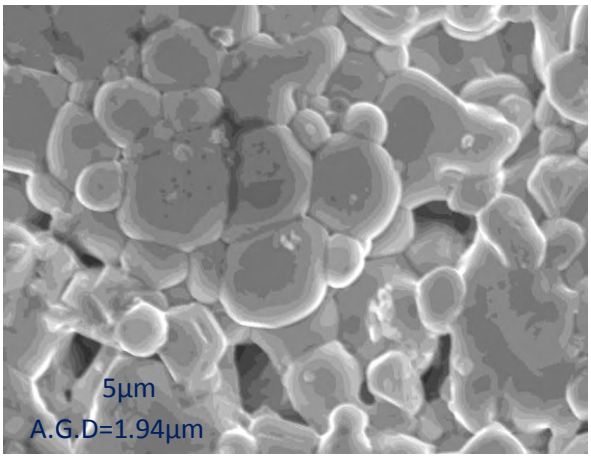

x=0.3

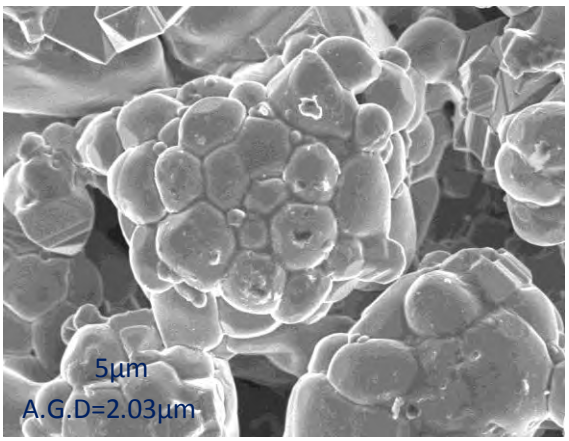

x=0.4

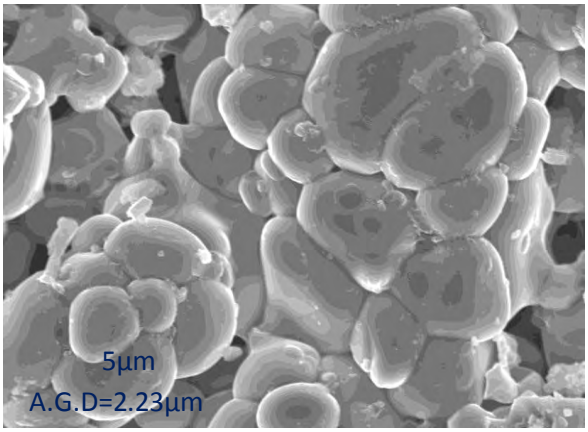

x=0.5

Fig. 4.6.a The optical micrographs of various $Fe_{2.5}Zn_{0.5-x}Mn_xO_4$ sintered at temperature 1100 ˚C.

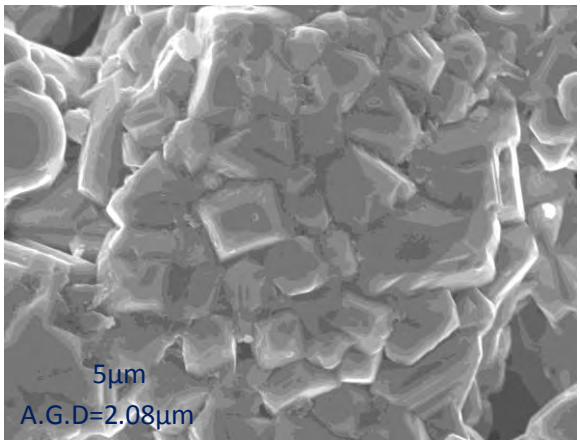

x=0.0

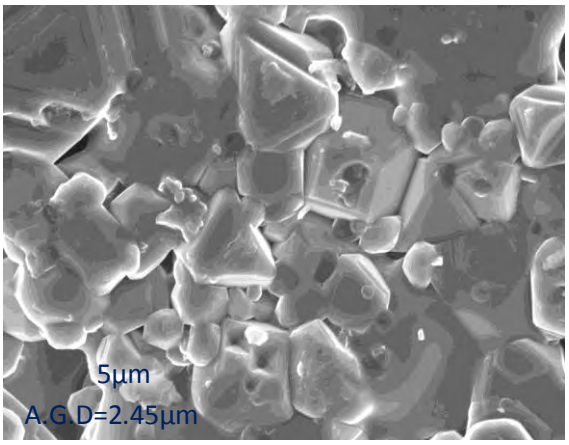

x=0.1

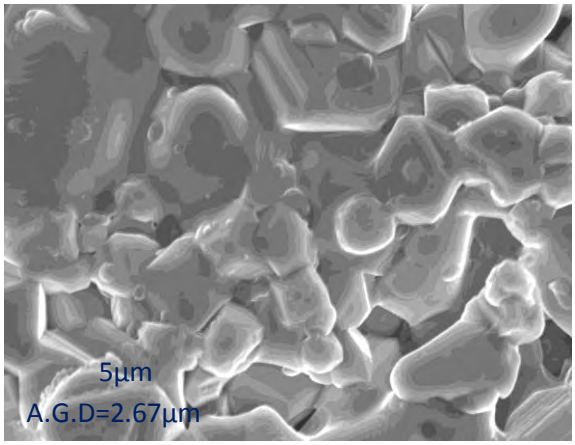

x=0.2

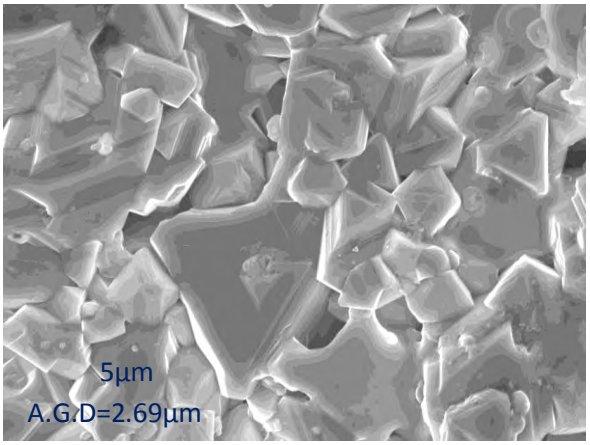

x=0.3

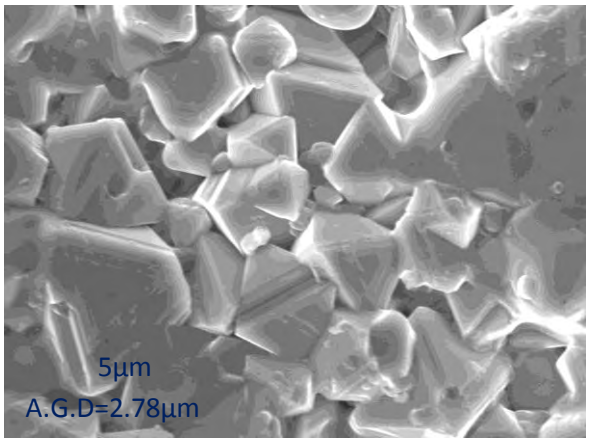

x=0.4

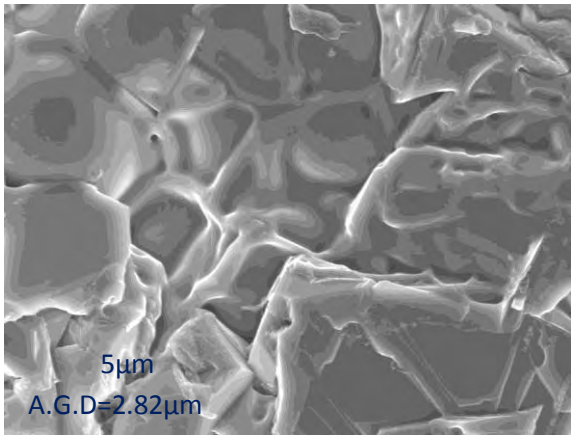

x=0.5

Fig. 4.6.b The optical micrographs of various $Fe_{2.5}Zn_{0.5-x}Mn_xO_4$ sintered at temperature 1150 ˚C.

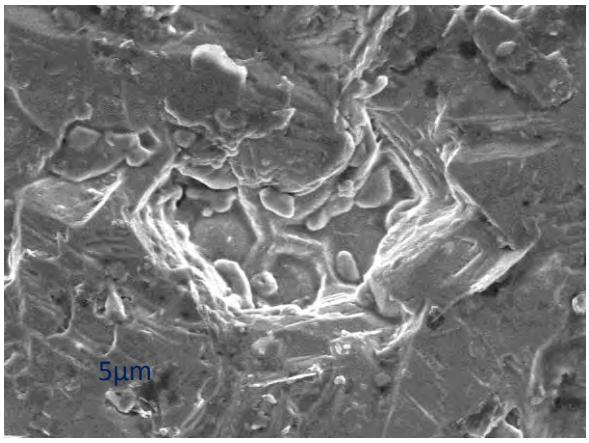

x=0.0

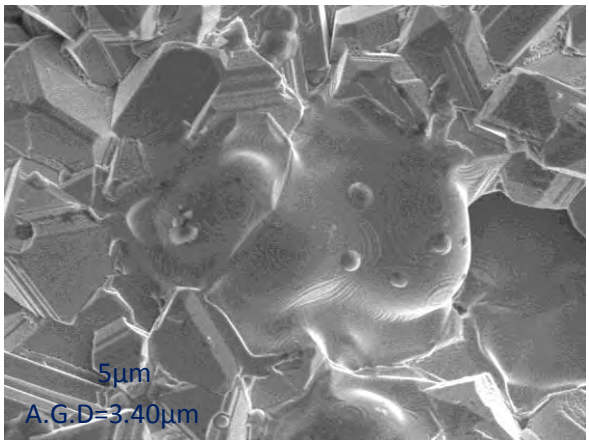

x=0.1

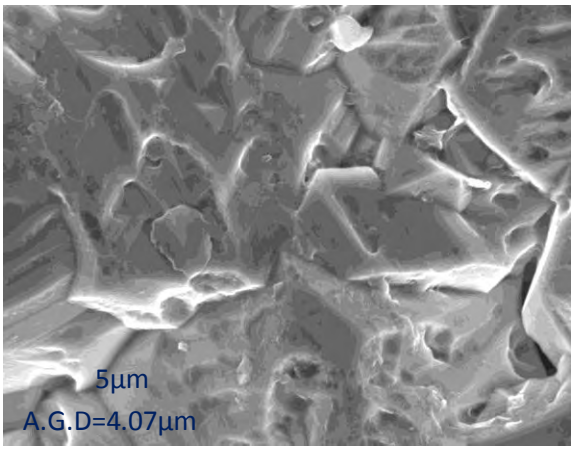

x=0.2

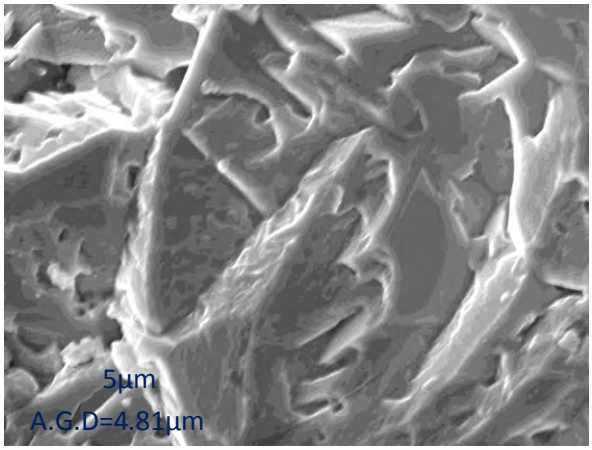

x=0.3

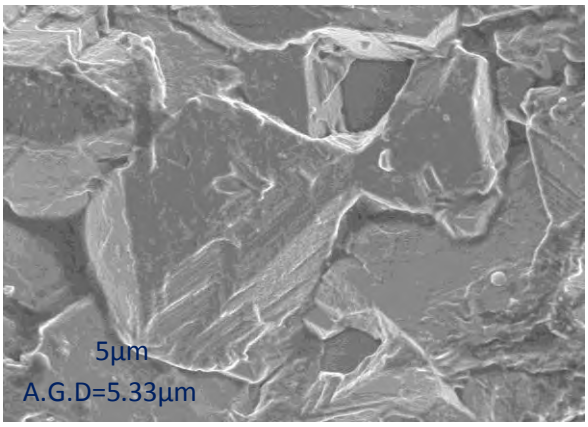

x=0.4

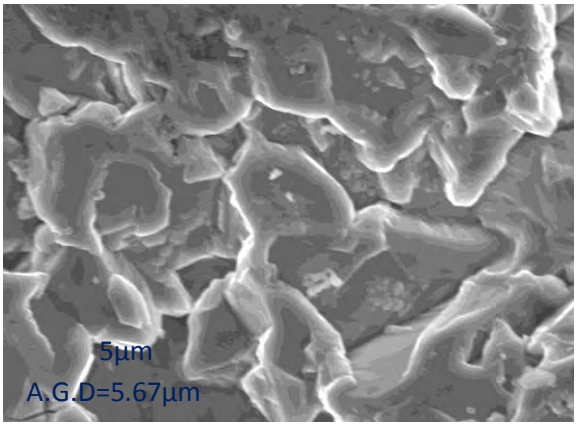

x=0.5

Fig. 4.6.c The optical micrographs of various $Fe_{2.5}Zn_{0.5-x}Mn_xO_4$ sintered at temperature 1200 ˚C.

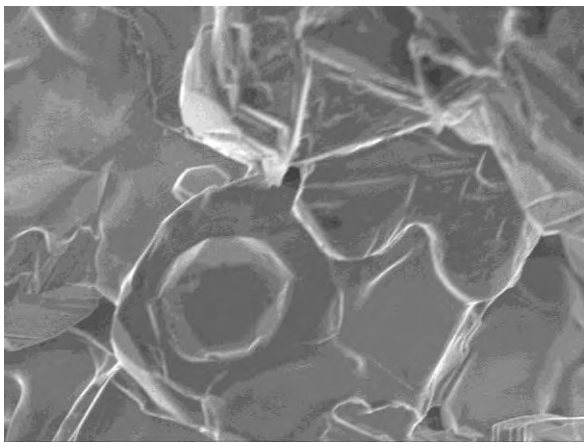

x=0.0

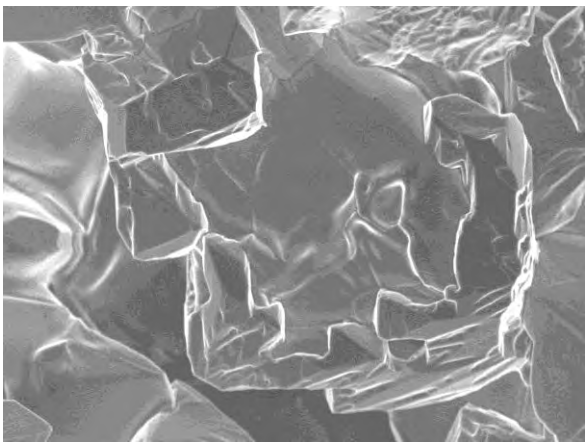

x=0.1

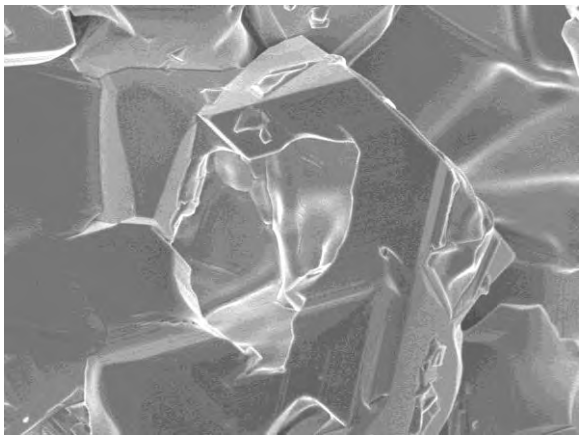

x=0.2

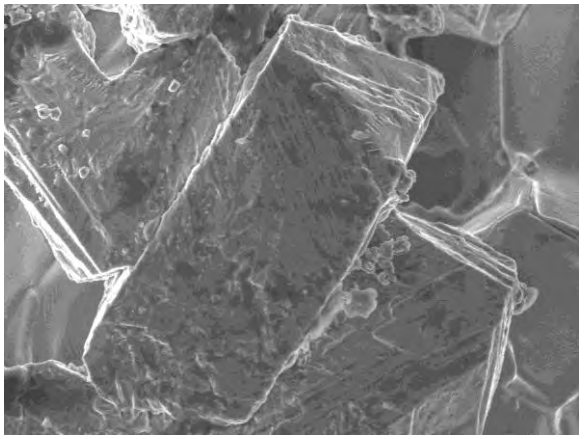

x=0.3

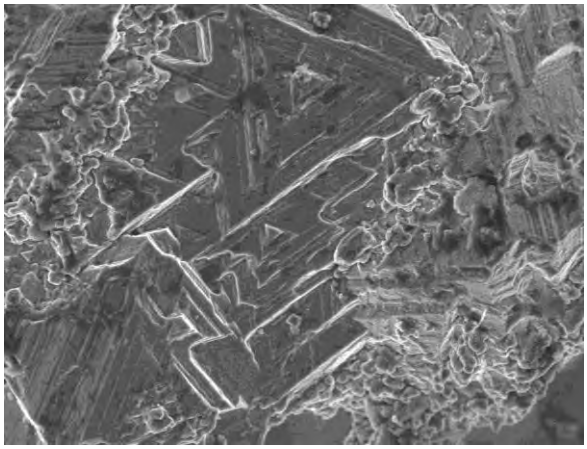

x=0.4

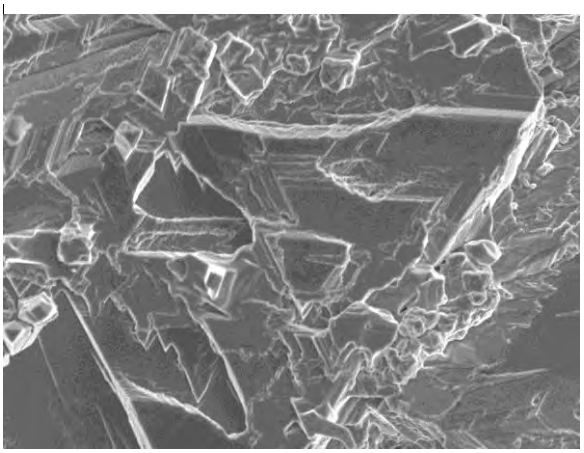

x=0.5

Fig. 4.6.d The optical micrographs of various $Fe_{2.5}Zn_{0.5-x}Mn_xO_4$ sintered at temperature 1250 ˚C.

4.5 Density and porosity of the polycrystalline $Fe_{2.5}Zn_{0.5-x}Mn_xO_4$

Density plays a key role in controlling the properties of polycrystalline ferrites. A significant decrease in the bulk density is observed with the Mn content. Fig 4.7 indicates that as Mn content increases in $Fe_{2.5}Zn_{0.5-x}Mn_xO_4$, density decreases.

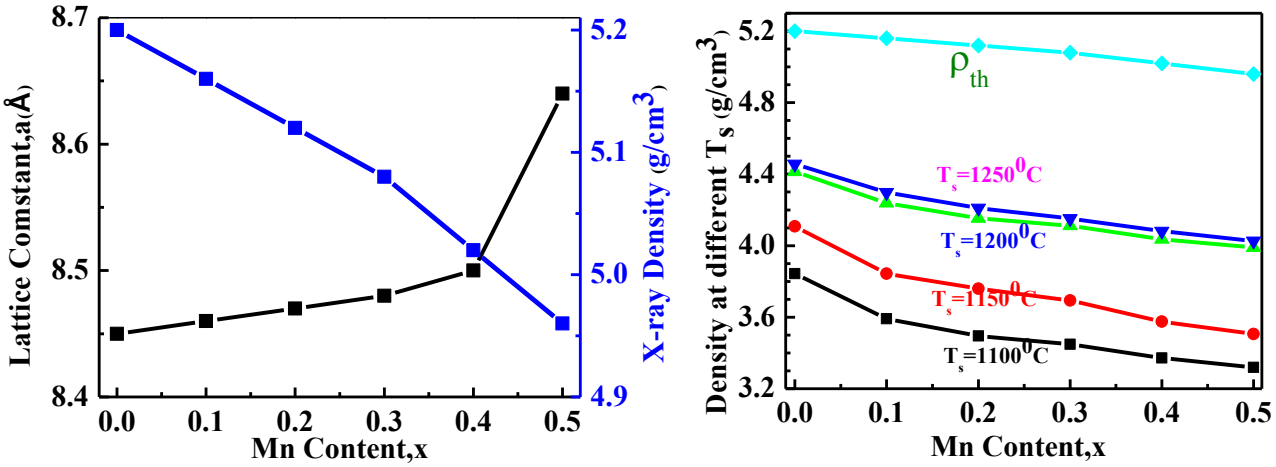

Fig.4.7 (a) The variation of Theoretical density, ρ_{th} and lattice constant, a_o(Å) with Mn content, x.(b) Theoretical density, ρ_{th} and bulk density, ρ_B with Mn content, x and different T_s for various $Fe_{2.5}Zn_{0.5-x}Mn_xO_4$.

It is known that the porosity of the ceramic samples results from two sources, intragranular porosity and intergranular porosity. When the grain growth rate is very high, pores may be left behind by rapidly moving grain boundaries, resulting in pores that are trapped inside the grains. This intragranular porosity leads to poor magnetic and mechanical properties. Thus the total porosity could be written as $P=P_{intra}+P_{inter}$. The intergranular porosity mainly depends on the grain size [8].

Fig 4.8 indicates that as Mn content increases in $Fe_{2.5}Zn_{0.5-x}Mn_xO_4$, density decreases and porosity increases. It is possible to explain this phenomenon in terms of the atomic weight and volume of the contents. As atomic mass of Mn is 54.938 and Zn is 65.38, where The ionic radii of the cation Mn^{2+} is 0.89 Å and Zn^{2+} is 0.74 Å densities are decreased for Mn substitution instead of Zn.

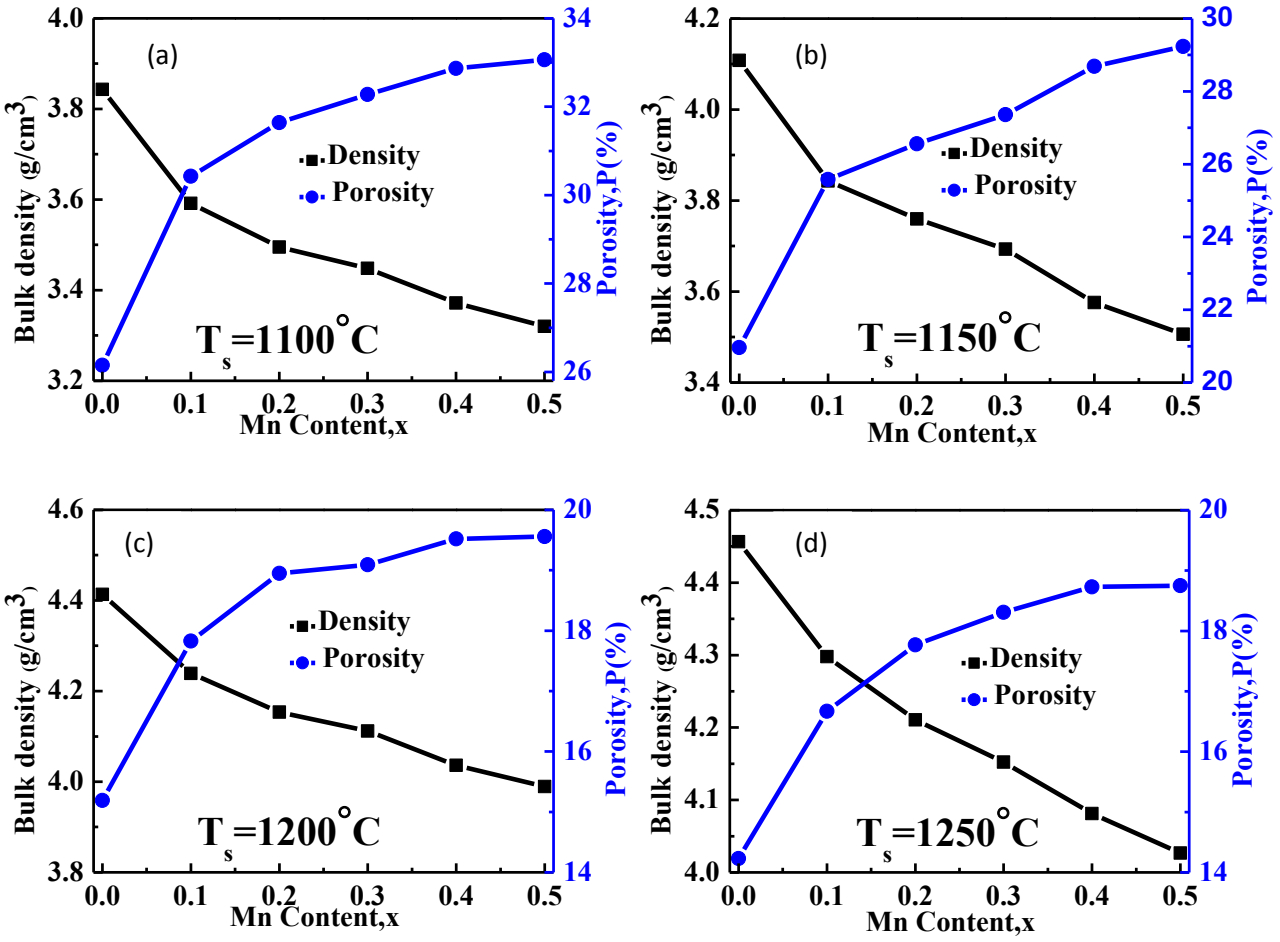

Fig.4.8 The variation of ρ_B and P (%) with Mn content, x for $Fe_{2.5}Zn_{0.5-x}Mn_xO_4$ sintered at (a) 1100, (b) 1150, (c) 1200 and (d) 1250°C in air.

Fig.4.9 shows the variation of ρ_B and P (%) with the variation of T_s for $Fe_{2.5}Zn_{0.5-x}Mn_xO_4$. Here volume of sample is decreasing with sintering temperature so density increases. Also for rising temperature trapped Oxygen is removed so density increases. During the sintering process, the thermal energy generates a force that drives the grain boundaries to grow over pores, thereby decreasing the pore volume and increasing density of the materials. For all content same trend is shown clearly.

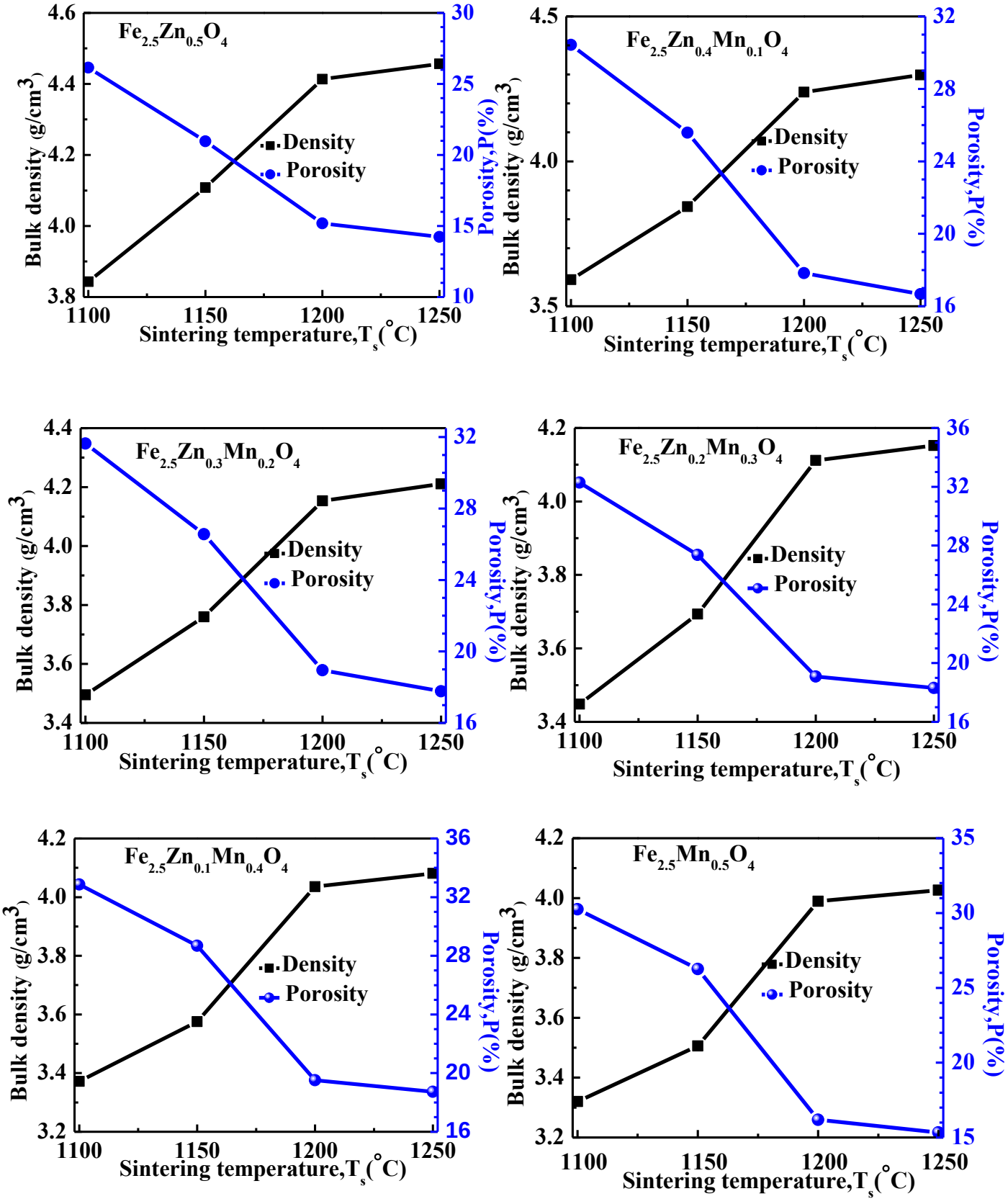

Fig.4.9 The variation of density and porosity for $Fe_{2.5}Zn_{0.5-x}Mn_xO_4$(x=0.0-0.5 in the step of 0.1)

4.6 Complex permeability of the polycrystalline$Fe_{2.5}Zn_{0.5-x}Mn_xO_4$

Initial permeability, μ_i of a magnetic material is an important parameter from the application point of view. Therefore the study of μ_i has been a subject of great interest from both the theoretical and practical points of view. The optimization of the dynamic properties such as complex permeability in the high frequency range requires a precise knowledge of the magnetization mechanisms involved [9,10].The magnetization mechanisms contributing to, $\mu_i = \mu_i^{/} - \mu_i^{//}$, in soft polycrystalline ferrites have been a controversial subject for a long time and can't be understood satisfactorily. Although it is admitted that two mechanisms are involved in this phenomenon, the domain wall displacement and the spin rotation in the domains.

μ_i has been calculated as a function of frequency up to 10 KHz-120 MHz at room temperature for all the samples of the series $Fe_{2.5}Zn_{0.5-x}Mn_xO_4$ by using the conventional technique based on the determination of the complex impedances of a circuit loaded with toroid shaped sample. A variation of $\mu_i^{/}$ and $\mu_i^{//}$ values for T_s for all compositions is observed. $\mu_i^{/}$ and $\mu_i^{//}$ increases with Mn substitution up to x=0.30 for T_s =1100 and 1250°C and x=0.40 for T_s =1150 and 1200°C in $Fe_{2.5}Zn_{0.5-x}Mn_xO_4$ and then the value of substitution permeability decrease. In contrast resonance frequency is found to decrease with Mn substitution. All samples show independence of frequency in their $\mu_i^{/}$ values up to the resonance frequency. Moreover, a sharp decrease in $\mu_i^{/}$ and increase in $\mu_i^{//}$ above the resonance frequency was noticed.

Fig.4.10 shows The variation of, $\mu_i^{/}$ for $Fe_{2.5}Zn_{0.5-x}Mn_xO_4$ (x=0.0-0.5 in the step of 0.1) sintered at 1100, 1150,1200 and 1250˚C in air.

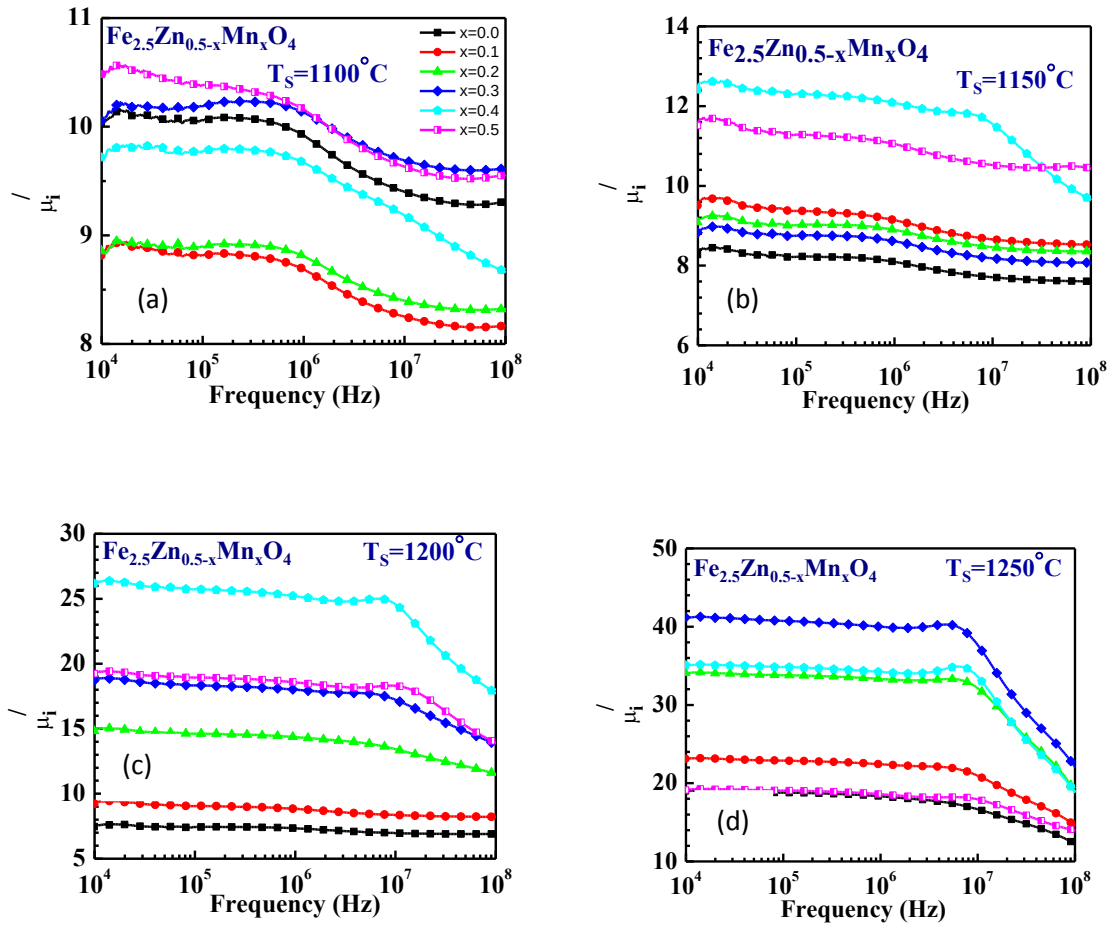

Fig.4.10 The variation of $\mu_i^{/}$ for $Fe_{2.5}Zn_{0.5-x}Mn_xO_4$ sintered at (a) 1100,(b) 1150,(c) 1200 and (d)1250˚C in air.

Fig.4.11 shows The variation of $\mu_i^{/}$ and $\mu_i^{//}$ with Mn content for $Fe_{2.5}Zn_{0.5-x}Mn_xO_4$ sintered at 1100,1150,1200 and 1250˚C in air and Fig.4.12 shows The variation of $\mu_i^{/}$ with T_s for $Fe_{2.5}Zn_{0.5-x}Mn_xO_4$.

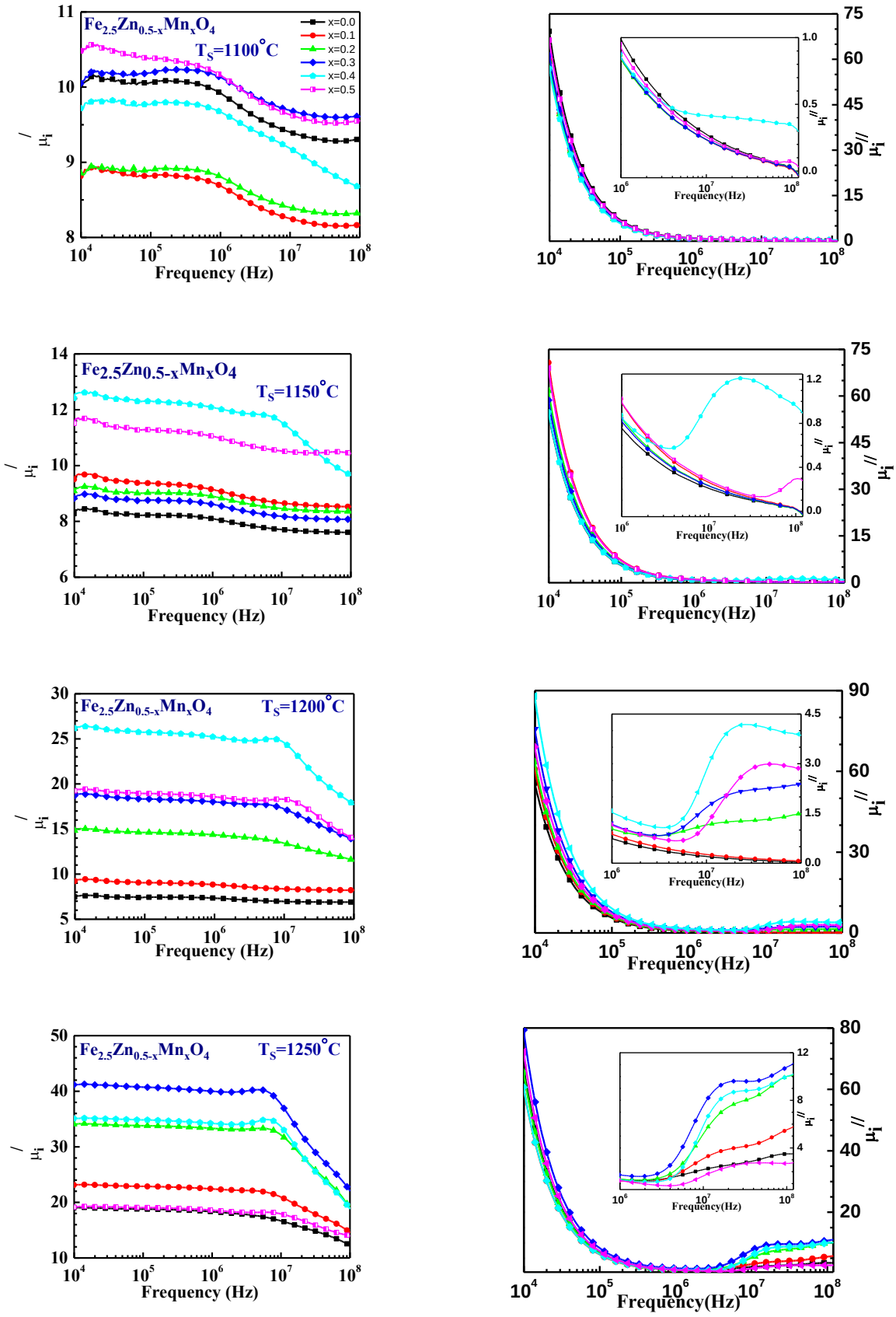

Fig.4.11 The variation of $\mu_i^{/}$ and $\mu_i^{//}$ with Mn content, x for $Fe_{2.5}Zn_{0.5-x}Mn_xO_4$ sintered at 1100, 1150, 1200 and 1250˚C in air.

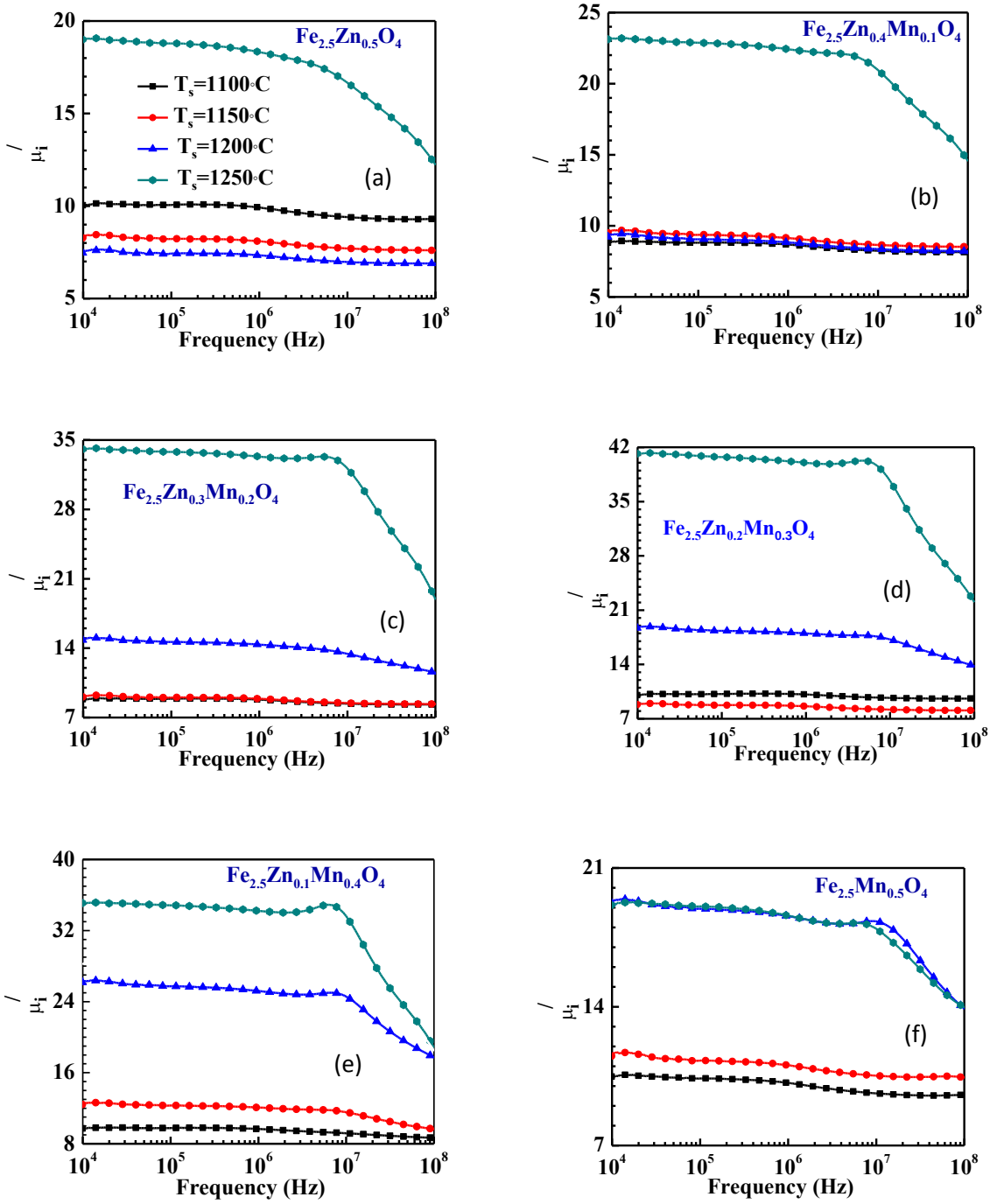

Fig.4.12 The variation of $\mu_i^{/}$ with T_S for $Fe_{2.5}Zn_{0.5-x}Mn_xO_4$, (a)x=0.0, (b) x=0.1,(c) x=0.2, (d)x = 0.3,(e)x= 0.4 and (f)x = 0.5.

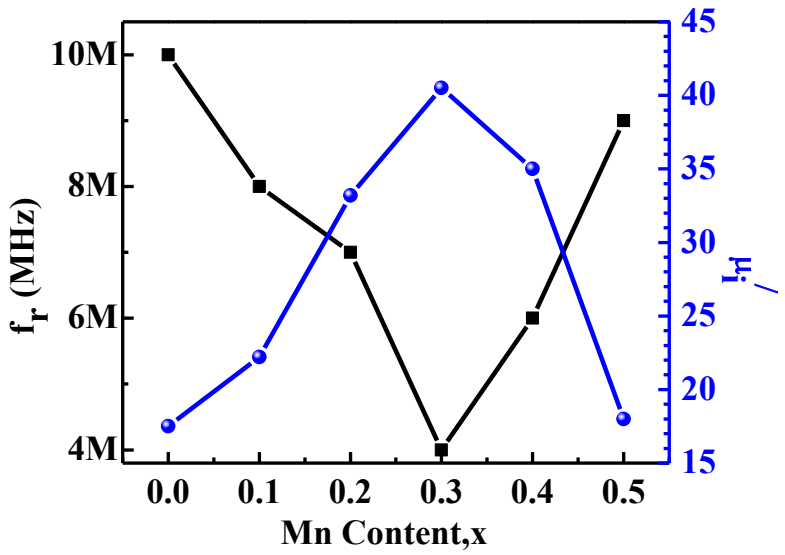

Fig.4.13 Variation of f_r and μ_i' with Mn content, x.

Fig 4.13 shows the Variation of f_r and μ_i' with *Mn* content (x) for $Fe_{2.5}Zn_{0.5-x}Mn_xO_4$ sintered at 1250 ˚C in air. In this figure it is found that as μ_i' increases then f_r decreases with the function of sintering temperature. An inversely proportional relation of μ_i' and f_r confirms the Snoek's limit [8]. Similar trend is observed for all other sintering temperatures.

The whole permeability phenomena can be explained as below .The permeability of polycrystalline ferrite is related to two different magnetizing mechanisms: spin rotation and domain wall susceptibility; χ_{spin} is intrinsic rotational susceptibility. χ_w and χ_{spin} may be written as : $\chi_w = 3\pi M_s^2 D/4\gamma$ and $\chi_{spin} = 2\pi M_s^2/K$ with M_s saturation magnetization, K the total anisotropy, D the average grain diameter, and γ the domain wall energy. In the present system room temperature DC magnetization value varying to Mn content increases up to x= 0.40 and start to decrease at x=0.40. Since μ_i' is a function of magnetization therefore, μ_i' increases with the increase of Mn content up to x=0.40 and beyond x=0.40, μ_i' decreases due to the non collinear spin arrangements [11]. Moreover, the magnetic properties of soft ferrite

are strongly influenced by its composition, additives and microstructures of the material. Among all these factors, the microstructures have great influence on magnetic properties. It is generally believed that larger the grain sizes, the higher the saturation magnetization and initial permeability. In microstructure studies of the present ferrite system, is also observed that average grain diameter increases with the function of Mn content.Therefore in the present case, variation of the initial permeability is strongly influenced by its grain size.

The increasing value of μ_i' with the increase of sintering temperature up to the 1250˚C is due to the lower porosity for samples sintered at higher sintering temperature. The porosity causes hindrance to the domain wall motion. As pores and voids are reduced with increasing sintering temperature.

The variation of initial permeability μ_i, with f_r, shown in Fig. 4.13 can be explained on the basis of Globus model. According to this model, the relaxation character is

$$(\mu_i - 1)^2 f_r = \text{constant.} \qquad (2)$$

μ_i in ferrites is due to domain wall displacement and remains constant with frequency as long as there is no phase lag between the applied field and the domain wall displacement. In ferrites, two resonance peaks are normally observed: one at lower frequency (10-120MHz) which is due to the domain wall oscillations [12,13] and the other at higher frequencies (~1GHz) due to Larmour precession of electron spins [14]. In the present case, the f_r of domain wall oscillations is found in the range of 4 MHz~10 MHz.

Fig.4.14 shows μ_i' Vs Mn Content, x graph at different Frequencies(1MHz, 5MHz, 10MHz and15MHz) for $Fe_{2.5}Zn_{0.5-X}Mn_XO_4$,.This shows that highest initial permeability is gained at x=0.3 for sintering temperature 1250^0C.

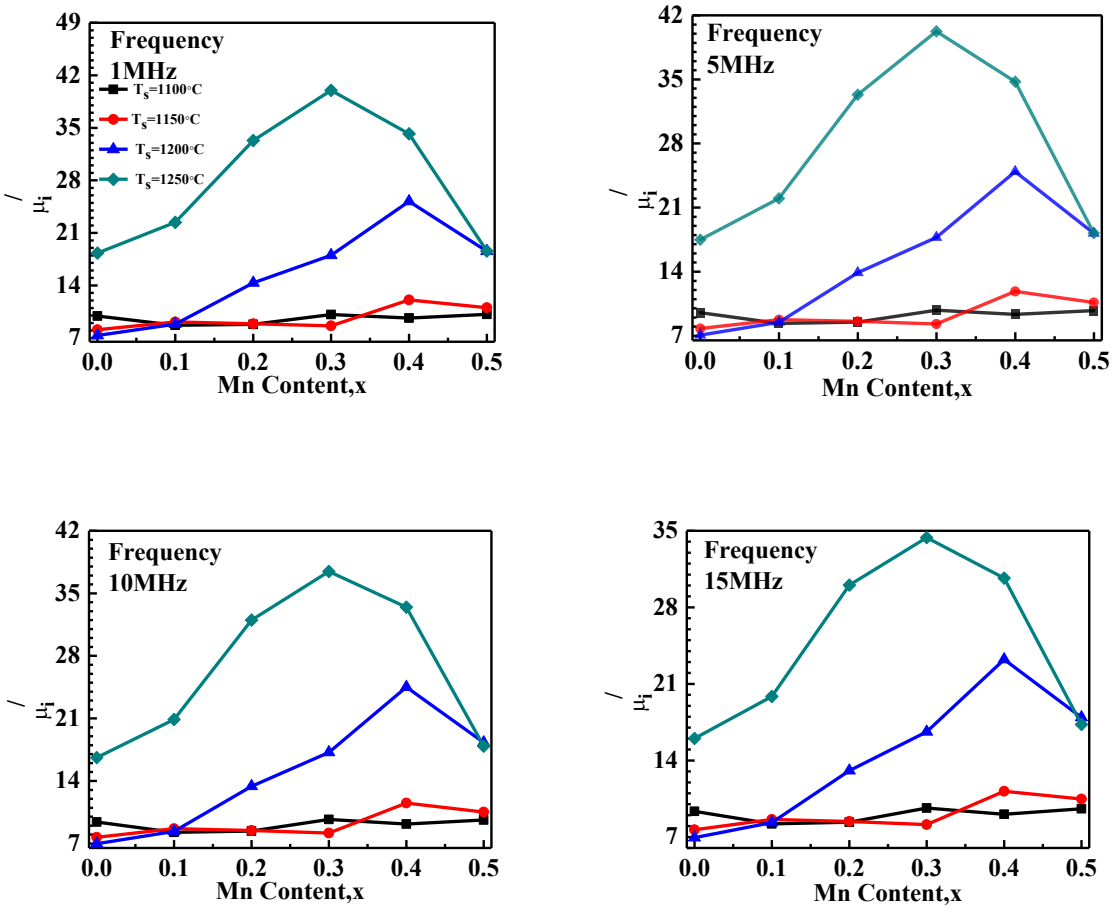

Fig.4.14 $\mu_i^{/}$ Vs Mn Content, x graph at different Frequency (a) 1MHz, (b) 5MHz, (c) 10MHz and (d)15MHz for $Fe_{2.5}Zn_{0.5-x}Mn_xO_4$.

4.7 loss factor of the polycrystalline $Fe_{2.5}Zn_{0.5-x}Mn_xO_4$

Energy loss is an extremely important subject in soft ferrimagnetic materials, since the amount of energy wasted on process other than magnetization can prevent the AC applications of a given material. The ratio of $\mu_i^{//}$ and $\mu_i^{/}$ representing the losses in the material are a measure of the inefficiency of the magnetic system. Obviously this parameter should be as low as possible. The magnetic losses, which cause the phase shift, can be split up into three components: hysteresis losses, eddy current losses and residual losses. This

gives the formula $\tan\delta_m = \tan\delta_h + \tan\delta_e + \tan\delta_r$. The μ_i is related to low applied magnetic field. Hysteresis losses vanish at very low field strengths. Thus at low field the remaining magnetic losses are due to eddy current losses and residual losses. Residual losses are independent of frequency. Eddy current losses increase with frequency and are negligible at very low frequency. Eddy current loss can be expressed as $P_e \approx f^2/\rho$, where P_e is the energy loss per unit volume and ρ is the resistivity [6, 7]. To keep the eddy current losses constant as frequency is increased; the resistivity of the material chosen must increase as the square of frequency. Eddy currents are not problem in the Mn-Zn ferrites until higher frequencies are encountered because they have very high resistivity about $10^5 \Omega cm$ to $10^8 \Omega cm$ [6]. The ferrite microstructure is assumed to consist of grains of low resistivity separated by grain boundaries of high resistivity. Thicker grain boundaries are preferred to increase the resistance.

The variations of loss factors with frequency of different compositions of the samples sintered at different T_s is observed. Loss factors are minimum for frequency up to 1≈10 MHz (depending on compositions and T_s).The loss factor is also observed that, at higher sintering temperature loss factor is low at low frequency (up to 1MHz) and increase gradually at higher frequency (after 10MHz) with the increase of sintering temperature.

At higher frequencies, a rapid increase in loss factor is observed. A resonance loss peak is shown in this rapid increase of magnetic loss. At the resonance, maximum energy transfer occurs from the applied field to the lattice which results the rapid increases in loss factor. As it is observed that phase lag between domain rotation and applied field is greater than that between applied field and domain wall displacement, the magnetic losses due to domain rotation overrides those due to domain wall displacement [15].

Fig.4.15 shows the variations of loss factors with frequency for $Fe_{2.5}Zn_{0.5-x}Mn_xO_4$ sintered at 1100, 1150, 1200 and 1250 ˚C.

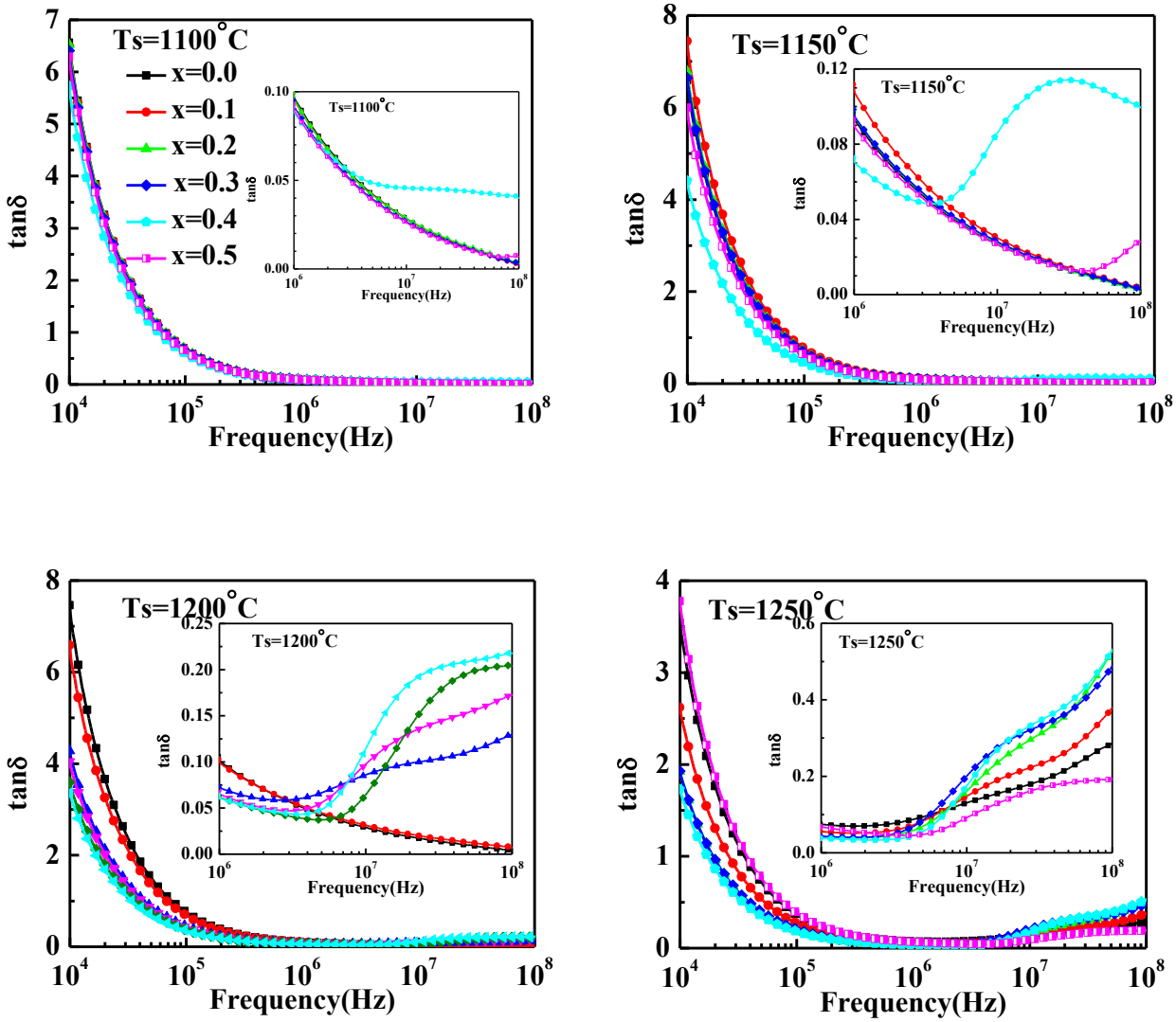

Fig.4.15 The variations of Loss factor with frequency for $Fe_{2.5}Zn_{0.5-x}Mn_xO_4$ sintered at (a) 1100, (b) 1150, (c) 1200 and (d) 1250^0C in air.

Fig.4.16 shows the variations of loss factors Vs frequency with Mn content for $Fe_{2.5}Zn_{0.5-x}Mn_xO_4$ (x=0.0-0.5 in the step of 0.1) sintered at 1100, 1150, 1200 and 1250˚C in air.

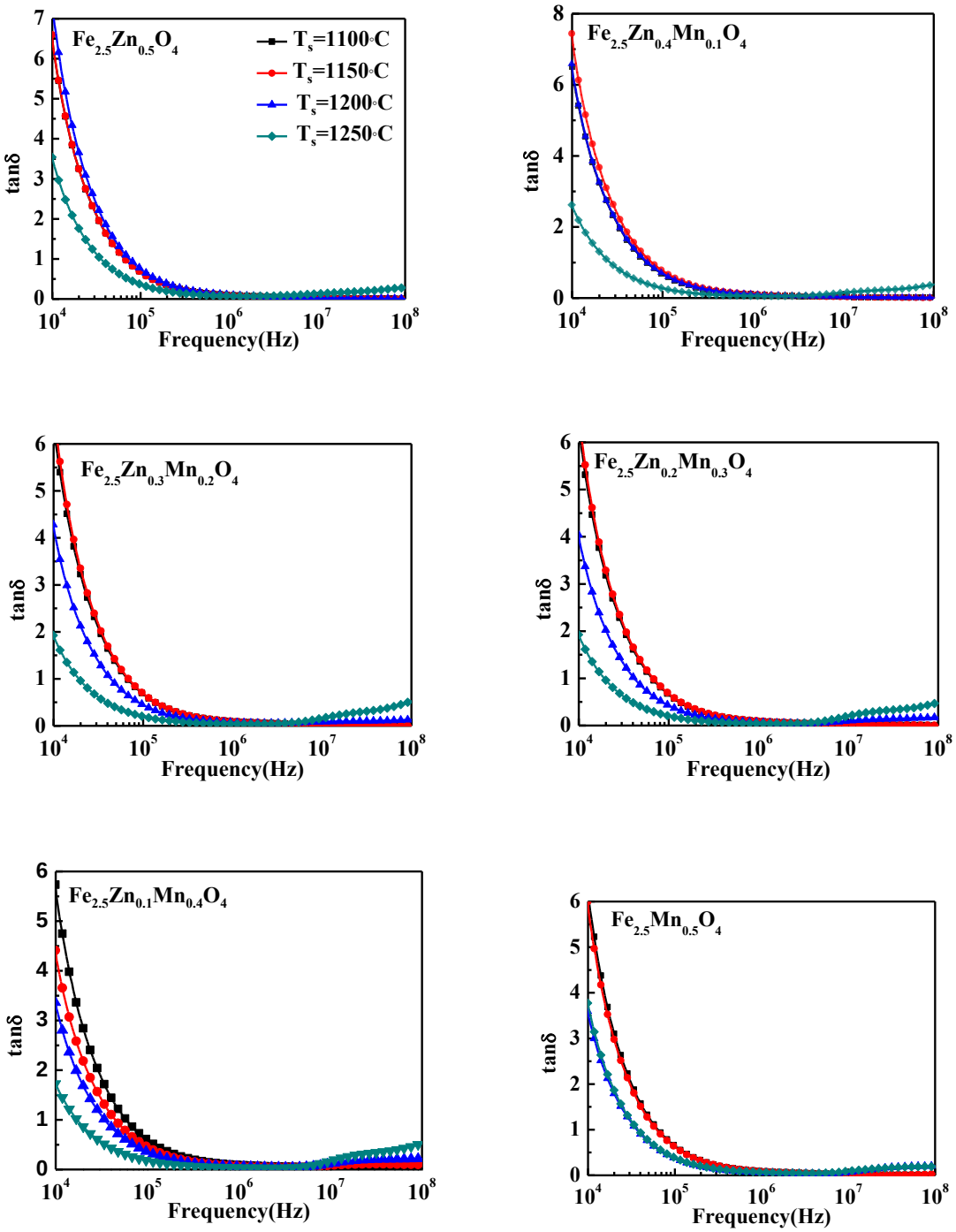

Fig.4.16 The variations of Loss factor with frequency for $Fe_{2.5}Zn_{0.5-x}Mn_xO_4$ sintered at 1100, 1150, 1200 and 1250^0C in air,(a)x=0.0, (b) x=0.1,(c) x=0.2,(d)x = 0.3 (e)x= 0.4and (f)x = 0.5.

4.8 Relative quality factor of the polycrystalline $Fe_{2.5}Zn_{0.5-x}Mn_xO_4$

From the loss factor, the relative quality factor (or Q-factor) is calculated. The Q-factor versus frequency plots of all the samples sintered at 1100, 1150, 1200 and 1250˚C are shown

in Fig. 4.17. It can be seen that the value of Q-factor increases with an increase of frequency and shows a peak around 1≈10MHz. It is also observed from the Fig 4.17(d) that the maximum value of Q-factor, Q_{max} increases with increasing Mn contents from x=0 to x=0.40 in $Fe_{2.5}Zn_{0.5-x}Mn_xO_4$, then it decreases. Similar variation is observed for $Fe_{2.5}Zn_{0.5-x}Mn_xO_4$ sintered at other temperatures as well. It shows a similar trend of $\mu_i^{/}$ of the present system as it is proportional to the Q-factor from the relation: $Q=\mu_i^{/}/\tan\delta$, as loss factor also shows an increasing trend with the increase of Mn content. Among all the studied samples, highest value of Q-factor (=1013) is observed for $Fe_{2.5}Zn_{0.10}Mn_{0.40}O_4$ sintered at 1250˚C, similar to $\mu_i^{/}$.

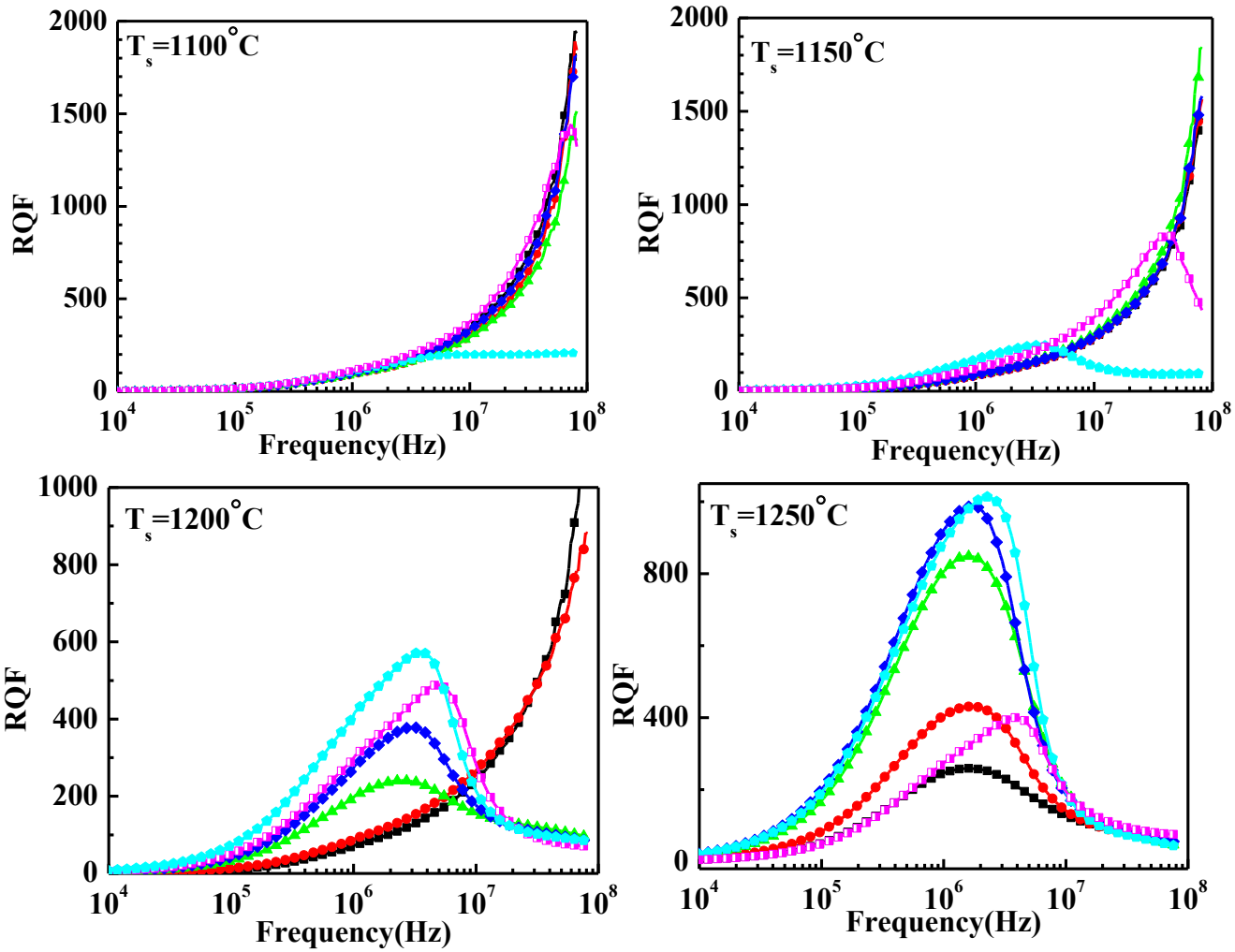

Fig.4.17 The variations of Q factors with frequency for $Fe_{2.5}Zn_{0.5-x}Mn_xO_4$ sintered at (a) 1100, (b) 1150 (c) 1200 and (d) 1250˚C in air.

Fig.4.18 shows the variations of Quality factors Vs frequency with Mn content for $Fe_{2.5}Zn_{0.5-x}Mn_xO_4$ (x=0.0-0.5 in the step of 0.1) sintered at 1100, 1150, 1200 and 1250˚C in air.

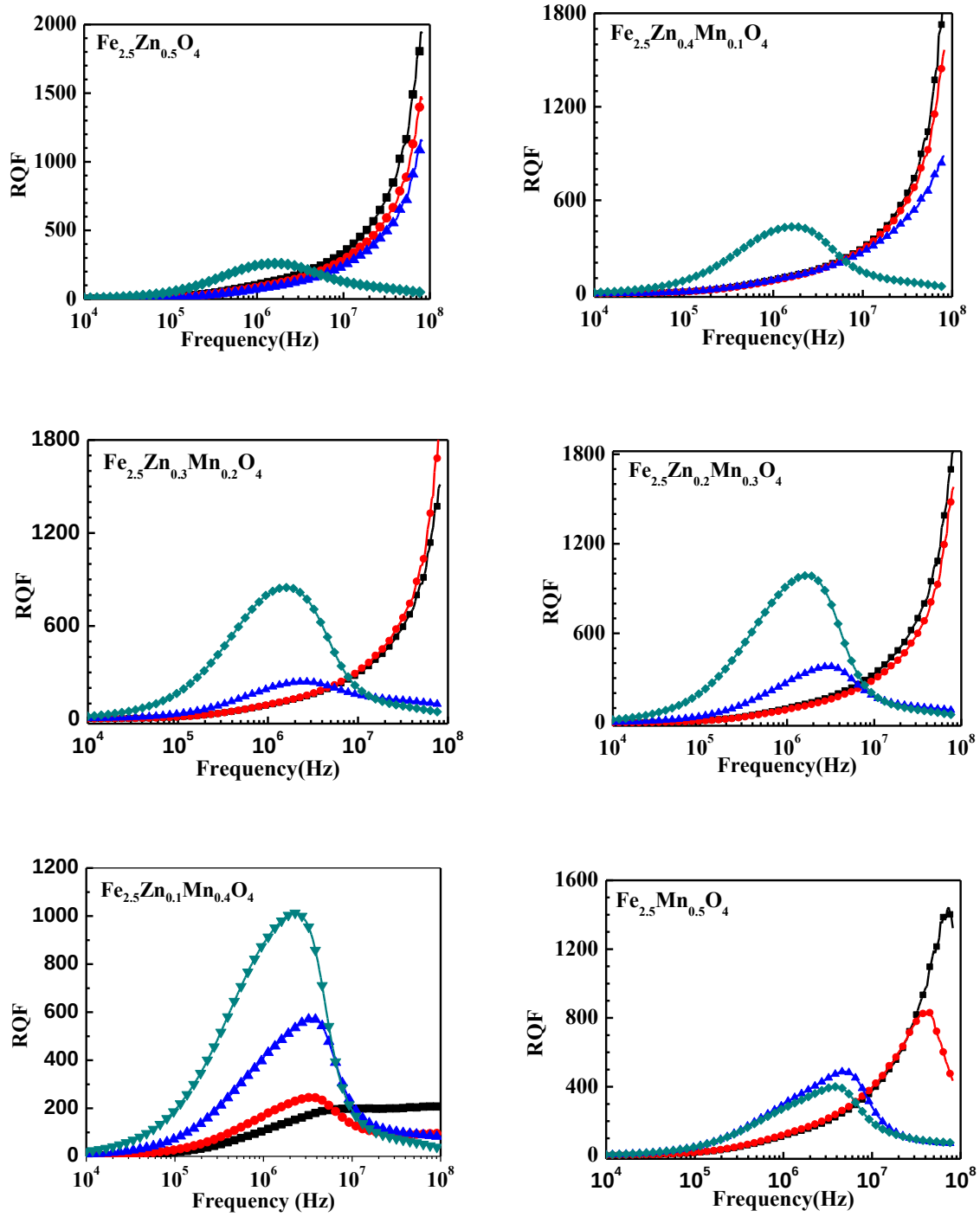

Fig.4.18 The variations of Q factor with frequency for $Fe_{2.5}Zn_{0.5-x}Mn_xO_4$ sintered at 1100, 1150, 1200 and 1250^0C in air (a) x=0.0, (b) x=0.1, (c) x=0.2, (d) x = 0.3, (e) x= 0.4 and (f) x = 0.5.

Fig 4.19 (b) shows the variation of Q value for $Fe_{2.5}Zn_{0.10}Mn_{0.40}O_4$ varying sintering temperatures .

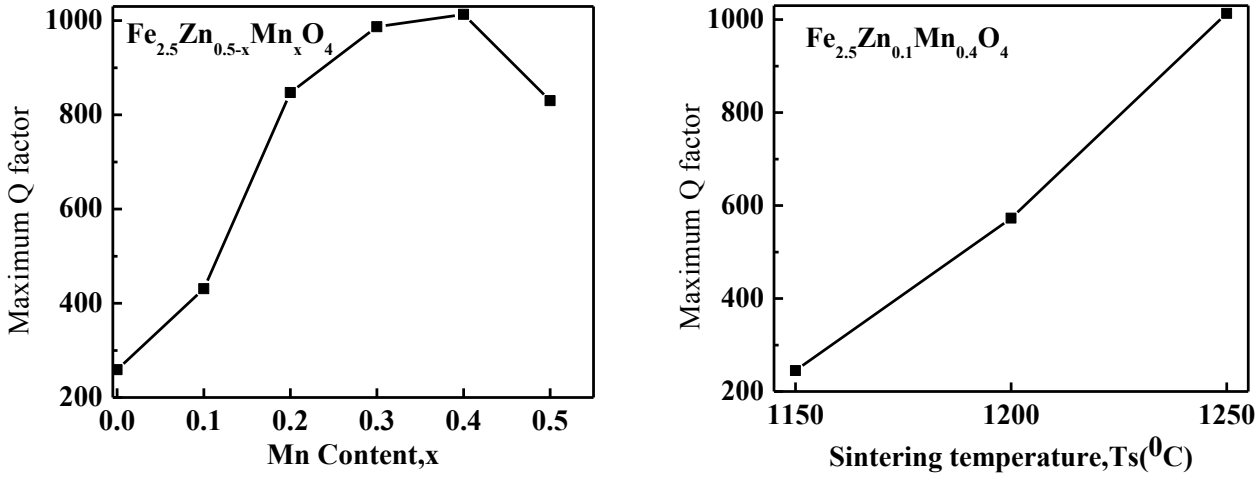

Fig.4.19(a) The variations of Q_{max} with Mn content for $Fe_{2.5}Zn_{0.5-x}Mn_xO_4$ and (b) the variations of $Q_{max}$for $Fe_{2.5}Zn_{0.10}Mn_{0.40}O_4$ sintered at 1100, 1150, 1200 and 1250˚C.

References:

[1] Doriguetto, A. C., Femandes, N.G., Calculated from ICSD using POWD 12++, ActaCrystallogr., Sec. C., volume 55,page 1751 (1999)

[2] Natl. Bur. Stand. (U.S.) Monogr. 25. volume 18,page 37 (1981) CAS Number:1309-37-1.

[3] Hossain, A. K. M. Akhter, Seki, M., Kawai, T. and Tabata, H., "Colossal magneto resistance in spinel type $Zn_{1-x}Ni_xFe_2O_4$", Journal of Applied Physics, Vol-96, pp 1273-1275, 2004.

[4] Nelson, J. B., Riley, D. P., 'An experimental investigation of extrapolation methods in the derivation of accurate unit-cell dimensions of crystals", Proc. Phys. Soc. London, Vol. 57, pp160, 1945.

[5] Whittaker, E.J.W., and Muntus, R., "Ionic radii for use in geochemistry", Geochim. Cosmochim. Acta, Vol - 34, No. 9, pp 945-956, 1970.

[6] Valenzuela, R., Magnetic Ceramics, Cambridge University Press, Cambridge, 1994

[7] Sheikh, A. M., Watae , S.C., Jadhav, S.A. and Chougule, B.K., "Preparation and Characterization of Zn substituted Li-Mg ferrites", Materials Research Bulletin, Vol-37, pp 2547-2555, 2002.

[8] Snoek, J.L., "Dispersion and absorption in magnetic ferrites at frequencies above one Mc/s", Physica, Vol-14, pp 207-217, 1948.

[9] Jun, Hu and Mi, Yan, "Preparation of high permeability Ni-Mn-Zn ferrite", Journal of Zhejiang University Science, Vol-6B (6), pp 580-583, 2005.

[10] Tsutaoka, T., Ueshima, M., Tokunaga,T., Nakamura, T. and Hatakeyama, K., "Frequency dispersion and temperature variation of complex permeability of Ni-Zn ferrite composite materials", Journal of Applied Physics, Vol-78(6), pp 3983-3991, 1995.

[11] Hossain, A. K. M. Akther, Mahmud, S.T., Seki, M., Kawaia, T. and tabata ,H., "Structural, electrical transport, and magntic properties of $Ni_{1-x}Zn_xFe_2O_4$", J. of Magn. and Magn. Mater.,Vol-312, pp 210-219, 2007.

[12] Rado ,G.T.,Wright ,R.W., Emerson, W. H. and Terris , A., "Ferromagnetism at Very High Frequencies. IV. Temperature Dependence of the Magnetic Spectrum of a Ferrite", Physical . Review ., Vol-88, pp 909-915,1952.

[13] Chauhan, B. S., Kumar, R., Jadhav, K. M. and Singh, M., "Magnetic study of substituted Mg-Mn Ferrites Synthesized by citrate precursor method", Journal of Magnetism and Magnetic Materials, Vol-283, pp 71-81, 2004.

[14] Smit, J., "Magnetic properties of materials", Mc-Graw Hill, NewYork, 1971.

[15] Jadhav, S.A., "Magnetic properties of Zn-substituted Li-Mn ferrites", Journal of Magnetism and Magnetic Materials, Vol-224, pp 167-172, 2001.

CHAPTER 5

CONCLUSIONS

5.1 Conclusions

The XRD patterns for the polycrystalline $Fe_{2.5}Zn_{0.5-x}Mn_xO_4$ confirm the formation of spinel ferrite. Lattice constant increases with increasing the Mn content for all compositions .This increase in lattice constant can be explained on the basis of ionic radii. Since the ionic radius of Mn^{2+} (0.89Å) is larger than that of Zn^{2+} (0.74Å), the increase in lattice constant with the increase in Mn substitution is expected. The ρ_B decrease and porosity increase with increasing Mn content. On the other hand, ρ_B increase and porosity decrease with increasing T_s for each composition. During the sintering process, the thermal energy generates a force that drives the grain boundaries to grow over pores, thereby decreasing the pore volume and increasing the density of the materials. The microstructural study shows that the average grain size increases with increasing Mn content. The μ_i' increases as Mn content increases up to x=0.40 for the samples sintered at 1150 and 1200ºC and x=0.30 for the samples sintered at 1100 and 1250ºC. It is also observed that μ_i' increases with increasing sintering temperatures for all compositions as this help to develop uniform grain. The μ_i' remains fairly constant in the frequency range up to some critical frequency which is called resonance frequency. The highest μ_i' for each sample has been observed sintered at 1250 ºC because the microstructure is homogeneous with a uniform size distribution.

The loss factor decreases with increasing of Mn content and sintering temperature. The relative quality factor increases with increasing sintering temperature and Mn content up to

x=0.40 then decreases. For inductors used in filter applications, the quality factor is often used as a measure of performance. It is observed that the sample sintered at 1250ºC is of the highest Q value (1013) for $Fe_{2.5}Zn_{0.10}Mn_{0.40}O_4$ sample, probably due to the growth of lesser imperfection in this sample.

5.2 Suggestions for future work

It was found that $Fe_{2.5}Zn_{0.10}Mn_{0.40}O_4$ has the maximum initial permeability μ_i' and maximum Q-factor. So Mn and other metals which prefer a sub lattice to occupy can be substituted in $Fe_{2.5}Zn_{0.10}Mn_{0.40}O_4$ ferrite to enhance the permeability value.